The International Journal of Advanced Manufacturing Technology (2019) 104:1785–1837
https://doi.org/10.1007/s00170-019-03809-9

ORIGINAL ARTICLE

Response surface methodology for advanced manufacturing technology optimization: theoretical fundamentals, practical guidelines, and survey literature review

Lucas Guedes de Oliveira[1] · Anderson Paulo de Paiva[1] · Pedro Paulo Balestrassi[1] · João Roberto Ferreira[1] · Sebastião Carlos da Costa[1] · Paulo Henrique da Silva Campos[1]

Received: 7 February 2019 / Accepted: 21 April 2019 / Published online: 18 June 2019

Abstract

Process optimization normally involves the combination of mathematical and statistical techniques which can be approached by distinct ways. Despite the fact that different methods can be found in the literature, the response surface methodology raised as one of the most effective ways for performing process optimization, by combining design and analysis of experiments, modeling techniques, and optimization methods. However, practical guidelines for response surface methodology and critical analysis of its applications are quite scarce. Thus, this paper aims to present the theoretical principles and practical guidelines for carrying response surface methodology as well as to provide empirical evidence on its critical aspects for manufacturing optimization. In order to accomplish with this objective, 49 papers published in the *International Journal of Advanced Manufacturing Technology* (IJAMT) from 2014 to 2017 were investigated and reproduced, allowing the analysis of 123 response surfaces. Surprisingly, more than 75.29% of the models have presented a saddle shape. The practical meaning of this finding is that the stationary point is not a suitable solution for the optimization of those surfaces. Besides, multiple response surfaces are more commonly found in the literature than individual ones. From this amount of papers, 71.88% of the works investigated have presented significant correlation with their peers and 87.61% have convexity incompatible with the optimization direction. Most of the optimization solutions have found outside of experimental region which reveals a preponderant neglect of the nonlinear constraints involving the definition of the experimental region. It was also verified that the proportion of functions in saddle format corresponds to 96.86% of the models estimated in flat regions. Moreover, it was found that the number of center points is commonly changed and all the manufacturing processes investigated are driven by at most five control parameters. Finally, considering the theoretical principles, the practical guidelines, and the obtained results, a follow-along example involving the optimization of AISI H13-hardened steel turning with PCBN wiper, previously published by the authors in IJAMT, was revisited by using response surface methodology. The results corroborated the proposed framework suitability.

Keywords Response surface methodology · Design of experiments · Central composite design · Advanced manufacturing technology · Convexity, eigenalysis, multivariate confidence regions

✉ Pedro Paulo Balestrassi
ppbalestrassi@gmail.com

Lucas Guedes de Oliveira
lucasguedesdeoliveira@gmail.com

Anderson Paulo de Paiva
andersonppaiva@unifei.edu.br

João Roberto Ferreira
jorofe@unifei.edu.br

Sebastião Carlos da Costa
sccosta@unifei.edu.br

Paulo Henrique da Silva Campos
paulohcamposs@unifei.edu.br

[1] Institute of Industrial Engineering and Management, Federal University of Itajuba, Itajuba, Minas Gerais, Brazil

Nomenclature

f	Feed rate
V_c	Cutting speed
d	Depth of cut
y	Response variable, function value, or estimated model
β	Model coefficient
x	Independent variable
ε	Experimental error or residual
N	Total number of experiments
k	Number of factors or input variables
n_C	Number of center points
α	Axial distance
n_F	Number of factorial points
SS	Squared sum
MS	Squared mean
F_0	Fisher-Snedecor statistics
$\varnothing$	Number of degrees of freedon of F_0
Γ	Gama function
δi	Spherical moments
m	Index of the space of the model
$\boldsymbol{M}$	Matrix of moments
$\boldsymbol{x}_s$	Stationary point coordinate vector
$\boldsymbol{B}$	Matrix of coefficients of second-order terms
$\boldsymbol{b}$	Vector of coefficients of first-order terms
ρ	Design radius or the Pearson correlation
y_s	Estimative of the response variable in the stationary point
λ	Eigenvalues of $\hat{\boldsymbol{B}}$
w	Canonical variables
$\boldsymbol{I}$	Identity matrix
$\boldsymbol{\mu}$	Mean vector
c	Chi-squared variable
$\tilde{\Sigma}$	Variance-covariance matrix
∇	Gradient vector
$\mathbf{P}$	Matrix of the eigenvectors of $\tilde{\boldsymbol{\Sigma}}^{-1}$
$\boldsymbol{X}$	Vector of experimental factors
$f(\boldsymbol{X})$	Objective function
$g_j(\boldsymbol{X})$	Generic inequality constraint
$l_j(\boldsymbol{X})$	Generic equality constraint
α_1, α_2	Relative weights of linearly combined functions
n	Total number of data
χ_0^2	Qui-squared statistic

Abbreviations

ABNT	Brazilian Association of Technical Standards
ANOVA	Analysis of variance
BBD	Box-Behnken design
CCD	Central composite design
DOE	Design of experiments
FCCD	Face-centered central composite design
FFD	Full factorial design
EWR	Electrode wear rate
GRG	Generalized reduced gradient
IQR	Interquartile range
NBI	Normal boundary intersection
NOMATI	Manufacturing Optimization and Innovation Technology Center
Ortho.	Orthogonal
MRR	Material removal rate
MRV	Multiple response variables
RSM	Response surface methodology
OLS	Ordinary least squares
PC	Principal component score
PCA	Principal component analysis
SAM	Steepest ascent method
SPV	Scaled prediction variance
UP	Uniform precision
WPCA	Weighted principal component analysis

1 Introduction

Due to the different phenomena that involve them, industrial processes are commonly constrained by operability regions, which are manifested by combinations of control parameters [1–3]. In turning processes, for instance, the well-known three control parameters—feed rate (f), cutting speed (Vc), and depth of cut (d)—are operational input variables subjected to machine specifications [4–7]. For this reason, the universe of possibilities of the output variables, known as response variables of the process, also becomes constrained, establishing a delimited operability region [8, 9], for different technical setups, there will be specific operability regions.

This causal relationship between input and output variables has been studied since the beginning of mathematics when the image of a function was conceptualized as a result of the processing of a domain [10]. In real cases, however, the functions that model the processes of interest are usually unknown [11–13], which makes difficult to fully recognize the operability regions.

Despite this, no technical barrier arises from this limitation, given that practitioners and engineers, in most cases, do not seek a global mapping of the processes in this mathematical sense, but specific regions that reveal potential for improvement or meeting project specifications, called regions of interest [9]. Nevertheless, other problems emerge, since the investigation of these regions implies, firstly, in the knowledge of the set of variables that driven the studied processes, which means that the control parameters, their main effects, and interactions, should be primarily identified [11, 14].

Historically, many techniques have been developed to address these initial issues, culminating in a large set of experimental designs that currently compose the design of experiments (DOE), central composite design (CCD), Box-Behnken design (BBD), and Taguchi designs are among the designs most frequently are presented in the literature. Depending on

the application, these designs have been used individually [15, 16] in combination [17] or comparatively in an attempt to present the best results [18]. Additionally, they also have been used in different areas of knowledge, such as chemical engineering [19–21], medical sciences [22–24], and manufacturing [25–27].

Allied to DOE techniques, analysis of variance (ANOVA), and other hypotheses tests based on *t* statistics are commonly employed to determine the significance of tested input variables and to numerically describe the main effects and the interactions of control parameters on response variables, which usually represent critical-to-quality characteristics of the final products, such as surface roughness [28] circularity [29], tensile strength [30], and critical-to-performance characteristics of the process, such as cutting forces [31], percent yield [32], and productivity [33].

To appropriately investigate the regions of interest, it is also crucial to examine the influence of the control parameters on the response variables in a combined fashion [34, 35]. For this purpose, modeling techniques, such as ordinary least squares (OLS), play an essential role, since they allow to obtain a mathematical representation of the region of interest, also called model, by fitting the experimental data [2, 36]. Based on the fitted model, researchers can take more rational and suitable decisions about the process enabling increasingly efficient production systems and high-quality products.

In this context of improvements, the decision-making process can become even better if the experimenter employs mathematical optimization methods in an association with modeling techniques. By doing so, one can forthrightly recognize setups in which there will be improvements for the process, according to an objective, such as the reduction of operational costs, the increase of the quality of the products or the minimization of the process time [33, 37].

Although other methods can be used to approach process optimization, response surface methodology (RSM) is the one that relies on the intersection of design and analysis of experiments, modeling techniques, and optimization methods, by combining these three components in a stronger approach. With this combination, RSM reveals a high level of statistical and mathematical sophistication for several reasons. First, before production starts, the results of a process can be equated based on a small number of control parameters [9]. Second, whenever certain setups are assigned to the control parameters, obtaining optimal responses can be guaranteed with minimum variance [38]. Third, new processes, as well as known processes, can be approached in the same way, using experimental designs and empirical data [9].

To endorse valid conclusions, however, several assumptions must be taken into account, since the compatibility of the statistical and mathematical solutions with the practical reality of the processes will depend on the criteria adopted in each step of the RSM. This fact comprises the data collection, the model fitting and optimization, and the interpretation of the results.

In this context, although many theoretical studies have been developed in the last 70 years, practical guidelines for RSM and critical analysis of its applications are quite scarce. Then, to fulfill this gap with a suitable approach, this paper presents the following objectives: (1) to provide practical guidelines and core theoretical principles of RSM, (2) to investigate some critical aspects of RSM in the context of experimental studies of advanced manufacturing technology, (3) to identify singularities of the critical aspects studied, (4) to raise discussions on the usage of RSM, as well as new research opportunities for RSM in manufacturing.

To reach these goals, this paper is organized as follows: Section 2 provides an in-depth literature review from the *International Journal of Advanced Manufacturing Technology* (IJAMT) on RSM and some of its critical aspects; Section 3 details the proposed method for performing the survey literature review and presents the questions and hypotheses of the problem; Section 4 presents the results with detailed discussion; Section 5 revisits a case of advanced manufacturing technology optimization by using RSM. Finally, some relevant conclusions are drawn in Section 6.

In order to better disseminate this research, the authors stress that this article derives from more than 20 years of experience on applying DOE and optimization methods in welding and machining process. The author's research group, called Manufacturing Optimization and Innovation Technology Center (NOMATI), belongs to the Institute of Production Engineering and Management of the Federal University of Itajuba, Itajuba, Brazil.

2 Response surface methodology

Response surface methodology (RSM) was developed by George Box and associates in the 1950s [39] and have been studied by many other researchers in the last decades [2, 3, 8, 9, 11, 14, 36, 38, 40–45]. In essence, RSM is the combination of design and analysis of experiments, modeling techniques, and optimization methods in a stronger approach that utilizes experimental data to obtain process improvements.

Figure 1 shows how RSM may be viewed as a combination of these components. This intersection of procedures implies that researchers should be very mindful in each one of the three steps involving RSM. Without this caution, this methodology will certainly fail, does not produce the expected and possible desired results.

2.1 Classical approach and practical guidelines

Due to its multiple perspectives, RSM has many formal definitions; in one of its more classic conceptions, RSM is

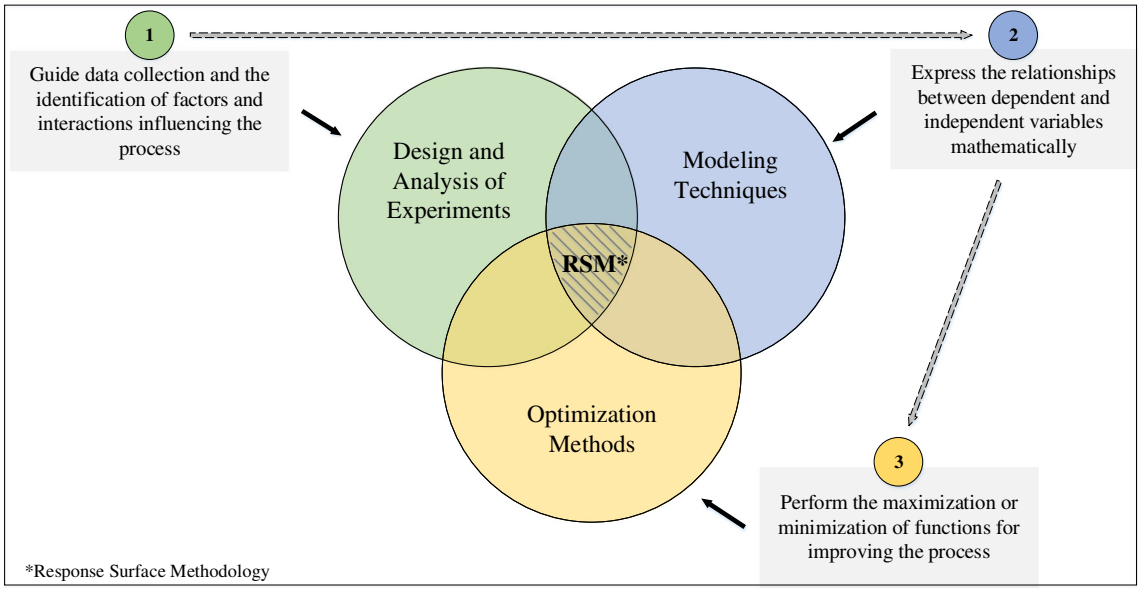

Fig. 1 Response surface methodology overview. Source: own authors

presented as a set of tools for improving the investigation of a particular experimental region [45]. More recent works describe the RSM as a useful method to establish mathematical relationships between the input and the output variables of a process in such a way that it can be optimized [46, 47].

A broader definition can be drawn from Myers and Montgomery [9], where the RSM has been conceptualized as "[...] a collection of statistical and mathematical techniques used to develop, improve and optimize processes." Based on this definition, the authors presented well-defined criteria for carrying RSM investigations. More applied studies have also provided practical examples for performing RSM according to the classical literature [48]. Considering the core principles [2, 3, 8, 9, 11, 14, 36, 38, 40–47], a roadmap for carrying RSM analysis was developed, as shown in Fig. 2.

The first step of RSM is to determine the variables governing the processes studied, i.e., the control parameters, also called factors [40, 49]. For this, the literature presents two approaches; the most conventional is to perform exploratory experiments, by using designs of few runs, such as fractional factorial or Taguchi arrays, which require a smaller number of experiments to investigate many factors than CCD and BBD, for example [41]. However, sometimes factors can also be adopted from practical experience [50], and then be followed by exploratory designed experiments with a smaller number of factors, which is preferable in some cases.

The second step of RSM is to determine the influence of the factors on the process investigated. For this purpose, ANOVA is the statistical technique most widely used in RSM studies because it allows distinguishing, among the factors evaluated, those that are truly significant and their individual effects on response variables [51].

Once the control parameters have been defined (Step 1) and their statistical significance confirmed (Step 2), the third step is to plan data collections according to an experimental design [42], for this purpose, CCD and BBD are the most usual [9]. Based on them, the responses variables are measured, as pointed in the Step 4.

After that, the fifth step is to evaluate if the experimental region is curve; this is a decision point because if the curvature is significant, the analysis should be continued by adding axial points to the design (Step 6A) and performing new experiments (Step 7), if not, the design should be moved to another direction [12, 52] by redefining the factor levels, as pointed in Step 6B.

In the curvature region, the collected data are used to fit mathematical models that adequately represent the process studied in function of its control parameters (Step 8), for this, OLS is typically employed to obtain a second-order model expanded in Taylor series expressed in Eq. 1 [39, 47]:

$$y = \beta_0 + \sum_{i=1}^{k} \beta_i x_i + \sum_{i=1}^{k} \beta_{ii} x_i^2 + \sum_{\substack{i=1 \\ j=1}}^{k} \beta_{ij} x_i x_j + \varepsilon \qquad (1)$$

where y is the modeled function, β_0 is the constant term of the model, β_i are the coefficients of the linear terms, β_{ii} are the coefficients of the quadratic terms, β_{ij} are the coefficients of the interation terms, and ε is the residual.

The last step of RSM (Step 9) is to find the set of control parameters that improve the process by applying an optimization method to minimize or maximize the functions modeled in Step 8.

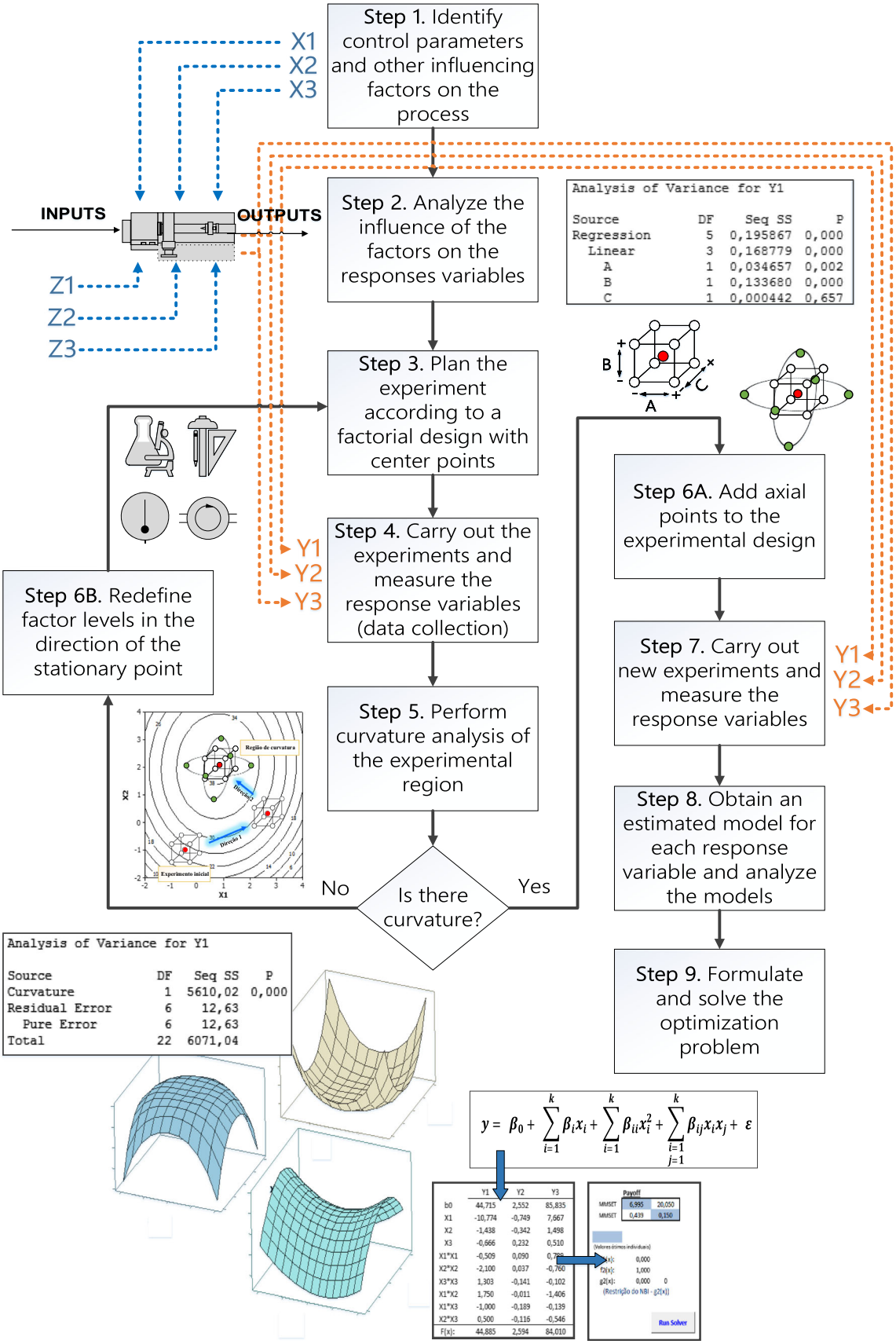

Fig. 2 Roadmap for an efficient conduction of response surface methodology. Source: own authors

2.2 Central composite design, center points, and curvature regions

Developed by Box and Wilson in 1951, CCD is the most used second-order design in experimental studies [9]. Typically, this design involves three kinds of experimental points: factorial (points that allow the generation of data for 2-sample *t* hypothesis tests), center points (a design element that allows the assessment of curvature in the region of interest), and the axial points (elements capable of estimating the quadratic effects observed in determinated region) [2].

The factorial points are placed at the vertices of a hypercubic design and are obtained from the combination of the levels of each factor. When used without axial and center points, these points characterize the factorial designs, as shown in Fig. 3.

Assuming that only two levels for each factor (− and +) are necessary (since the 2-sample *t* test requires only two set of data for each input variable), if the researcher is interested in studying *k* factors, then $N = 2^k$ experiments will be generated. Figure 3 a up to c show the displacement of a full factorial design (FFD) for 2, 3, and 4 factors, respectively. The design of Fig. 3 b represents the ethanol production process studied by Yücel and Göycıncık [53], in which the final ethanol concentration was modeled by NH_4Cl concentration (factor A), amount of yeast (factor B), and temperature (factor C). Another example is found in Lin et al. [54] and can be characterized by the design of Fig. 3 c. In this case, three critical

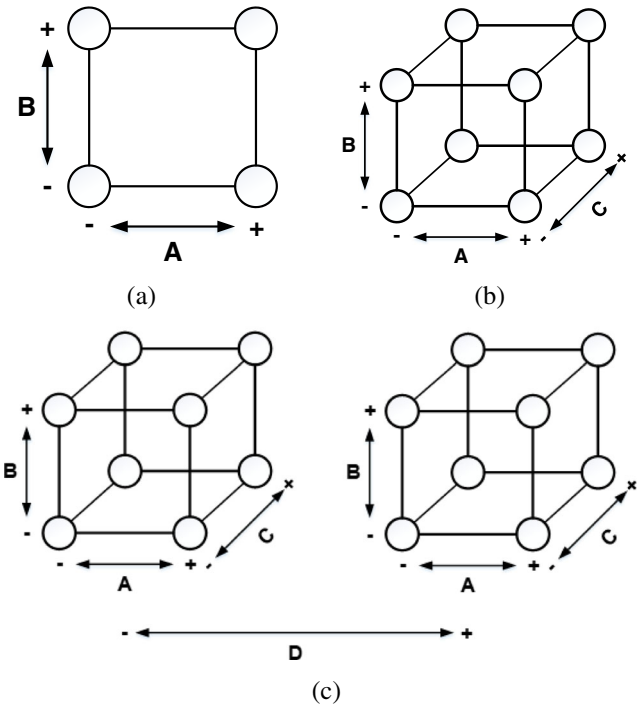

Fig. 3 Examples of full factorial designs with two levels in each factor: (a) $k = 2$, (b) $k = 3$, and (c) $k = 4$. Source: own authors

characteristics of microelectrical discharge machining were modeled by peak current, pulse on-time, pulse off-time, and electrode rotation speed.

Considering a sequential approach [38], the center points form the second typology of points to be included in the CCD, since they allow curvature analysis in the investigated region and reduce the prediction variance in the design center [55]. When the curvature is identified, the axial points are finally added, determining the total number of experiments of a CCD, as expressed by Eq. 2:

$$N = 2^k + 2k + n_c \tag{2}$$

where *N* is the total number of experiments, *k* is the number of factors, 2^k is the number of factorial points, $2k$ the number of axial points, and n_c is the number of center points.

The center points are placed exactly in the design center and can be obtained by the average values of the factors levels (usually identified by the code 0). The axial points, in turn, extrapolate the lower and upper levels of each factor and are placed outside the cuboidal experimental region, allowing a better estimation of the quadratic terms [9]. Figure 4 shows a schematic view of a CCD for two and three factors. They are, in truth, a rotation of the factorial points.

The distance from the axial points to the design center is given in Eq. 3:

$$\propto = 2^{k/4} \tag{3}$$

where $\propto$ is the axial distance and *k* is the number of factors.

As mentioned in Section 2.1, experimental designs allow planned data collection in such a way that it is possible to model a particular region of interest. This region generally defines a location of significant curvature. For this reason, the literature converges on the need to precisely identify the curve region within the operability region [2, 9, 38].

Steepest ascent method (SAM) is one of the most used optimization methods for searching curvature regions. Originated in pure mathematics, its formulation has been applied to the experimental context since the early days of RSM [33, 56]. By applying SAM, the function fitted to experimental data is differentiated to obtain the gradient vector; with this procedure, the direction of the stationary point can be verified, ensuring the correct location of the curve region.

Figure 5 provides an overview of Steepest Ascent Method, by reproducing a problem proposed in the literature [38]. This illustration alludes to a generic stationary point, obtained by virtue of multiple iterations. Based on the coefficient of the linear model built with a FFD, a search direction is defined. Moving the original center point along this line search direction, the experimenter will find more suitable regions for curvature. Sometimes, it will be necessary to redo the FFD to define new directions like that shown in Fig. 5 (3). Along the line search the response of interest will increase

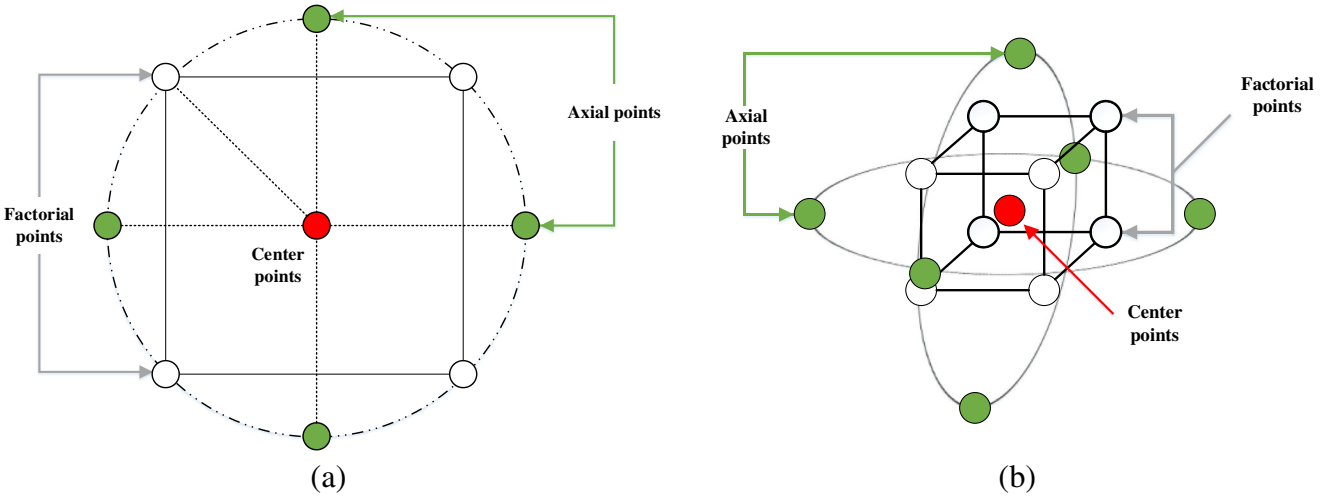

Fig. 4 Schematic view of a central composite design: (**a**) for two factors ($k = 2$) and (**b**) for three factors ($k = 3$). Source: own authors

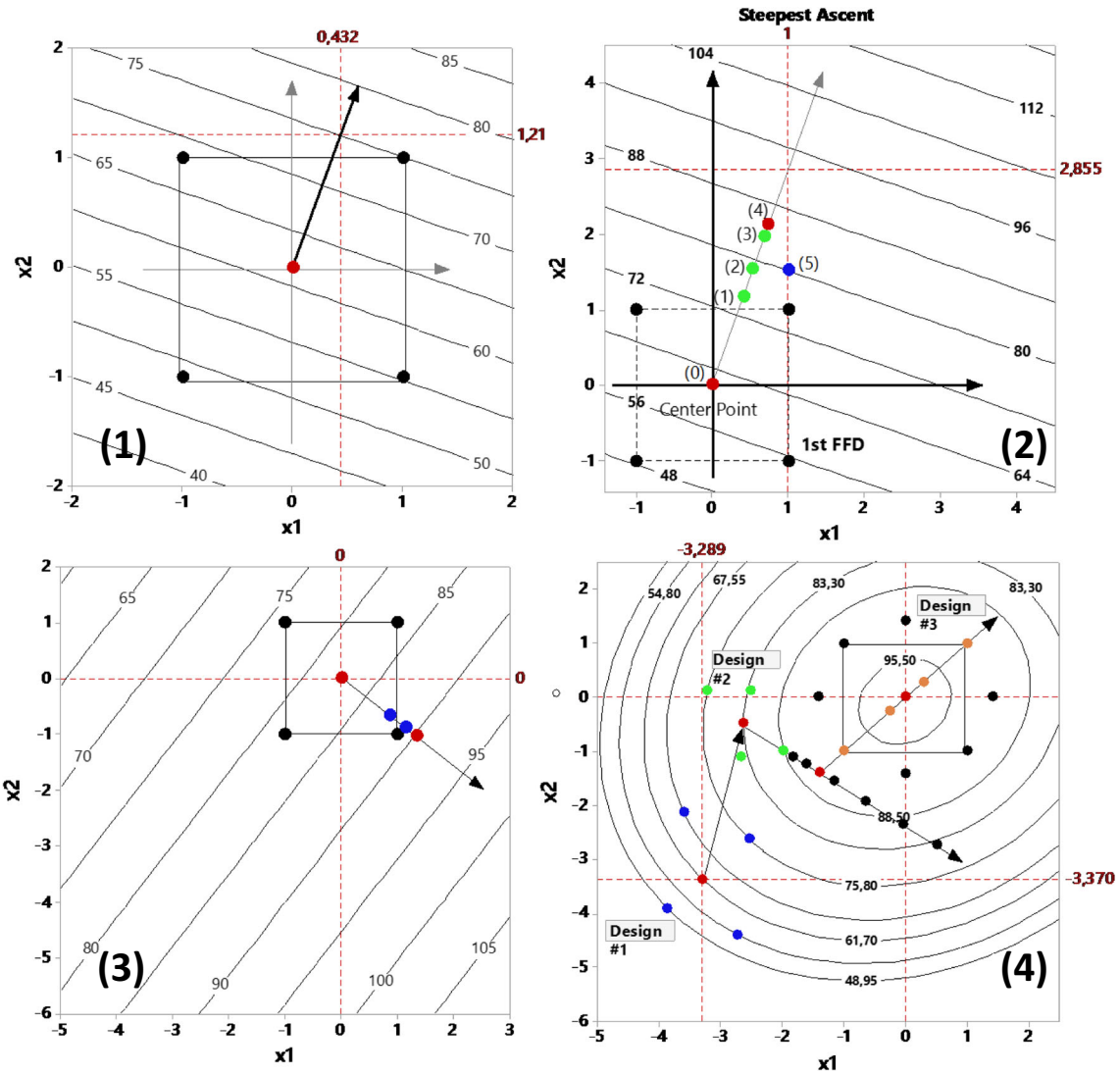

Fig. 5 Schematic view of steepest ascent method. Source: adapted from Khuri and Cornell [38]

accordingly until the region of a possible curvature, where the response starts to diminish sequentially. At this inflection point, a curvature test must be conducted.

A typical curvature test consists of comparing the average of the responses measured in the factorial points with the average of the responses measured in the center points [9], so that it is possible to evaluate if the sum of the coefficients of the quadratic terms is equal to or different from zero, as stated in Eq. 4:

$$\begin{aligned} H_0 &: \sum_{j=1}^{k} \beta_{jj} = 0 \\ H_1 &: \sum_{j=1}^{k} \beta_{jj} \neq 0 \end{aligned} \tag{4}$$

where β_{jj} is the coefficients of quadratic terms of jth order

The test uses the sum of squares presented in Eq. 5, which combines the averages of the measured responses and the amounts of factorial and center points of the experimental design. Considering that the calculation of $SS_{\text{pure quadratic}}$ has one degree of freedom, the mean of squares associated with the quadratic terms of the model will be given by the same expression:

$$MS_{\text{pure quadratic}} = SS_{\text{pure quadratic}} = \frac{n_F n_C \left(\bar{y}_F - \bar{y}_C\right)^2}{n_F + n_C} \tag{5}$$

where n_F is the number of factorial points, n_C is the number of center points, $\bar{y}_F$ is the average of the responses measured in the factorial points, $\bar{y}_C$ is the average of the responses measured in the center points.

The sum of squares of the experimental error is obtained in the ANOVA by Eq. 6.

$$SS_{\text{error}} = \sum_{i=1}^{n_c} \left(y_i - \bar{y}_C\right)^2 \tag{6}$$

where y_i is the responses measured in the ith center point.

With $(n_C - 1)$ degrees of freedom, an unbiased estimator for the natural variability of the process is obtained, accounting for the variance between responses measured under the same experimental conditions (i.e., center points):

$$MS_{\text{error}} = \frac{SS_{\text{error}}}{n_C - 1} = \frac{\sum_{i=1}^{n_c} \left(y_i - \bar{y}_C\right)^2}{n_C - 1} \tag{7}$$

From the quotient of the variance estimated between the factorial and center points (variance between) and the experimental error (variance within), F statistics can be computed by Eq. 8:

$$F_0 = \frac{MS_{\text{pure quadratic}}}{MS_{\text{error}}} = \frac{\left[\dfrac{n_F n_C \left(\bar{y}_F - \bar{y}_C\right)^2}{n_F + n_C}\right]}{\left[\dfrac{\sum_{i=1}^{n_c} \left(y_i - \bar{y}_C\right)^2}{n_C - 1}\right]} \tag{8}$$

The p value comes from the improper integral of the Fisher-Snedecor distribution with degrees of freedom $\varnothing_1$ and $\varnothing_2$ [57], as shown in Eq. 9:

$$P(X > F_0) = \int_{x=F_{calc}}^{+\infty} \frac{\Gamma[(\varnothing_1 + \varnothing_2)/2]}{\Gamma(\varnothing_1/2)\Gamma(\varnothing_2/2)} \left(\frac{\varnothing_1}{\varnothing_2}\right)^{\varnothing_2/2} \frac{x^{(\varnothing_2 - 2)/2}}{[1 + (\varnothing_1/\varnothing_2)x]^{(\varnothing_1 + \varnothing_2)/2}} dx \tag{9}$$

where $\varnothing_1$ is the number of degrees of freedom of the numerator of F_0, $\varnothing_2$ is the number of degrees of freedom of the denominator of F_0, and Γ is the gamma function. Replacing $\varnothing_1$ by 1 and $\varnothing_2$ by $(n_C - 1)$ in Eq. 9, we arrive at:

$$P(X > F_0) = \int_{x=F_{calc}}^{+\infty} \frac{\Gamma[(1 + n_C - 1)/2]}{\Gamma(1/2)\Gamma((n_C - 1)/2)} \left(\frac{1}{n_C - 1}\right)^{(n_C - 1)/2} \frac{x^{(n_C - 1 - 2)/2}}{[1 + (1/n_C - 1)x]^{(1 + n_C - 1)/2}} dx \tag{10}$$

from where we obtain an expression for the p value as a function of the number of center points in the design and the continuous variable x, with a domain in the interval $[0, +\infty)$:

$$P(X > F_0) = \int_{x=F_{calc}}^{+\infty} \frac{\Gamma[(n_C)/2]}{\Gamma(1/2)\Gamma((n_C - 1)/2)} \left(\frac{1}{n_C - 1}\right)^{(n_C - 1)/2} \frac{x^{(n_C - 3)/2}}{[1 + (1/n_C - 1)x]^{(n_C)/2}} dx \tag{11}$$

2.3 Spherical moments, rotatability, and orthogonality of central composite designs

This section provides the mathematical and statistical fundamentals on the ideal values for the factorial, axial, and center points based on the spherical moments, rotatability, and orthogonality of CCD.

Suppose we have a CCD for $k = 2$, whose factorial block consists of a FFD with levels equal to $L = \pm r$. For a traditional FFD, $r = \pm 1$. Besides the two factors, let us consider the computation of the following quartic and quadratic terms: x_1^2, x_2^2,

Table 1 Central composite design and its spherical moments δ_i even

x_1 [1]	x_2 [2]	x_1^2 [11]	x_2^2 [22]	x_1^4 [1111]	x_2^4 [2222]	$x_1^2x_2^2$ [1122]
$-r$	$-r$	r^2	r^2	r^4	r^4	r^4
r	$-r$	r^2	r^2	r^4	r^4	r^4
$-r$	R	r^2	r^2	r^4	r^4	r^4
r	R	r^2	r^2	r^4	r^4	r^4
0	0	0	0	0	0	0
0	0	0	0	0	0	0
⋮	⋮	⋮	⋮	⋮	⋮	⋮
0	0	0	0	0	0	0
$-\rho$	0	ρ^2	0	ρ^4	0	0
ρ	0	ρ^2	0	ρ^4	0	0
0	$-\rho$	0	ρ^2	0	ρ^4	0
0	P	0	ρ^2	0	ρ^4	0
$\sum_{u=1}^{N} x_{iu} = 0$		$\sum_{u=1}^{N} x_{iu}^2 = 2^k r^2 + 2\rho^2$		$\sum_{u=1}^{N} x_{iu}^4 = 2^k r^4 + 2\rho^4$		$\sum_{u=1}^{N} x_{iu}^2 x_{ju}^2 = 2^k r^4$

x_1^4, x_2^4, and $x_1^2x_2^2$. In this way, we may obtain the design structure shown in Table 1.

According to Box and Hunter [36], a moment of order δ for an experimental "rotatable" design of order d using k factors is given by:

$$\left[1^{\delta_1}2^{\delta_2}\cdots k^{\delta_k}\right] = \frac{1}{N}\sum_{u=1}^{N} x_{1u}^{\delta_1}x_{2u}^{\delta_2}\cdots x_{ku}^{\delta_k} \tag{12}$$

$$\left[1^{\delta_1}2^{\delta_2}\cdots k^{\delta_k}\right] = \begin{cases} \dfrac{\lambda_\delta \prod_{i=1}^{k}\delta_i!}{2^{\delta/2}\prod_{i=1}^{k}\left(\frac{\delta_i}{2}\right)!} & \forall \quad \delta_i \text{ even} \\ 0 & \forall \quad \delta_i \text{ odd} \end{cases} \tag{13}$$

The moments associated to the columns x_1^2, x_1^4, and $x_1^2x_2^2$ in Table 1 are as follows, respectively:

$$[11] = \left[1^2 2^0\right] = \frac{\lambda_2 2!}{2} = \lambda_2 \text{ and } [11] = \frac{1}{N}\sum_{u=1}^{N} x_{iu}^2 = \frac{2^k r^4 + 2\rho^4}{N} \tag{14}$$

$$[1111] = \left[1^4 2^0\right] = \frac{\lambda_4 4!}{2^2 \times 2!} = 3\lambda_4 \text{ and } [1111] = \frac{1}{N}\sum_{u=1}^{N} x_{iu}^4 = \frac{2^k r^4 + 2\rho^4}{N} \tag{15}$$

$$[1122] = \left[1^2 2^2\right] = \frac{\lambda_4 2!2!}{2^2 \times 1!1!} = \lambda_4 \text{ and } [1122] = \frac{1}{N}\sum_{u=1_{i\neq j}}^{N} x_{iu}^2 x_{ju}^2 = \frac{2^k r^4}{N} \tag{16}$$

A CCD is rotatable if the second-, mixed-, and fourth-order moments are, respectively, equal to $\lambda_2 = [ii] = 1$, $\lambda_4 = [iijj]$, $3\lambda_4 = [iiii]$. Similarly, a CCD is orthogonal if the mixed fourth-order moment, [iijj], or equivalently, λ_4, is equal to unity, $\lambda_4 = 1$. Taking these design moments into account, the necessary and sufficient condition for rotatability of a second-order model is:

$$[iiii] = 3[iijj] \tag{17}$$

From Table 1, $\lambda_4 = N^{-1}2^k r^4$ and $3\lambda_4 = N^{-1}(2^k r^4 + 2\rho^4)$, which implies that, to assure the design rotatability, the following equality must be satisfied:

$$3N^{-1}2^k r^4 = N^{-1}2^k r^4 + 2N^{-1}\rho^4 \tag{18}$$

Hence, when the CCD is designed in terms of (− 1) and (+ 1) levels, it is possible to obtain the well-known mathematical expression for the radius of CCD with k factors that is capable of keeps the rotatability property, such as:

$$\rho = \sqrt[4]{2^k} \tag{19}$$

If we take the variables in coded units, it is possible to observe that the coded design satisfies the constraint $\sum_{u=1}^{N} x_{iu}^2 = 0$ but keeps $\sum_{u=1}^{N} x_{iu}^2 \neq N$. So, it is necessary to use a scale factor g to correct this misspecification. Introducing the scale factor g, N may be expressed as:

$$N = \sum_{u=1}^{N} (g x_{ui})^2 = g^2 \sum_{U=1}^{N} x_{ui}^2 = g^2\left(2^k + 2\rho^2\right) \tag{20}$$

And the scale factor becomes:

$$g = \sqrt{\frac{N}{2^k + 2\rho^2}} \tag{21}$$

Using this result, we find the pure fourth-order moment [iiii] as:

$$[iiii] = \frac{1}{N}\sum_{U=1}^{N}(gx_{ui})^4 = \frac{g^4}{N}\left(2^k + 2\rho^4\right) \tag{22}$$

$$[iiii] = \left(\frac{N}{2^k + 2\rho^2}\right)^2\left(\frac{2^k + 2\rho^4}{N}\right) \tag{23}$$

Adopting $\rho = 2^{k/4}$, we have:

$$[iiii] = \frac{N^2}{2^{2k} + 4\left(2^k\right)\rho^2 + 4\rho^4}\left(\frac{2^k + 2\rho^4}{N}\right) = \frac{3\left(2^k\right)N}{2^{2k} + 4\left(2^{3k/2}\right) + 4\left(2^k\right)} = \frac{3N}{2^k + 4\left(2^{k/2}\right) + 4} \tag{24}$$

Since [iiii] = 3[iijj], we obtain:

$$\lambda_4 = \frac{N}{2^k + 4\left(2^{k/2}\right) + 4} \tag{25}$$

In order to be orthogonal, the design must have the following number of center points:

$$n_0 = 4\left(2^{k/2}\right) + 4 - 2k \tag{26}$$

Box and Hunter [36] defined the variance function for a general second-order rotatable design as:

$$\mathrm{Var}\left[\hat{y}(\rho)\right] = \frac{2(k+2)\lambda_4^2 + 2\lambda_4(\lambda_4 - 1)(k+2)\rho^2 + [(k+1)\lambda_4 - (k-1)]\rho^4}{2\lambda_4[(k+2)\lambda_4 - k]} \tag{27}$$

In their original concept, Box and Hunter [36] established that the most important aspect in response surface design is that the variance function be as "low" and "flat" as possible everywhere in the experimental region. To accomplish with this assumption, the researchers proposed to choose the value of λ_4 in order to obtain the prediction variance at the origin equals to the prediction variance at a distance of 1.0 (in coded units). This constraint was coined as "uniform precision." Mathematically, λ_4 must be chosen to satisfy the constraint below:

$$\mathrm{Var}\left[\hat{y}(x)|\rho = 0\right] = \mathrm{Var}\left[\hat{y}(x)|\rho = 1\right] \tag{28}$$

Replacing this initial condition in the variance function, it is possible to write that:

$$\mathrm{Var}\left[\hat{y}(x)|\rho = 0\right] = \frac{2(k+2)\lambda_4^2}{2\lambda_4[(k+2)\lambda_4 - k]} \tag{29}$$

Table 2 Values of λ_4 for different values of k

k	2	3	4	5	6	7	8
λ_4	0.7844	0.8385	0.8705	0.8918	0.9070	0.9185	0.9274

$$\mathrm{Var}\left[\hat{y}(x)|\rho = 1\right] = \frac{2(k+2)\lambda_4^2 + 2\lambda_4(\lambda_4 - 1)(k+2) + [(k+1)\lambda_4 - (k-1)]}{2\lambda_4[(k+2)\lambda_4 - k]} \tag{30}$$

The value of λ_4 that satisfies these conditions is obtained by:

$$\lambda_4 = \frac{(k+3) + \sqrt{9k^2 + 14k - 7}}{4(k+2)} \tag{31}$$

For different values of k, we obtain the values of λ_4 as shown in Table 2.

The number of center points needed to satisfy the uniform precision may be written as:

$$\frac{2^k + 2k + n_0}{2^k + 4\left(2^{k/2}\right) + 4} = \frac{(k+3) + \sqrt{9k^2 + 14k - 7}}{4(k+2)} \tag{32}$$

Integer solutions of this equation will be the exception, but we can still use an integer solution as close as possible to the value that solves it exactly. This will provide rotatable, near uniform precision designs:

$$n_0 = \left\{\left[2^k + 4\left(2^{k/2}\right) + 4\right]\left[\frac{(k+3) + \sqrt{9k^2 + 14k - 7}}{4(k+2)}\right]\right\} - \left(2^k + 2k\right) \tag{33}$$

Table 3 Number of design points for a CCD with k input variables. Source: adapted from Box and Hunter [36]

k	2	3	4	5
λ_4	0.7844	0.8385	0.8705	0.8918
n_0 (UP)	4.55	5.55	7.34	10.28
n_0 (UP)[1]	5	6	7	10
n_0 (Ortho.)	8.00	9.30	12.00	16.60
n_0 (Ortho.)[1]	8	9	12	17
Factorials	4	8	16	32
Axials	4	6	8	10
N (UP)	13	20	31	52
N (Ortho.)	16	23	36	59

[1] Values recommended by [36] after rounding

The number of center points required for a rotatable CCD in k input variables to be either nearly orthogonal (Ortho.) or nearly having the uniform precision (UP) is described in Table 3.

2.4 Response surfaces modeling

Considering the sequential approach of RSM [38], the CCD is used to model the process in the curvature region by using the empirical data. A second-order response surface model can be written in canonical form or in matrix notation [39, 47, 58]:

$$\hat{Y}(\mathbf{x}) = \beta_0 + \sum_{i=1}^{k}\beta_i x_i + \sum_{i=1}^{k}\beta_{ii}x_i^2 + \sum_{i<j}\sum\beta_{ij}x_i x_j = \beta_0 + \mathbf{x}^{\mathbf{T}}\mathbf{b} + \mathbf{x}^{\mathbf{T}}\mathbf{B}\mathbf{x}$$

$$\hat{Y}(\mathbf{x}) = \beta_0 + \underbrace{\begin{bmatrix} x_1 & x_2 & \cdots & x_k \end{bmatrix}}_{\mathbf{x}^{\mathbf{T}}}\underbrace{\begin{bmatrix} \beta_1 \\ \beta_2 \\ \vdots \\ \beta_k \end{bmatrix}}_{\mathbf{b}} + \underbrace{\begin{bmatrix} x_1 & x_2 & \cdots & x_k \end{bmatrix}}_{\mathbf{x}^{\mathbf{T}}}\underbrace{\begin{bmatrix} \beta_{11} & 1/2\,\beta_{21} & \cdots & 1/2\,\beta_{k1} \\ 1/2\,\beta_{12} & \beta_{22} & \cdots & 1/2\,\beta_{k2} \\ \vdots & \vdots & \ddots & \vdots \\ 1/2\,\beta_{1k} & 1/2\,\beta_{2k} & \cdots & \beta_{kk} \end{bmatrix}}_{\mathbf{B}}\underbrace{\begin{bmatrix} x_1 \\ x_2 \\ \vdots \\ x_k \end{bmatrix}}_{\mathbf{x}} \tag{34}$$

where β is the polynomial coefficient, k is the number of factors, and ε is the error term.

A traditional approach to estimating the β parameters is known as OLS method [2, 36] and consists of an optimization problem in which the function L, given by the sum of squares of the residuals, must be minimized as a function of β:

$$\min_{\beta} L = \sum_{i=1}^{n}\varepsilon_i^2 = \sum_{i=1}^{n}\left(Y_i - \beta_0 + \sum_{i=1}^{k}\beta_i x_i + \sum_{i=1}^{k}\beta_{ii}x_i^2 + \sum_{i<j}\sum\beta_{ij}x_i x_j\right)^2 \tag{35}$$

In matrix notation:

$$\min_{\beta}\ \mathbf{L} = \mathbf{y}^T\mathbf{y} - \beta^T\mathbf{X}^T\mathbf{y} - \mathbf{y}^T\mathbf{X}\beta + \beta^{\mathbf{T}}\mathbf{X}^{\mathbf{T}}\mathbf{X}\beta \tag{36}$$

Then, to minimize $\boldsymbol{L}$, the derivative of $\boldsymbol{L}$ with respect to β is calculated by:

$$\frac{\partial \mathbf{L}}{\partial \boldsymbol{\beta}} = \frac{\partial\left(\mathbf{y}^{\mathbf{T}}\mathbf{y} - \boldsymbol{\beta}^{\mathbf{T}}\mathbf{X}^{\mathbf{T}}\mathbf{y} - \mathbf{y}^{\mathbf{T}}\mathbf{X}\boldsymbol{\beta} + \boldsymbol{\beta}^{\mathbf{T}}\mathbf{X}^{\mathbf{T}}\mathbf{X}\boldsymbol{\beta}\right)}{\partial \boldsymbol{\beta}} = \frac{\partial\left(\mathbf{y}^{\mathbf{T}}\mathbf{y} - 2\boldsymbol{\beta}^{\mathbf{T}}\mathbf{X}^{\mathbf{T}}\mathbf{y} + \boldsymbol{\beta}^{\mathbf{T}}\mathbf{X}^{\mathbf{T}}\mathbf{X}\boldsymbol{\beta}\right)}{\partial \boldsymbol{\beta}} = 0 \tag{37}$$

$$\frac{\partial \mathbf{L}}{\partial \boldsymbol{\beta}} = -2\mathbf{X}^{\mathbf{T}}\mathbf{y} + 2\mathbf{X}^{\mathbf{T}}\mathbf{X}\hat{\boldsymbol{\beta}} = 0 \therefore \hat{\boldsymbol{\beta}} = \left(\mathbf{X}^{\mathbf{T}}\mathbf{X}\right)^{-1}\mathbf{X}^{\mathbf{T}}\mathbf{y} \tag{38}$$

With this procedure, the OLS method has two important properties; so $\hat{\boldsymbol{\beta}}$ be considered a good estimator of the coefficients of the model, the expected value $E\left(\hat{\boldsymbol{\beta}}\right) = \boldsymbol{\beta}$ and the covariance of $\hat{\boldsymbol{\beta}}$, which depends on the data variance and the experimental matrix, are given by $\mathrm{Cov}\left(\hat{\boldsymbol{\beta}}\right) = \sigma^2\left(\mathbf{X}^{\mathbf{T}}\mathbf{X}\right)^{-1}$, where $\mathbf{X}$ is design matrix and σ^2 is mean square error. It can be shown that:

$$\mathrm{Cov}\left(\hat{\boldsymbol{\beta}}\right) = E\left\{\left[\hat{\boldsymbol{\beta}} - E\left(\hat{\boldsymbol{\beta}}\right)\right]^T\left[\hat{\boldsymbol{\beta}} - E\left(\hat{\boldsymbol{\beta}}\right)\right]\right\} = E\left[\left(\hat{\boldsymbol{\beta}} - \boldsymbol{\beta}\right)\left(\hat{\boldsymbol{\beta}} - \boldsymbol{\beta}\right)\right] \tag{39}$$

$$\mathrm{Cov}\left(\hat{\boldsymbol{\beta}}\right) = E\left\{\left[\left(\mathbf{X}^{\mathbf{T}}\mathbf{X}\right)^{-1}\left(\mathbf{X}^{\mathbf{T}}\boldsymbol{\varepsilon}\right)\right]\left[\left(\mathbf{X}^{\mathbf{T}}\mathbf{X}\right)^{-1}\left(\mathbf{X}^{\mathbf{T}}\boldsymbol{\varepsilon}\right)\right]\right\} = E\left\{\left[\left(\mathbf{X}^{\mathbf{T}}\mathbf{X}\right)^{-1}\left(\mathbf{X}^{\mathbf{T}}\boldsymbol{\varepsilon}\right)\right]\left[\left(\boldsymbol{\varepsilon}^{\mathbf{T}}\mathbf{X}\right)\left(\mathbf{X}^{\mathbf{T}}\mathbf{X}\right)^{-1}\right]\right\} \tag{40}$$

$$\mathrm{Cov}\left(\hat{\boldsymbol{\beta}}\right) = E\left\{\left[\left(\mathbf{X}^{\mathbf{T}}\mathbf{X}\right)^{-1}\left(\mathbf{X}^{\mathbf{T}}\mathbf{X}\right)\left[\left(\boldsymbol{\varepsilon}^{\mathbf{T}}\boldsymbol{\varepsilon}\right)\left(\mathbf{X}^{\mathbf{T}}\mathbf{X}\right)^{-1}\right]\right\} = E\left(\boldsymbol{\varepsilon}^{\mathbf{T}}\boldsymbol{\varepsilon}\right)\left(\mathbf{X}^{\mathbf{T}}\mathbf{X}\right)^{-1} = \sigma^2\left(\mathbf{X}^{\mathbf{T}}\mathbf{X}\right)^{-1} \tag{41}$$

Since the response surface model is an approximation of the region of interest, any point on the surface will be contained in a confidence interval; this interval is a result of the variance effect of the model at the analyzed point. By using the covariance matrix $\mathrm{Cov}\left(\hat{\boldsymbol{\beta}}\right)$ of Eq. 41, a (1-α)% confidence interval for new observations of a model can be built as shown in Eq. 42:

$$(1-\alpha)CI = \hat{y}(\mathbf{x}_0) \pm t_{\alpha/2,n-p}\sqrt{\hat{\sigma}^2\left[1 + \mathbf{z}^{\mathbf{T}}(\mathbf{x}_0)\left(\mathbf{X}^{\mathbf{T}}\mathbf{X}\right)^{-1}\mathbf{z}^{\mathbf{T}}(\mathbf{x}_0)\right]} \tag{42}$$

With the following properties:

$$E\left[\hat{Y}(\mathbf{x})|\mathbf{x}_0\right] = \mathbf{z}_0^{(m)\mathbf{T}}\left[\left(\mathbf{X}^T\mathbf{X}\right)^{-1}\left(\mathbf{X}^{\mathbf{T}}\mathbf{Y}\right)\right] \text{ and } \mathrm{Var}\left[\hat{Y}(\mathbf{x})|\mathbf{x}_0\right] = \sigma^2\left[\mathbf{z}_0^{(m)\mathbf{T}}\left(\mathbf{X}^{\mathbf{T}}\mathbf{X}\right)^{-1}\mathbf{z}_0^{(m)}\right] \tag{43}$$

For $k = 2$, for instance, $\mathbf{z}_0^{(m)\mathbf{T}} = \mathbf{z}_0^{(2)\mathbf{T}} = \left[1, x_1, x_2, x_1^2, x_2^2, x_1x_2\right]$.

2.5 Convexity, optimization direction, and experimental region constraint

Several critical aspects of RSM arise from the interface between modeling techniques and optimization methods. Among them, the convexity [2] and the optimization direction of the function [59] can be highlighted. While convexity is an intrinsic characteristic of the mathematical models conceptualized in the previous section, optimization direction is an extrinsic characteristic, defined by the experimenter in the phase of obtaining the optimal values.

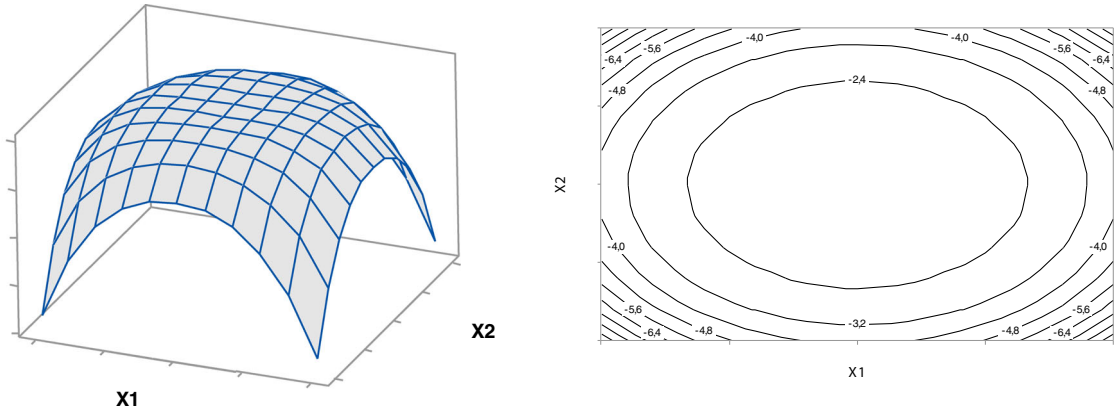

(a) Surface and contour plots of a concave response surface model. Stationary point is a maximum.

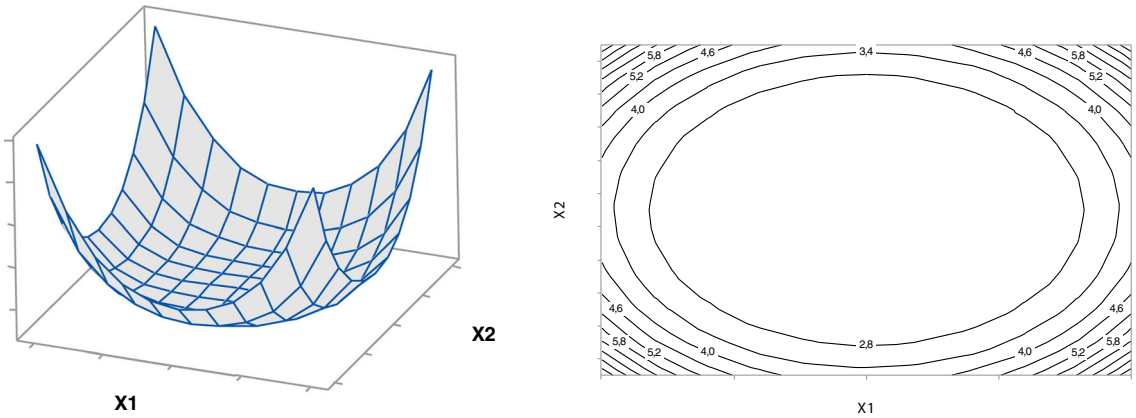

(b) Surface and contour plots of a convex response surface model. Stationary point is a minimum.

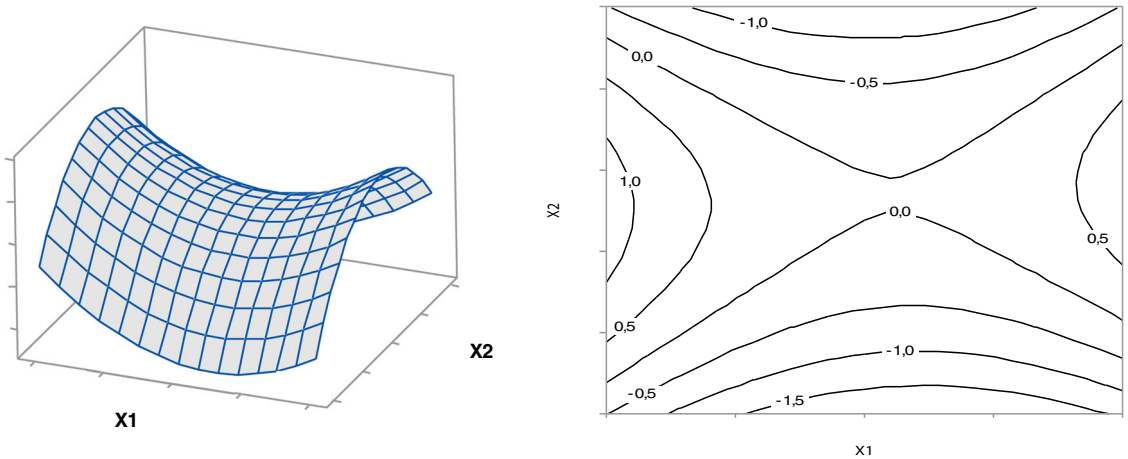

(c) Surface plots of a saddle surface. Stationary point is neither maximum nor minimum.

Fig. 6 Surfaces and contour plots for different convexities: (a) concave, (b) convex, and (c) saddle. Source: own authors

The literature provides a wide range of approaches on function convexity [44, 46, 60], in which there is a consensus about the three types of convexities of surfaces originating from quadratic functions. Figure 6 illustrates surfaces and contour plots for the different types of convexities. Concave functions are similar to domes (Fig. 6a); convex functions exhibit bucket-like contours (Fig. 6b) [61]; saddle-shaped functions, in turn, carry in its own nomenclature the description of its geometrical format—that is, saddle—and are also known by other names such as col. and minimax (Fig. 6c) [2].

Since graphs may induce misinterpretations [46], especially for a larger number of factors, analytical methods are required to characterize the stationary points and, accordingly, the convexity of the functions [62].

From the optimization theory, an unconstrained stationary point of response surface model may be written as:

$$\nabla_x\left[\beta_0 + \mathbf{x^T b} + \mathbf{x^T B x}\right] = 0 \therefore \mathbf{b} + 2\mathbf{x^T}[\mathbf{B}] = 0 \rightarrow \mathbf{x} = -\frac{1}{2}\mathbf{b}[\mathbf{B}]^{-1} \quad (44)$$

However, if we are interested in solutions constrained to the spherical region formed by CCD, then one must solve the following optimization system:

$$\underset{x\in\Omega}{\text{Min}}\ \beta_0 + \mathbf{x^T b} + \mathbf{x^T}[\mathbf{B}]\mathbf{x} \qquad S.t.: \mathbf{x^T x} \le \rho^2 \quad (45)$$

Using the concept of the Lagrangian function $\ell(\mathbf{x}, \rho)$, the optimization problem becomes:

$$\underset{x\in\Omega}{\text{Min}}\ \ell(x,\rho) = \beta_0 + x^T b + x^T[B]x + \left\lfloor \lambda\left(x^T x - \rho^2\right)\right\rfloor \quad (46)$$

Applying the KKT's first-order condition, the gradient of the Lagrangian will be:

$$\nabla\ell(x,\rho) = \begin{bmatrix} b + 2x(B+\lambda I) \\ x^T x - \rho^2 \end{bmatrix} = \begin{bmatrix} 0 \\ 0 \end{bmatrix} \quad (47)$$

Which results in:

$$x = -\frac{1}{2} b(B+\lambda I)^{-1} \quad (48)$$

This is the well-known form for the constrained stationary point of response surface model. As a straightforward consequence, it is possible to write that the CCD axial distance is equal to:

$$\rho = \sqrt{\frac{1}{4}\left[(B+\lambda I)^{-1} b\right]^T \left[(B+\lambda I)^{-1} b\right]} \quad (49)$$

where $\boldsymbol{B}$ is the matrix of coefficients of the second-order terms, and $\boldsymbol{b}$ is the vector of coefficients of the first-order terms, $\boldsymbol{I}$ is the identity matrix, and λ are the eigenvalues of $\boldsymbol{B}$, for $i = 1, 2, 3, ..., k$.

To obtain the eigenvalues λ of $\boldsymbol{B}$, the determinant of the difference between the matrix of coefficients $\boldsymbol{B}$ and the identity matrix $\boldsymbol{I}$ must equal zero:

$$|\boldsymbol{B} - \lambda \boldsymbol{I}| = 0 \quad (50)$$

The response surface in the vicinity of the stationary points can also be written as a function of the response at the stationary point by using the eigenvalues of $\boldsymbol{B}$:

$$\hat{y} = \hat{y}_s + \sum_{i=1}^{k} \lambda_i w_i^2 \quad (51)$$

where $\hat{y}_s$ is the estimate of the response variable at the stationary point and w_i are canonical variables.

Under mathematical arguments, if in any direction of the canonical variable w_i, the increment is negative ($\lambda < 0$), it means that the stationary point is the maximum response of the function—the maximum point. Similarly, if in any direction of these canonical variables, the increment is positive ($\lambda > 0$), it means that the response grows by moving away from the stationary point, which makes it a minimum point. If in each direction w_i, the signal of the increment is different (sometimes positive, sometimes negative), the stationary point is not an extreme of the function, but a saddle point.

In practice, if all eigenvalues are negative, there is a maximum point, and therefore the function is concave. On the other hand, if all eigenvalues are positive, there is a minimum point, which indicates a convex function. However, if, among the eigenvalues, there are both positive and negative signals, then the function is a saddle-shaped surface [63].

Given the stochastic nature of the RSM, the stationary point of a response surface will be always associated to a variability component. In the following paragraphs, we demonstrate the variance propagation of the response surface to the stationary point.

The stationary point may be found using the first partial derivatives of the response surface in terms of each factor. For example, let us consider a full quadratic model for $k = 2$ variables, such as:

$$\hat{Y}(x) = \hat{\beta}_0 + \hat{\beta}_1 x_1 + \hat{\beta}_2 x_2 + \hat{\beta}_{11} x_1^2 + \hat{\beta}_{22} x_2^2 + \hat{\beta}_{12} x_1 x_2 \quad (52)$$

For this model, the stationary point can be defined considering the gradient of this function, such that:

$$f_1(x) = \left[\frac{\partial \hat{Y}(x)}{\partial x_1}\right] = \beta_1 + 2\beta_{11}x_1 + \beta_{12}x_2 \quad f_2(x) = \left[\frac{\partial \hat{Y}(x)}{\partial x_2}\right] = \beta_2 + 2\beta_{22}x_2 + \beta_{12}x_1 \quad (53)$$

The gradient vector will be then:

$$\nabla_x\left[\hat{Y}(x)\right] = \begin{bmatrix} \dfrac{\partial \hat{Y}(x)}{\partial x_1} \\ \dfrac{\partial \hat{Y}(x)}{\partial x_2} \end{bmatrix} = \begin{bmatrix} \beta_1 + 2\beta_{11}x_1 + \beta_{12}x_2 \\ \beta_2 + 2\beta_{22}x_2 + \beta_{12}x_1 \end{bmatrix} \quad (54)$$

And the respective Hessian will be given by:

$$\nabla_x^2\left[\hat{Y}(x)\right] = \begin{bmatrix} \dfrac{\partial^2 \hat{Y}(x)}{\partial x_1^2} & \dfrac{\partial^2 \hat{Y}(x)}{\partial x_1 \partial x_2} \\ \dfrac{\partial^2 \hat{Y}(x)}{\partial x_2 \partial x_1} & \dfrac{\partial^2 \hat{Y}(x)}{\partial x_2^2} \end{bmatrix} = \begin{bmatrix} 2\beta_{11} & \beta_{12} \\ \beta_{12} & 2\beta_{22} \end{bmatrix} \quad (55)$$

Consider that the variance-covariance matrix of the coefficients of the full quadratic model is described by:

$$\sigma_x^2(\mathbf{X}^{\mathbf{T}}\mathbf{X})^{-1} = \begin{array}{c} \\ \beta_0 \\ \beta_1 \\ \beta_2 \\ \beta_{11} \\ \beta_{22} \\ \beta_{12} \end{array} \begin{array}{c} \begin{array}{cccccc} \beta_0 & \beta_1 & \beta_2 & \beta_{11} & \beta_{22} & \beta_{12} \end{array} \\ \begin{bmatrix} \sigma^2_{\beta_0} & & & & & \text{sym} \\ 0 & \sigma^2_{\beta_1} & & & & \\ 0 & 0 & \sigma^2_{\beta_2} & & & \\ \sigma_{\beta_0\beta_{11}} & 0 & 0 & \sigma^2_{\beta_{11}} & \sigma_{\beta_{11}\beta_{22}} & \\ \sigma_{\beta_0\beta_{22}} & 0 & 0 & \sigma_{\beta_{11}\beta_{22}} & \sigma^2_{\beta_{22}} & \\ 0 & 0 & 0 & 0 & 0 & \sigma^2_{\beta_{12}} \end{bmatrix} \end{array} \quad (56)$$

It is clear that all covariances σ_{β_i,β_j} are null and only covariance $\sigma_{\beta_{11}\beta_{22}} \neq 0$. Thus, the variance equation for the derivatives will not contain terms of covariance. Therefore, it can be written that:

$$\mathrm{Var}[f_i(x)] = \sum_{i=1}^{p}\left[\frac{f_i(x)}{\partial\beta_i}\right]^2\sigma^2_{\beta_i} + 2\sum_{i<j}^{p}\sum^{p}\left[\frac{f_i(x)}{\partial\beta_i}\right] \times \left[\frac{f_i(x)}{\partial\beta_j}\right]\sigma\beta_i,\beta_j \quad (57)$$

or in another arrangement:

$$\mathrm{Var}[f_1(x)] = \sum_{i=1}^{p}\left[\frac{\partial^2\hat{Y}(x)}{\partial x_i\partial\beta_i}\right]^2\sigma^2_{\beta_i} + 2\sum_{i<j}^{p}\sum^{p}\left[\frac{\partial^2\hat{Y}(x)}{\partial x_i\partial\beta_i}\right] \times \left[\frac{\partial^2\hat{Y}(x)}{\partial x_i\partial\beta_i}\right]\sigma_{\beta i,\beta j} \quad (58)$$

Analogously, the covariances between the partial derivatives can be defined as:

$$\mathrm{Cov}\left[f_i(x), f_j(x)\right] = \sum_{i=1}^{p}\left[\frac{f_i(x)}{\partial\beta_i}\right] \times \left[\frac{f_j(x)}{\partial\beta_i}\right]\sigma^2_{\beta_i} + \sum_{i<j}^{p}\sum^{p}\left[\frac{f_i(x)}{\partial\beta_i}\right] \times \left[\frac{f_j(x)}{\partial\beta_j}\right]\sigma_{\beta_i,\beta_j} \quad (59)$$

For the quadratic model, it is obtained:

$$Cov\left[f_1(\mathbf{x}), f_2(\mathbf{x})\right] = \underbrace{\left(\frac{f_1(\mathbf{x})}{\partial\beta_1}\right)\left(\frac{f_2(\mathbf{x})}{\partial\beta_1}\right)}_{0}\sigma^2_{\beta_1} + \left(\frac{f_1(\mathbf{x})}{\partial\beta_{11}}\right)\underbrace{\left(\frac{f_2(\mathbf{x})}{\partial\beta_{11}}\right)}_{0}\sigma^2_{\beta_{11}} + \underbrace{\left(\frac{f_1(\mathbf{x})}{\partial\beta_{22}}\right)}_{0}\left(\frac{f_2(\mathbf{x})}{\partial\beta_{22}}\right)\sigma^2_{\beta_{22}} + \left(\frac{f_1(\mathbf{x})}{\partial\beta_{12}}\right)\left(\frac{f_2(\mathbf{x})}{\partial\beta_{12}}\right)\sigma^2_{\beta_{12}} + \left(\frac{f_1(\mathbf{x})}{\partial\beta_{11}}\right)\left(\frac{f_2(\mathbf{x})}{\partial\beta_{22}}\right)\sigma_{\beta_{11},\beta_{22}} \quad (60)$$

Simplifying:

$$\mathrm{Cov}[f_1(x), f_2(x)] = \left(\frac{f_1(x)}{\partial\beta_{12}}\right)\left(\frac{f_2(x)}{\partial\beta_{12}}\right)\sigma^2_{\beta_{12}} + \left(\frac{f_1(x)}{\partial\beta_{11}}\right)\left(\frac{f_2(x)}{\partial\beta_{22}}\right)\sigma_{\beta_{11},\beta_{22}} \quad (61)$$

Taking the partial derivatives of the gradient with respect to the estimated coefficients, for the first partial derivative, the equation of the variance can be written as:

$$\mathrm{Var}[f_1(x)] = \left(\frac{\partial^2\hat{Y}(x)}{\partial x_1\partial\beta_1}\right)^2\sigma^2_{\beta_1} + \left(\frac{\partial^2\hat{Y}(x)}{\partial x_1\partial\beta_{11}}\right)^2\sigma^2_{\beta_{11}} + \left(\frac{\partial^2\hat{Y}(x)}{\partial x_1\partial\beta_{12}}\right)^2\sigma^2_{\beta_{12}} = \sigma^2_{\beta_1} + 4\sigma^2_{\beta_{11}}x_1^2 + \sigma^2_{\beta_{12}}x_2^2 \quad (62)$$

Similarly, for the second derivative, the variance equation will be equal to:

$$\mathrm{Var}[f_2(x)] = \left(\frac{\partial^2\hat{Y}(x)}{\partial x_2\partial\beta_2}\right)^2\sigma^2_{\beta_2} + \left(\frac{\partial^2\hat{Y}(x)}{\partial x_2\partial\beta_{22}}\right)^2\sigma^2_{\beta_{22}} + \left(\frac{\partial^2\hat{Y}(x)}{\partial x_2\partial\beta_{12}}\right)^2\sigma^2_{\beta_{12}} = \sigma^2_{\beta_2} + 4\sigma^2_{\beta_{22}}x_2^2 + \sigma^2_{\beta_{12}}x_1^2 \quad (63)$$

And the covariance equation:

$$\mathrm{Cov}[f_1(\mathbf{x}), f_2(\mathbf{x})] = x_1x_2\left(\sigma^2_{\beta_{12}} + 4\sigma_{\beta_{11},\beta_{22}}\right) \quad (64)$$

Thus, for the complete quadratic model, the variance-covariance matrix of the gradient can be written as:

$$\tilde{\boldsymbol{\Sigma}}_{\left[\nabla\hat{y}(\mathbf{x})\right]} = \mathrm{Var}\left[\nabla\hat{y}(\mathbf{x})\right] = \begin{bmatrix} \mathrm{Var}[f_1(\mathbf{x})] & \mathrm{Cov}[f_1(\mathbf{x}), f_2(\mathbf{x})] \\ \mathrm{Cov}[f_1(\mathbf{x}), f_2(\mathbf{x})] & \mathrm{Var}[f_2(\mathbf{x})] \end{bmatrix} \quad (65)$$

In the specific case of a full quadratic model for $k = 2$ variables, the variance-covariance matrix of the partial derivatives can be written as:

$$\underset{(2\times2)}{\tilde{\boldsymbol{\Sigma}}}_{\left[\nabla\hat{y}(\mathbf{x})\right]} = \mathrm{Var}\left[\nabla\hat{y}(\mathbf{x})\right] = \begin{bmatrix} \sigma^2_{\beta_1} + 4\sigma^2_{\beta_{11}}x_1^2 + \sigma^2_{\beta_{12}}x_2^2 & x_1x_2\left(\sigma^2_{\beta_{12}} + 4\sigma_{\beta_{11},\beta_{22}}\right) \\ x_1x_2\left(\sigma^2_{\beta_{12}} + 4\sigma_{\beta_{11},\beta_{22}}\right) & \sigma^2_{\beta_2} + 4\sigma^2_{\beta_{22}}x_2^2 + \sigma^2_{\beta_{12}}x_1^2 \end{bmatrix} \quad (66)$$

This particular proof emphasizes how the uncertainty in a response surface coefficients may be propagated to the stationary point, since there is a nonzero variance-covariance matrix associated to the response surface gradient.

Based on this fact, enclosing any point on the surface, including the stationary and the optimum points (which not always are the same, as will be discussed later in this section), there will be a confidence ellipse.

Consider the ellipse equation written in terms of vector of normal random variables $\mathbf{x}$ with a respective mean vector $\boldsymbol{\mu}$ and a variance-covariance matrix $\tilde{\boldsymbol{\Sigma}}^{-1}$. The constant c^2 is a chi-squared variable and can change depending on the desired confidence level (1-α).

$$(\mathbf{x}-\boldsymbol{\mu})^{\mathbf{T}}\tilde{\boldsymbol{\Sigma}}^{-1}(\mathbf{x}-\boldsymbol{\mu}) = c^2 \quad (67)$$

Applying a spectral decomposition, the variance-covariance matrix $\tilde{\boldsymbol{\Sigma}}^{-1}$ may be replaced by its respective eigenvalues and eigenvectors. If $\mathbf{P}$ is matrix of the eigenvectors of $\tilde{\boldsymbol{\Sigma}}^{-1}$ and $\boldsymbol{\Lambda}^{-1}$ is the diagonal matrix of its eigenvalues, then the ellipse may be written as:

$$(x-\mu)^T P \Lambda^{-1} P^T (x-\mu) = c^2 \tag{68}$$

Since $\boldsymbol{\Lambda}^{-1} = \boldsymbol{\Lambda}^{-1/2}\boldsymbol{\Lambda}^{-1/2}$, then:

$$\left[\mathbf{P}^{\mathbf{T}}(\mathbf{x}-\boldsymbol{\mu})\right]^{\mathbf{T}} \boldsymbol{\Lambda}^{-1/2}\boldsymbol{\Lambda}^{-1/2}\left[\mathbf{P}^{\mathbf{T}}(\mathbf{x}-\boldsymbol{\mu})\right] = c^2 \tag{69}$$

Taking $c^2 = k(MSE)F_{(\alpha,k,df_{\text{error}})}$ and applying the square root over the expressions of both sides of the former equation, it is possible to write that:

$$\sqrt{\left[\mathbf{P}^{\mathbf{T}}(\mathbf{x}-\boldsymbol{\mu})\right]^{\mathbf{T}} \boldsymbol{\Lambda}^{-1/2}\boldsymbol{\Lambda}^{-1/2}\left[\mathbf{P}^{\mathbf{T}}(\mathbf{x}-\boldsymbol{\mu})\right]} = \sqrt{k(MSE)F_{(\alpha,k,df_{\text{error}})}} \tag{70}$$

Which results in:

$$\left[\mathbf{P}^{\mathbf{T}}(\mathbf{x}-\boldsymbol{\mu})\right]^{\mathbf{T}} \boldsymbol{\Lambda}^{-1/2} = \sqrt{k(MSE)F_{(\alpha,k,df_{\text{error}})}} \tag{71}$$

or:

$$\mathbf{x}-\boldsymbol{\mu} = \frac{\boldsymbol{\Lambda}^{1/2}}{\mathbf{P}^{\mathbf{T}}}\sqrt{k(MSE)F_{(\alpha,k,df_{\text{error}})}} \tag{72}$$

Since the matrix of eigenvalues is orthogonal, then $\mathbf{P}^{\mathbf{T}} = \mathbf{P}^{-1}$. Therefore:

$$\mathbf{x} = \boldsymbol{\mu} + \mathbf{P}\boldsymbol{\Lambda}^{1/2}\sqrt{k(MSE)F_{(\alpha,k,df_{\text{error}})}} \tag{73}$$

The former equation describes any point in an ellipse. Therefore, in order to draw the ellipse, one may use the following expression:

$$\begin{bmatrix} x_1 \\ x_2 \end{bmatrix} = \begin{bmatrix} \mu_1 \\ \mu_2 \end{bmatrix} + \sqrt{k(MSE)F_{(\alpha,k,df_{error})}} \times \underbrace{\begin{bmatrix} h_{11} & h_{12} \\ h_{21} & h_{22} \end{bmatrix}}_{\mathbf{P}} \underbrace{\begin{bmatrix} \sqrt{\lambda_1} & 0 \\ 0 & \sqrt{\lambda_2} \end{bmatrix}}_{\Lambda^{1/2}} \begin{bmatrix} \cos\alpha \\ \sin\alpha \end{bmatrix} \tag{74}$$

With $0 \le \alpha \le 2\pi$

The most important particularity of optimization problems involving objective functions or constraints estimated by response surface models is that the coefficients of nonlinear functions will be stochastic. Therefore, the optimum or the stationary points (they are not always the same) are, in truth, just estimated values and, depending on the experimental error level, may be, in practice, a very unstable solution.

To avoid such drawbacks, the optimization problem may be improved by adding three kinds of constraints: (a) a constraint $g_1(\mathbf{x})$ representing the experimental space (or the CCD region); (b) a constraint $g_2(\mathbf{x})$ involving the confidence ellipse for the optimum or for the stationary point if it is the case and, and (c) a constraint $g_3(\mathbf{x})$ added to control the prediction variance. The resulting optimization system may be defined as:

$$\begin{aligned} &\underset{x\in\Omega}{\text{Min}} \;\; f(x) = \beta_0 + x^T b + x^T B\, x \\ &S.t.: g_1(x) = x^T x - \rho^2 \le 0 \\ &\quad g_2(x) = \nabla_x^{\mathrm{T}}\left[\hat{y}\left(x_0^*\right)\right]\left(\tilde{\Sigma}_{\nabla_x}^{-1}\right)\nabla_x\left[\hat{y}\left(x_0^*\right)\right] \le k(\text{MSE})F_{(\alpha,k,df_{\text{error}})} \\ &\quad g_3(x): \xi_{\text{Lower}} \le \sum_{i=1}^{n}\left\{\frac{\partial\left[\hat{y}(x)\right]}{\partial\beta_i}\right\}_{\hat{\beta}_i}^{2}\sigma_{\beta_i}^2 \le \xi_{\text{Upper}} \\ &\quad \xi_{\text{Lower}} = \frac{(n-p)\hat{\sigma}^2}{\chi^2_{(n-p,1-\alpha/2)}} \\ &\quad \xi_{\text{Upper}} = \frac{(n-p)\hat{\sigma}^2}{\chi^2_{(n-p,\alpha/2)}} \end{aligned} \tag{75}$$

Figure 7 shows how the experimental space, prediction variance, and confidence level for the optimum can substantially change the optimization results.

As noted throughout this section, the convexity of the functions has many characteristics and mathematical implications. Notably, the correct understanding of the nature of the stationary points and the convexities of the models provides valuable information about the behavior of the response variables in terms of their factors and interactions [38]. However, considering optimization methods as a third component of RSM, the optimization direction also appears as a relevant analytical paradigm, capable of interconnecting the logical nature of modeling and optimization with its practical meaning.

Although often used in the literature, there seems to be no formal definition for the optimization direction, which can be understood as a necessary attribute to the objective functions, to be deliberated according to the nature of the problem [59, 64]. In this way, the optimization direction provides the correct direction for optimizing functions, indicating their minimization or maximization [65, 66]. As a result, it is common to minimize the surface roughness of machined parts [67, 68], to maximize the tensile strength of welded alloys [69, 70], to minimize the energy consumption in pelleting of wheat straw [71], and to maximize the biodiesel yield [72].

In most works, the convexity and the optimization direction are usually treated in isolation, but a few papers provide joint approaches and demonstrate the interdependence of both concepts [35, 73, 74]. From these studies, it is observed that, by its very nature, a concave function is compatible with the maximization direction, since it has a maximum point. Similarly, it is noted that a convex function is proper for minimization, since it has a minimum point.

Despite this, there are cases in which the optimization direction is incompatible with the convexity of the function to be optimized. That is, it is required to minimize a concave function, maximize a convex function, or even minimize or maximize a saddle-shaped function. When these cases occur,

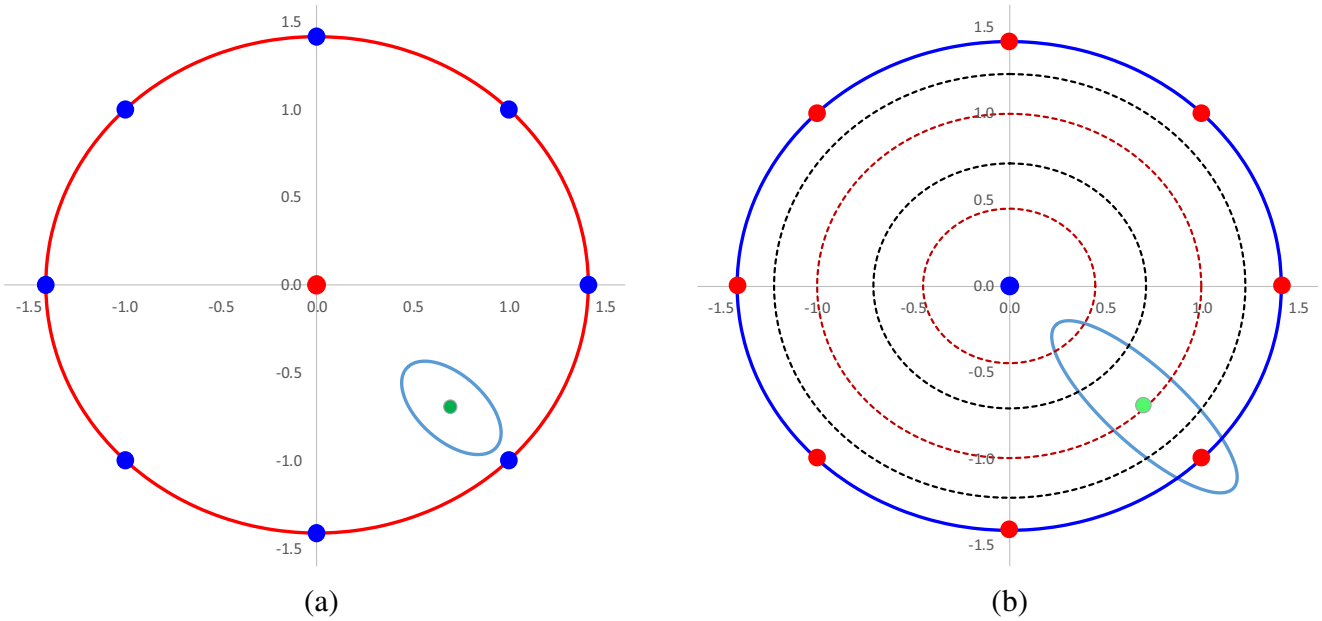

Fig. 7 Spherical CCD region, prediction variance, and confidence ellipse. (**a**) Low level of uncertainty on response surface coefficients. (**b**) Optimum uncertainty based on a larger experimental error (MSE). Source: own authors

the optimum will not be the stationary point, but a point in the boundary of the experimental design. Since solutions outside the experimental design cannot be predicted consistently, the researcher should use an experimental region constraint to solve the optimization problem, as expressed by Eq. 76 [43, 58]:

$$\boldsymbol{x}^T\boldsymbol{x} \leq \rho^2 \tag{76}$$

where ρ is the radius of the experimental region.

However, depending on its location inside the experimental design, the optimum $\mathbf{x_0}$ may present low predictability, especially in the borderline where the optimum will most likely rely on. Then, there will be a trade-off between the expected value E[f(**x**)] and the variance Var [f(**x**)], as shown in Fig. 8.

Figure 9 summarizes the relationship between the three critical aspects addressed in this section: convexity, optimization direction, and experimental region constraint. For this, the illustration draws on an analogy between the presented concepts and the walking in a mountain. In this case, the mountain represents the function obtained with the response surface modeling; the shape of the mountain is a fixed condition, insensitive to any external desire, as well as the convexity is an intrinsic characteristic of the model.

In this sense, Fig. 9 also expresses the will of two individuals (A and B), who, as an external part of the mountain (i.e., extrinsically), wish to go down or to climb it. In the context of RSM, if the function should be minimized, there is a minimization direction (individual A). Similarly, if the function is required to be maximized, there is a maximization direction (individual B). Assuming that Eq. 76 provides an experimental region constraint as shown in Fig. 9, the minimization will be constrained to the height indicated by the mountain level curve. This limit would represent the impossibility of access to lower heights due to physical barriers (such as the presence of abysses, and plains). In turning cases, for example, it would be impossible to achieve certain levels of surface roughness depending on the machine.

If there is an overall maximum point (characteristic of the concave function) and a maximization direction, the experimental region constraint will become inactive. This is because the stationary point itself delimits the optimization, that is, there is no possibility of climbing beyond the highest peak of the mountain (Fig. 9). Thus, the usage of this type of constraint, besides leading to real solutions in the cases of incompatibility between the convexity and the optimization direction, does not cause any type of interference when these aspects are harmonic.

2.6 Multiple responses and correlation

The production systems, by their very nature, present several critical characteristics. In general, each of them defines an intervening aspect of the quality of the products or the efficiency of the processes. In view of this, such characteristics are usually treated as response variables [14, 75]. For welding processes, the width of the fusion zone and the size of the heat affected zone can be used to define the quality of the weld bead [76]. For biodiesel synthesis, the percentage of fuel produced can be used to characterize the process efficiency [77].

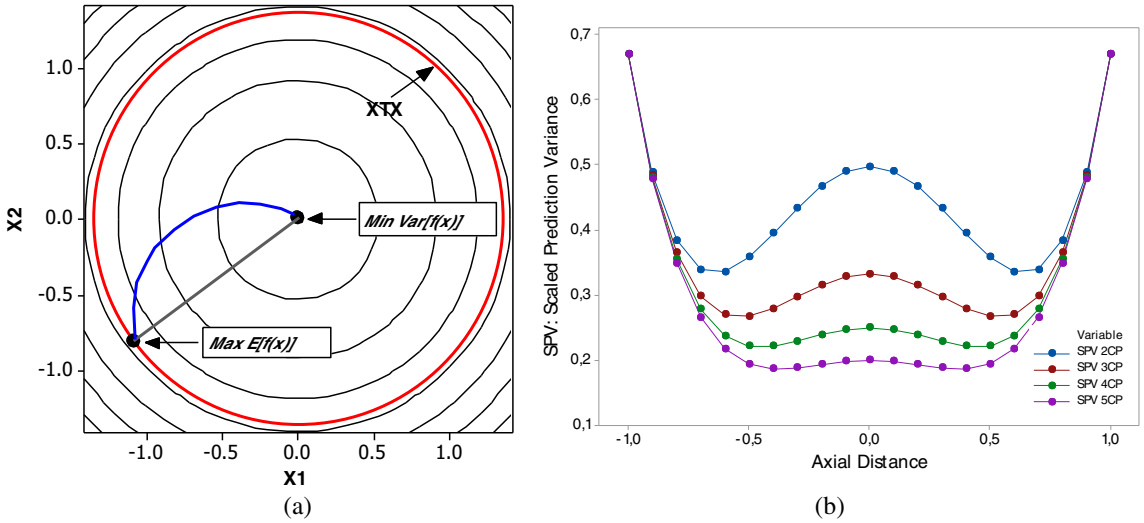

Fig. 8 Schematic illustration of the (a) duality between E[f(**x**)] and Var [f(**x**)], (b) scaled prediction variance (SPV) for different amounts of center points. Source: own authors

In manufacturing studies, the surface roughness is frequently used to define the quality of manufactured items [67, 78]. Bajíc et al. [79] stated that "[...] the major indicator of surface quality on machined parts is surface roughness." However, many other aspects can also be used to represent the quality of the machining process, such as the wear and the tool life, the cutting forces and the cutting temperature, and the properties of the chip [80].

For the optimization stage, when addressed together, these aspects configure the multiobjective problems, by converting the response variables models into objective functions, as formulated by Eq. 77. According to Rao [64], the solution of multiobjective problems reveals much higher levels of complexity because "with multiple objectives, there arises a possibility of conflict [...]."

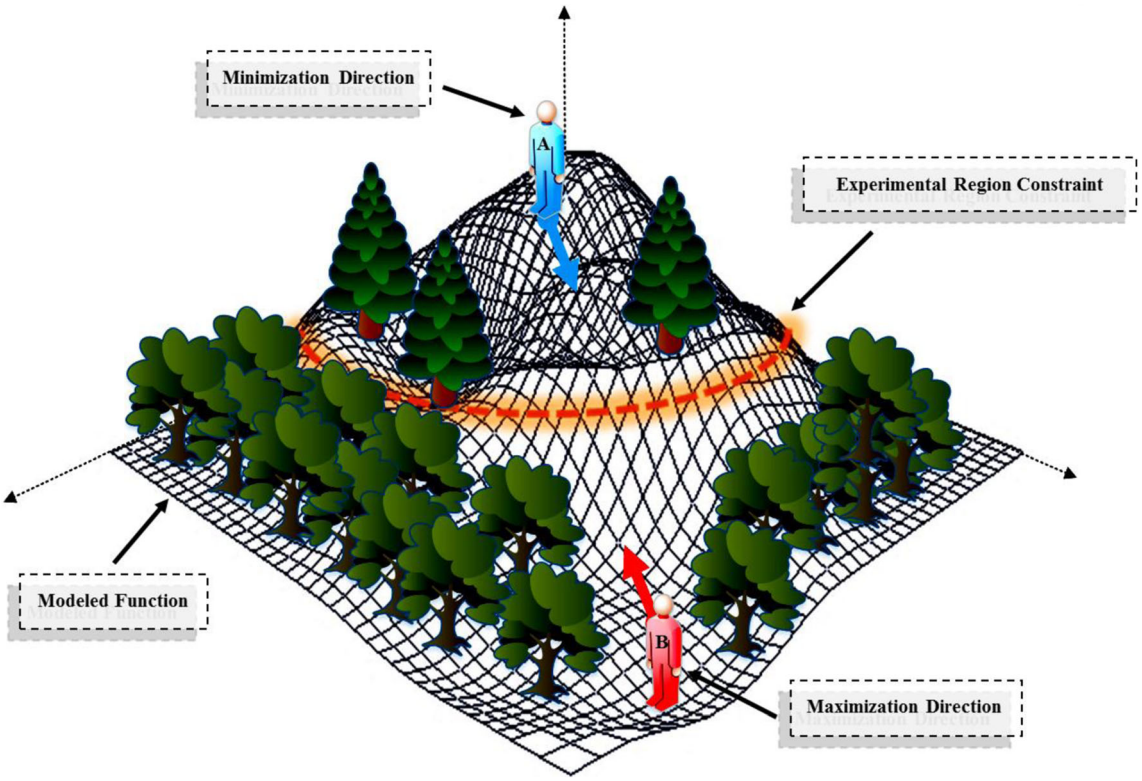

Fig. 9 Mountain analogy: the relationship between the convexity of functions, optimization direction, and experimental region constraint. Source: own authors

$$\text{Find } \boldsymbol{X} = \begin{Bmatrix} x_1 \\ x_2 \\ \vdots \\ x_n \end{Bmatrix} \text{that minimize } f(\boldsymbol{X}) \tag{77}$$

Subjected to :
$g_j(\boldsymbol{X}) \leq 0, j = 1, 2, \ldots, m$
$l_j(\boldsymbol{X}) \leq 0, j = 1, 2, \ldots, p$

where $\boldsymbol{X}$ is the vector of factors of the experimental matrix, $f(\boldsymbol{X})$ is the objective function and $g_j(\boldsymbol{X})$ and $l_j(\boldsymbol{X})$ are inequality and equality constraints, respectively.

In welding processes, for example, it is common to maximize the penetration, the area, and the bead width, and minimize the reinforcement and the convexity index, concomitantly [81]. In machining processes, it is common to minimize the surface roughness, cutting time, total time, and cost, and maximize the material removal rate (MRR) [37]. In these cases, the presence of multiple responses puts the optimization direction as the first obstacle to conventional solutions. According to Rao [64], "one simple way to handle the problem is to construct an overall objective function as a linear combination of the conflicting multiple objective functions." Conventionally, the optimization methods propose the minimization of this global function [82] as shown in Eq. 78 [64]:

$$f(X) = \propto_1 f_1(X) + \propto_2 f_2(X) \tag{78}$$

where $f(\boldsymbol{X})$ is the objective function resulting from the linear combination, $f_1(\boldsymbol{X})$ and $f_2(\boldsymbol{X})$ are two distinct objective functions, and $\propto_1$ and $\propto_2$ are constants denoting the relative importance of the functions $f_1(\boldsymbol{X})$ and $f_2(\boldsymbol{X})$, respectively.

Although this is a satisfactory solution if the models are not correlated, Eq. 78 cannot be used if there is linear dependence between the objective functions, because the global mathematical model may present instability, overfitting and/or imprecision [37, 83]. For this reason, multivariate techniques have been used to obtain linearly independent functions, capable of representing correlated functions without losing their original information [75].

To extract correlation, for instance, Purkayastha et al. [84] applied principal component analysis (PCA) in eight models of a chemical process. Gomes et al. [85] used PCA to analyze four response variables obtained from the turning of AISI 12L14 steel. Routara et al. [86] examined four response variables of a grinding process of the UNS C34000 Brass alloy based on a weighted principal component analysis (WPCA). In all cases, uncorrelated variables were created as linear composites of the original variables [87].

3 Method

This section is intended to describe the proposed method. As mentioned previously, the objectives of this paper are as follows: (1) to provide practical guidelines and core theoretical

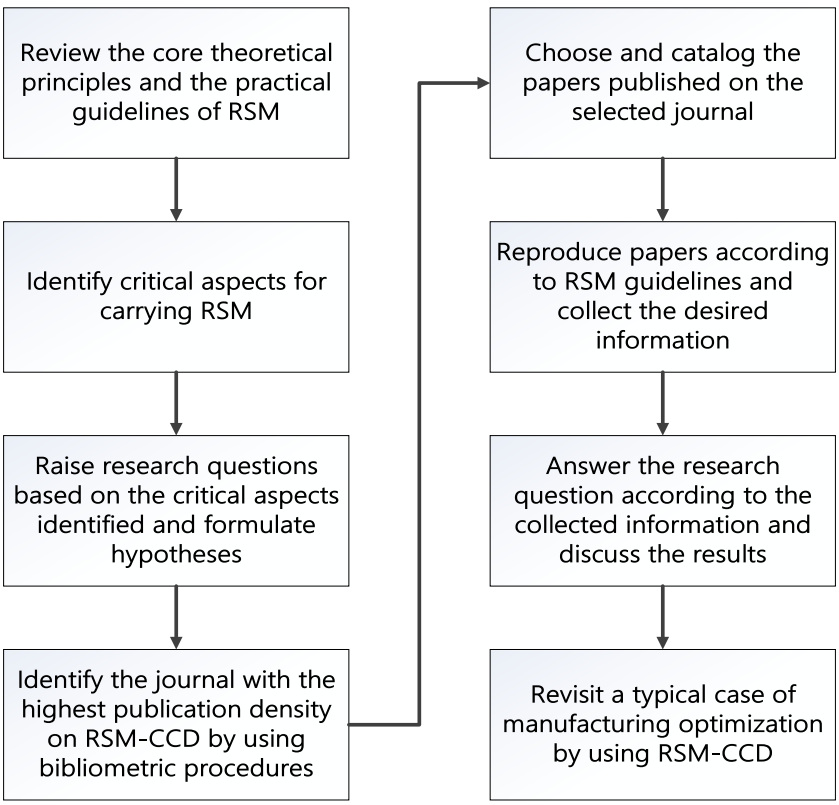

Fig. 10 Flowchart of the proposed method

principles of RSM; (2) to investigate some critical aspects of RSM in the context of experimental studies on advanced manufacturing technology; (3) to identify singularities of the critical aspects studied; and (4) to raise discussions on the usage of RSM, as well as new research opportunities for RSM in manufacturing. For this, the sequence of stages shown in Fig. 10 was adopted.

Initially, a profound literature review on RSM was carried out, addressing its core theoretical principles and practical guidelines, as presented in Section 2. Based on this review, the authors identified critical aspects to be considered in RSM analysis, as detailed in Section 3.1. Then, 13 research questions were raised based on the critical aspects identified and related hypotheses were formulated, which are described in Section 3.2.

To answer these research questions, a bibliometric procedure was adopted, to explore the journals that publish in the studied topic and find papers with RSM-CCD applications, as presented in Section 3.3. Within the journal with the highest publication density on RSM-CCD, papers were chosen and cataloged, as described in Section 3.4.

By applying RSM guidelines to the data available in each of the papers chosen, the research questions were answered and the results discussed, as presented in Section 4. Finally, by considering the practical guidelines, the core theoretical principles and the results of this study, a typical case of manufacturing optimization was revisited by using RSM-CCD, as presented in Section 5.

3.1 Critical aspects

Considering the core theoretical principles and the practical guidelines of RSM discussed in Section 2, eight critical aspects were chosen: three from the intersection between design and analysis of experiments and modeling techniques—number of control parameters, number of center points, and regions of curvature; three from modeling techniques and optimization methods—convexity of the functions, optimization direction, and correlated models; and two from optimization methods and design and analysis of experiments—number of response variables, and experimental region constraint, as pointed in Fig. 11.

The justification for the choice of these eight aspects covers several arguments, which were discussed in more details in Section 2. Based on the existing literature, there are not enough elements to suggest a hierarchy among them, but the relevance of each aspect can be clearly proven in the context of RSM. This fact highlights the importance of present study since it intends to deal with a very little discussed topic, involving the RSM scientific practice and the impacts of some critical aspects on its analysis. Briefly, these critical aspects were chosen for the following reasons:

a) the number of control parameters defines the experimental design structure and the universe of possibilities for improving the process [2, 14, 38];
b) the number of center points influence the prediction variance in the design center and the proper identification of

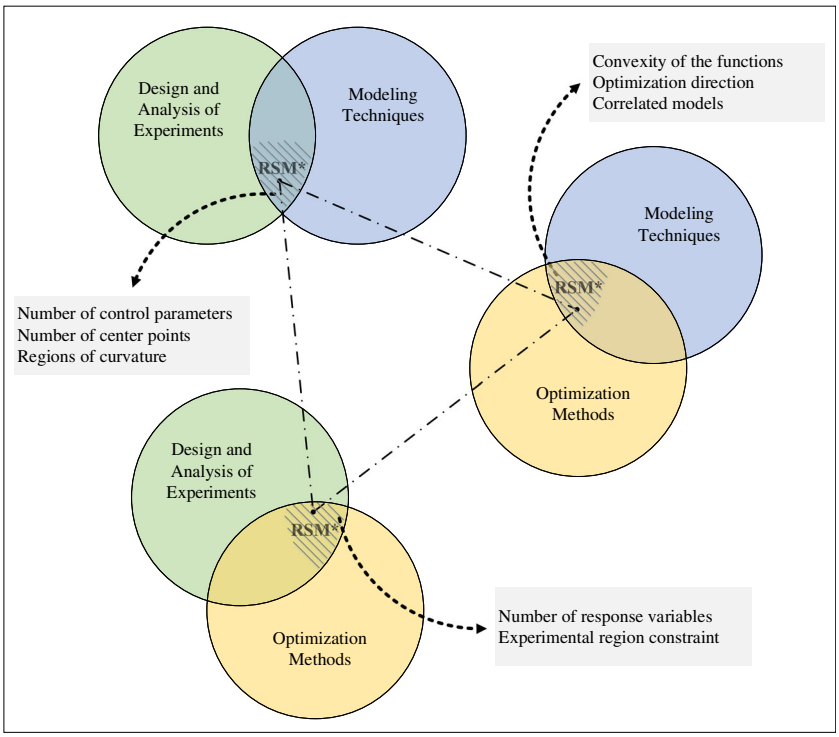

Fig. 11 Detailed view of the intersections between the technical components and some critical aspects of the response surface methodology. Source: own authors

Table 4 Research questions, problem hypotheses, and fundamentals and results sections

Related critical aspect[a]	Research question (RQ)	Hypothesis	Fundamentals	Results
CP	RQ1. What is the typical number of control parameters of manufacturing processes?	H1. Most manufacturing processes are controlled by a maximum of five parameters.	Sections 2.1, 2.2 and 2.3	Section 4.2.1
CP	RQ2. What is the typical number of factorial and axial points used for each quantity of control parameters (k = 2, 3, 4, ...)?	H2. Most studies use the number of factorial and axial points prescribed in the literature according to the number of control parameters.	Sections 2.2 and 2.3	Section 4.2.2
CPT	RQ3. What is the typical number of center points used for each quantity of control parameters (k = 2, 3, 4, ...)?	H3. Most studies use the number of center points prescribed in the literature according to the number of control parameters.	Sections 2.2 and 2.3	Section 4.2.2
RV	RQ4. What is the typical number of response variables measured in manufacturing processes?	H4. Most manufacturing processes measure multiple response variables.	Sections 2.3 and 2.6	"Response Variables" section
CM	RQ5. What is the typical number of pairs of models correlated in manufacturing processes?	H5. Most pairs of models of manufacturing processes have a significant correlation.	Sections 2.3 and 2.6	"Correlated Models" section
CR	RQ6. Is the response surfaces modeling performed only in regions of curvature?	H6. Most studies perform response surfaces modeling only in regions of curvature.	Section 2.2 and 2.4	"Regions of curvature" section
CR CF	RQ7. Is there an association between curvature and convexity?	H7. Convexity is distorted in regions without a significant curvature.	Sections 2.2 and 2.5	"Regions of curvature" section
CF	RQ8. Is there dominance of one of the types of convexity?	H8. Most models are saddle-shaped.	Section 2.5	"Convexity Analysis" section
CF	RQ9. Is there an association between convexity and rotatability?	H9. Modified rotatability distorts model convexity.	Sections 2.2, 2.3 and 2.5	"Convexity Analysis" section
CF	RQ10. Is there an association between convexity and the terms used in the models?	H10. Removing model terms distorts convexity.	Sections 2.2, 2.3, 2.4, and 2.5	"Convexity Analysis" section
OD	RQ11. Is there a preponderance of one of the optimization directions?	H11. Minimization and maximization directions occur with the same frequency in manufacturing studies.	Section 2.5	"Optimization Direction" section
CF OD	RQ12. Is the process optimization direction compatible with the convexity of the models?	H12. In most manufacturing processes it is required to minimize convex models and maximize concave models.	Section 2.5	"Optimization Direction" section
ERC	RQ13. In the optimization stage, is the experimental region constraint used?	H13. When the optimization direction is incompatible with the convexity of the models, most studies employ the experimental region constraint.	Section 2.5	"Optimization Direction" section

[a] In this table, the related critical aspects are the following: number of control parameters (CP), number of center points (CPT), number of response variables (RV), correlated models (CM), regions of curvature (RC), convexity of the functions (CF), optimization direction (OD), and experimental region constraint (ERC)

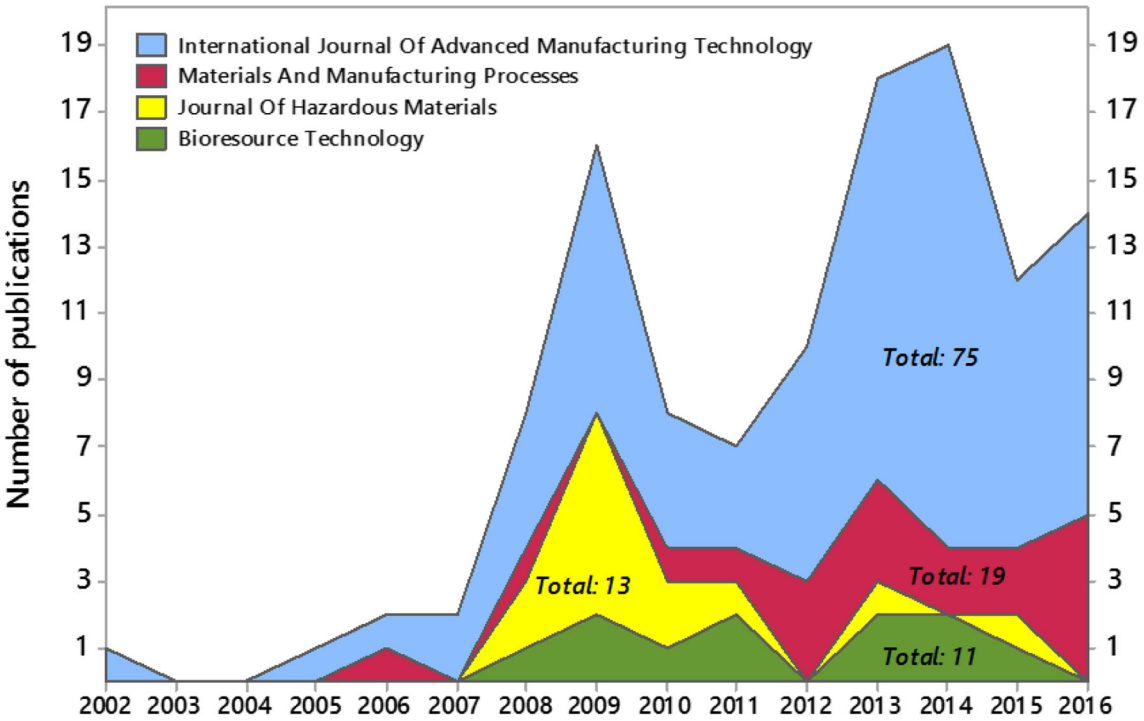

Fig. 12 Number of papers published on response surface methodology and central composite design in the highest density journals by year. Source: own authors

the regions of curvature, where there are great potentials for process improvement [9, 55];

c) the convexity and the optimization direction of a function allow inferring on the importance of the stationary point in the RSM analysis; if they are compatible, the optimal is the stationary point; if not, the optimal is a point in the design boundary [43];

d) correlation between models can cause deformations on the linearly combined global function such as instability, overfitting, and inaccuracy, influencing the way of approaching multiobjective problems [37, 83];

e) the number of response variables defines the dimensions of improvement called critical-to-quality and critical-to-performance characteristics [40, 75];

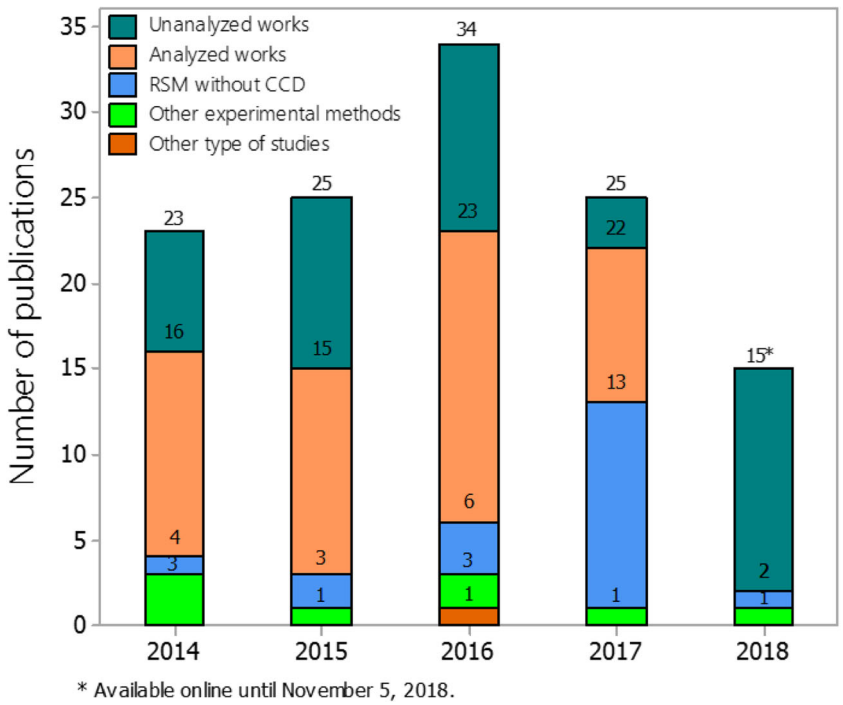

Fig. 13 Classification of the available papers by year according to five categories. Source: own authors

Table 5 Advanced manufacturing technology applications investigated

Process	Paper	Brief description	Paper	Brief description
Machining				
	[93]	Wire electrical discharge machining of Inconel 718	[94]	End milling of Aluminum 6063 with High-speed steel (HSS) end mill cutters
	[95]	Ball-burnishing crossed strategy of a 2017A-T451 aluminum alloy flat surface	[96]	Hard turning of AISI 52100 steel with mixed ceramic tool
	[97]	Grooves into cylindrical shapes of mild steel by wire electrochemical Machining	[98]	Nd:YAG laser drilling on austenitic stainless steel
	[99]	Electrochemical machining of 20MnCr5 alloy steel	[100]	AISI H13 hardened steel turning with PCBN wiper tool
	[78]	Turning of high-strength low-alloy steel AISI 4340 with multilayer coated carbide tools	[101]	High-speed ball-end milling of Inconel-718 thin cantilevers
	[102]	12L14 free machining steel turning process	[103]	Machining fixture layout for end milling operation
	[104]	Orthogonal machining of aluminum alloys Al2024-T3, Al6061-T6 and Al7075-T6	[105]	Wire electric discharge machining of EM 353 case-carburized steel
	[106]	High-speed milling of titanium alloy Ti-6Al-4V with carbide inserts	[107]	Tool design for SS 304 stainless steel magnetic abrasive finishing (MAF)
	[108]	Electrical discharge machining (EDM) of an Al-Mg2Si metal matrix composite (MMC)	[109]	Electrical discharge drilling of aerospace alloys Inconel 718 Brass (D2NiBr) and Ti-6Al-4 V
	[110]	Micro-rotary ultrasonic machining (μ-RUM) of borosilicate glass BK7	[111]	Abrasive waterjet turning (AWJT) of 96% alumina ceramic
	[112]	Drilling of ceramic materials with rotary ultrasonic machining (USM)	[113]	Grinding and polishing process for integrally bladed rotors (IBR) of aero-engine
	[114]	Broaching of heat-resistant steel X12CrMoWVNb N-10-1-1	[115]	Microgrinding of nickel-based single crystal superalloy DD98
Welding				
	[116]	Friction stir welding (FSW) of dissimilar aluminum alloys AA6061 and AA5010	[117]	Friction stir welding (FSW) of dissimilar alloys A5052H32 and high-strength low-alloy (HSLA) steel IRS M-42-97
	[118]	Friction stir welding (FSW) of dissimilar aluminum alloys AA7075-AA6061	[119]	Friction stir welding (FSW) of aluminum alloys AA6061-T6
	[120]	Plasma arc welding (PAW) of High-strength low-alloy (HSLA) steel	[121]	Multi-pass narrow-gap laser welding with filler wire of AH32 high-strength ship steel
	[122]	Tungsten inert gas welding (A-TIG) of duplex stainless steel 2205	[123]	Friction welding (FW) of AISI 1020 and ASTM A536 steel joints
	[124]	Friction stir welding (FSW) of AA7075-T6 aluminum alloys with preheating system	[125]	Gas metal arc (GMA) welding of low carbon steel thick-walled plates.
	[126]	Electron beam welding of ultra-thin FeCo-V magnetic foils	[127]	Bobbin tool friction stir welding (BTFSW) of 2219-T87 aluminum alloy
	[128]	Friction stir spot welding (FSSW) of transformation-induced plasticity (TRIP) steels		
Other				
	[129]	Pre-form design for hydro-forming of 6063-T4 aluminum alloy automotive cross members	[130]	Multi-scan laser forming of AISI 304 stainless steel sheet
	[131]	Plastic injection molding (PIM)	[132]	Plasma spray coating of AISI 316 austenitic stainless steel
	[133]	Fiber volume fraction test of aircraft composite structures	[134]	Diffusion bonding of titanium and AA 7075 aluminum alloy dissimilar joints
	[135]	Tube drawing process used to produce squared sections from round pure copper tubes	[136]	Hydro-bulging of stainless steel sheet SUS304
	[137]	Deep drawing of aluminum alloy AA 5754-O	[138]	Radial knurling connection process of assembled camshaf
	[139]	High-power direct diode laser (HPDDL) cladding of ASTM A36 mild steel	[140]	Hydro-forming of 780 MPa torsion beam

f) the experimental region constraint, based on the control parameters, is a necessary solution to deal with the incompatibility between convexity and optimization direction, ensuring real solutions in the optimization stage [58].

3.2 Questions and hypotheses of the problem

Considering RSM as a structured method (Section 2), this paper aims to address 13 research questions related to the eight critical aspects presented in Section 3.1. Table 4 presents these questions, the associated hypotheses and the sections in which the statistical analyzes are based (fundamentals) and discussed (results).

3.3 Search criteria and papers selection

To properly investigate the critical aspects presented in Section 3.1, some criteria were established to search and choose the papers. Firstly, international journals dealing with RSM and CCD were analyzed; for this initial search, the Scopus academic base was used because it is one of the collections with the highest density of scientific papers [88, 89]. Then, the terms "response surface methodology" and "central composite design" were defined as the search criteria in all fields, and the search was restricted only to papers, disregarding books and other available documents.

From 1971 to 2016, 6740 papers were found in the topic of interest. Adding the term "manufacturing" as the third search criterion; however, 735 papers were found between 1987 and 2016. Based on this analysis, four journals showed a density of publications greater than 10 articles. Among them, the *International Journal of Manufacturing Technology* (IJAMT) presented the largest number of publications, surpassing by 74.42% the sum of papers published in the other journals (*Materials And Manufacturing Processes*, *Journal Of Hazardous Materials e Bioresource Technology*).

Figure 12 provides a comparison between the main journals and allows to verify both the number of papers published in each year and the total volume of publications by journal. From this, it can be observed that the IJAMT has maintained the highest density of publications since the beginning of the period, contributing, fundamentally, to its performance in the overall sum.

By reproducing the above analysis in the Web of Science academic base, similar results were obtained, albeit in smaller proportions. With the terms "response surface methodology" and "central composite design," 4024 publications were observed between the years 1973 and 2016. Adding the term "manufacturing," on the other hand, this number was reduced to only 55 published papers between 1993 and 2016.

As was the case in the Scopus collection, IJAMT also led the volume of publications in the Web of Science with four papers, followed by the *Journal of the Taiwan Institute of Chemical Engineers* with three papers and the *Bioresource Technology, Food Chemistry* and *Journal of Manufacturing Processes* with two papers each. All other sources contributed, in isolation, with only one paper over the period.

Although a consultation on academic bases does not necessarily result in all publications on the subject, most of them tend to demonstrate a proportionality relationship. Thus, the analysis shown in Fig. 12 is not intended to accurately indicate the presence of only 75 articles in the history of IJAMT. However, it seeks to illustrate the prominence of this journal, given the difficulty in gathering all the publications related to a particular object of study in a unique academic collection. This fact is one of the main advantages of bibliometric researches [89].

Considering that IJAMT is the biggest source of papers on the investigated topic, the present study adopted it as the only source for the selection of the papers, allowing a deeper understanding of its applications, as will be presented throughout Section 4. Specifically, the terms "response surface methodology" and "central composite design" were used as search criteria within the IJAMT.

At the same time, it was considered a time window from 2014 to 2017, with the purpose of evaluating the latest applications of RSM with CCD in manufacturing. During this period, 107 papers were obtained, which represent almost half of the total IJAMT publications in the topic, whose entire collection accounts for 219 papers published between 1999 and 2017.

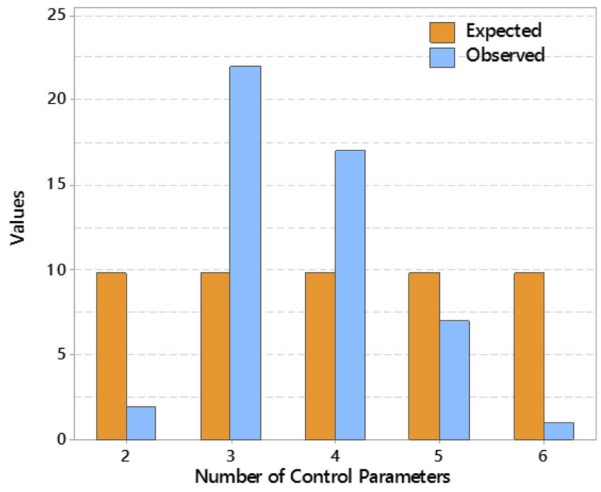

Chi-Square Goodness-of-Fit Test:
Variable – Number of Control Parameters

Category	Observed	Test proportion	Expected	Contribution to Chi-Sq
2	2	0.2	9.8	6.2082
3	22	0.2	9.8	15.1878
4	17	0.2	9.8	5.2898
5	7	0.2	9.8	0.8000
6	1	0.2	9.8	7.9020

N	DF	Chi-Sq	P-value
49	4	35.3878	0.000

Fig. 14 Chi-squared test result for the number of control parameters

3.4 Cataloging and classification of the papers

Once obtained from the IJAMT online base, each paper was cataloged and classified according to five categories, as shown in Fig. 13. Initially, the papers which employed different proposals from those ideally intended were labeled as "other type of studies." Despite this classification, only the paper of Omrani et al. [90] was classified in this category, since the authors carried out a literature review instead of an experimental study.

In the same way, some studies did not use RSM, although they have performed processes optimization. Most of them applied Taguchi's method [16, 91], and one paper used a factorial design to determine the parameters of greatest influence on a drilling process [92]; these cases were classified as "other experimental methods."

Despite this, most of the accessed papers employed the RSM. When not using a CCD, the papers were labeled as "RSM without CCD." On the other hand, when using RSM-CCD (the applications of interest), the papers were divided into "analyzed works" and "unanalyzed works." In all, from 81 publications that effectively applied the RSM with CCD, 49 papers were analyzed, from which 12 were published in 2014, 12 in 2015 and 17 in 2016, maintaining a proportion of analysis around 60% of the available databases in these years. In 2017, 9 papers were analyzed, accounting for 75% of the papers available. In percental terms, 60.49% of the papers published between 2014 and 2017 were analyzed. As shown in Fig. 13, the present study did not analyze the papers published in 2018, considering that the base has not yet been consolidated and proportions cannot be well defined.

Table 6 Test for the proportion of experiments compatible with standard values by type of points and number of control parameters (CP)[a]

Experiments	Standard	2014		2015		2016		2017		Total				
		N	f_o	N	f_o	N	f_o	N	f_o	N	f_o	$P = f_o/N$	95% lower limit	p value
Total														
2^a (CP)	13	0	0	0	0	2	2	0	0	2	2	1.000	0.223607	0.250
3	20	5	3	3	1	6	5	5	3	19	12	0.632	0.418064	0.180
4	31	4	1	4	1	5	2	3	2	16	6	0.375	0.177766	0.895
5	52	2	1	0	0	1	0	0	0	3	1	0.333	0.016952	0.875
								Total		40	21	0.525	0.384797	0.437
Factorial														
2 (CP)	4	0	0	0	0	2	2	0	0	2	2	1.000	0.223607	0.250
3	8	5	5	3	3	6	6	5	5	19	19	1.000	0.854131	0.000
4	16	4	4	4	4	5	5	3	3	16	16	1.000	0.829250	0.000
5	32	2	2	0	0	1	1	0	0	3	3	1.000	0.368403	0.125
									Total	40	40	1.000	0.927842	0.000
Center														
2^b (CP)	5	0	0	0	0	2	2	0	0	2	2	1.000	0.223607	0.250
3	6	5	3	3	1	6	5	5	3	19	12	0.632	0.418064	0.180
4	7	4	1	4	1	5	2	3	2	16	6	0.375	0.177766	0.895
5	10	2	1	0	0	1	0	0	0	3	1	0.333	0.016952	0.875
								Total		40	21	0.525	0.384797	0.437
Axial														
2 (CP)	4	0	0	0	0	2	2	0	0	2	2	1.000	0.223607	0.250
3	6	5	5	3	3	6	6	5	5	19	19	1.000	0.854131	0.000
4	8	4	4	4	4	5	5	3	3	16	16	1.000	0.829250	0.000
5	10	2	2	0	0	1	1	0	0	3	3	1.000	0.368403	0.125
									Total	40	40	1.000	0.927842	0.000

[a] In this analysis, it was considered only the papers based on full factorial designs without replicates, given the comparison with the standard values discussed in Sections 2.2 and 2.3

[b] Due to the lower density of publications, categories with two or five control parameters did not present satisfactory results

Table 7 Median and interquartile range (IQR) for the number of experiments used in the analyzed works by point typology and number of control parameters (CP)

Experiments	Standard	2014			2015			2016			2017			Total		
		N	Median	IQR	*N*	Median	IQR	*N*	Median	IQR	*N*	Median	IQR	*N*	Median	IQR
Total[a]																
2 (CP)	13	0	–	–	0	–	–	2	13	–	0	–	–	2	13	–
3	20	5	20	4.00	3	18	4.00	6	20	0.75	5	20	1.50	19	20	2.00
4	31	4	30	0.75	2	28.5	4.50	5	30	6.00	3	31	1.00	14	30	3.25
5	52	2	51	–	0	–	–	1	43	–	0	–	–	3	50	9.00
Factorial[a]																
2 (CP)	4	0	–	–	0	–	–	2	4	–	0	–	–	2	4	–
3	8	5	8	0.00	3	8	0.00	6	8	0.00	5	8	0.00	19	8	0.00
4	16	4	16	0.00	2	16	0.00	5	16	0.00	3	16	0.00	14	16	0.00
5	32	2	32	–	0	–	–	1	32	–	0	–	–	3	32	0.00
Center																
2 (CP)	5	0	–	–	0	–	–	2	5	–	0	–	–	2	5	–
3	6	5	6	4.00	3	4	4.00	6	6	0.75	5	6	1.50	19	6	2.00
4	7	4	6	0.75	2	4.5	4.50	5	6	6.00	3	7	1.00	14	6	3.25
5	10	2	9	–	0	–	–	1	1	–	0	–	–	3	8	9.00
Axial																
2 (CP)	4	0	–	–	0	–	–	2	4	–	0	–	–	2	4	–
3	6	5	6	0.00	3	6	0.00	6	6	0.00	5	6	0.00	19	6	0.00
4	8	4	8	0.00	2	8	0.00	5	8	0.00	3	8	0.00	14	8	0.00
5	10	2	10	–	0	–	–	1	10	–	0	–	–	3	10	0.00

[a] In this analysis, it was considered only the papers based on full factorial designs without replicates, given the comparison with the standard values discussed in Sections 2.2 and 2.3

4 Results and discussions

4.1 Main observations and papers description

In this study, different applications of RSM on advanced manufacturing technology were analyzed. Although this field involves a large number of industrial processes, the present analysis uses this terminology only to address papers published in the IJAMT. In other words, since this research performs an exploratory study involving critical aspects of RSM, this paper does not cover all existing manufacturing processes.

However, several applications are investigated, including machining, welding, deep drawing, tool design, hydroforming, tube drawing, and other processes. Table 5 presents the main catalytic information of the analyzed papers, associating the type of the manufacturing process, the reference number, and a brief description of the process.

4.2 Data collection and analysis of the critical aspects

In this section, the main contributions of the present study are presented. In order to correctly address the questions and hypotheses of the problem raised in Section 3.2, this section was divided into four parts, through which all the results are discussed.

4.2.1 Control parameters

The number of control parameters used in each of the papers was investigated; firstly, the papers were categorized into the interval from two to six control parameters, which corresponds, respectively, to the minimum and the maximum numbers of control parameters found in the analysis.

Then a chi-square goodness of fit test for the number of control parameters was performed as shown in Fig. 14. As can be seen, a significant difference was observed between the testing categories (p value = 0.000), which means that there are preponderances of certain quantities of control parameters. In specific terms, (a) most manufacturing processes have three or four control parameters, and (b) it is unusual a manufacturing process controlled by two or more than five parameters.

This result confirms the first hypothesis raised in Section 3.2 (H1), which stated that most manufacturing processes have a number of control parameters equal to or less than five. This thesis is also corroborated through a more

Table 8 Hypothesis tests for the number of papers in each category of response variables by manufacturing process

Response variables	2014	2015	2016	2017	Total			
	N1	*N2*	*N3*	*N4*	*N*	*P*	Stat.[a]	*p* value
Total								
Test 1[b]								
1	3	3	9	3	18	0.37	–	–
2	4	2	2	2	10	0.20	–	–
3	3	3	3	2	11	0.22	–	–
4	2	3	1	2	8	0.16	–	–
5	0	0	0	0	0	0.00	–	–
6	0	1	1	0	2	0.04	–	–
Total	*12*	*12*	*16*	*9*	*49*	1.00	26.061	0.000
Test 2[c]								
1	3	3	9	3	18	0.37	–	–
MVR (> 1)[d]	9	9	7	6	31	0.63	–	–
Total	*12*	*12*	*16*	*9*	*49*	1.00	–	0.043
Machining								
Test 1								
1	2	2	3	1	8	0.35	–	–
2	3	2	0	0	5	0.22	–	–
3	2	3	0	2	7	0.30	–	–
4	0	2	0	1	3	0.13	–	–
5	0	0	0	0	0	0.00	–	–
6′	0	0	0	0	0	0.00	–	–
Total	*7*	*9*	*3*	*4*	*23*	1.00	15.348	0.009
Test 2								
1	2	2	3	1	8	0.16	–	–
MRV (> 1)	5	7	0	3	15	0.65	–	–
Total	*7*	*9*	*3*	*4*	*23*	1.00	–	0.105
Welding								
Test 1								
1	0	0	3	1	4	0.29	–	–
2	1	0	0	2	3	0.21	–	–
3	0	0	2	0	2	0.14	–	–
4	2	0	0	1	3	0.21	–	–
5	0	0	0	0	0	0.00	–	–
6	0	1	1	0	2	0.14	–	–
Total	*3*	*1*	*6*	*4*	*14*	*1.00*	4.000	0.549
Test 2								
1	0	0	3	1	4	0.29	–	–
MRV (> 1)	3	1	3	3	10	0.71	–	–
Total	*3*	*1*	*6*	*4*	*14*	*1.00*	–	0.090
Other processes								
Test 1								
1	1	1	3	1	6	0.50	–	–
2	0	0	2	0	2	0.17	–	–
3	1	0	1	0	2	0.17	–	–
4	0	1	1	0	2	0.17	–	–
5	0	0	0	0	0	0.00	–	–
6	0	0	0	0	0	0.00	–	–
Total	***2***	***2***	*7*	***1***	***12***	1.00	12.000	0.035
Test 2								
1	0	0	3	1	4	0.50	–	–
MRV (> 1)	3	1	3	3	10	0.50	–	–
Total	***2***	***2***	*7*	***1***	***12***	1.00	–	0.927

[a] Test statistic: test 1, χ^2; test 2, Z

[b] Chi-square goodness of fit test

[c] Tests for one proportion

[d] *MRV*, multiple response variables

detailed analysis, since, although Aggarwal et al. (2015) were the only to use six control parameters; the authors identified that only four were significant, further highlighting the central categories of Fig. 14.

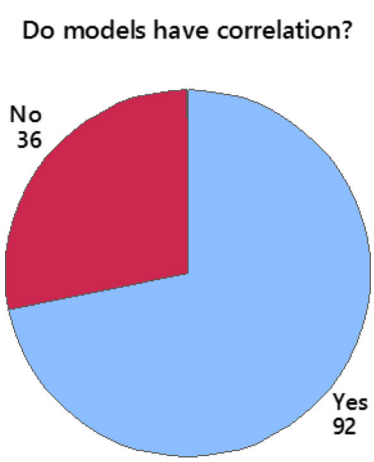

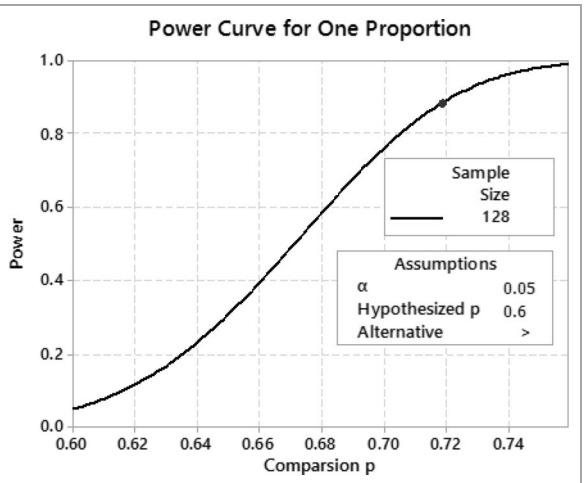

Test and CI for one proportion:
Test for p = 0.60 *vs* p > 0.60

Sample	X	N	Sample p	Lower Limit 95%
1	92	128	0.718750	0.646063
P-value: 0.000				

Power and Sample Size:
tested p = 0.60 (*vs* > 0.60)

Sample	Comparison p	Size	Power
1	0.718750	128	0.884134

Fig. 15 One proportion test result for correlated models

4.2.2 Number of experiments and the use of factorial, axial, and center points

To investigate the number of experimental points conventionally employed in RSM-CCD analysis, the papers were stratified by year and number of control parameters, as shown in Table 6. According to the formulations set out in Sections 2.2 and 2.3, Table 6 provides the standard number of experiments calculated for each of the categories of points and number of control parameters, and the frequency of agreement between the papers and the standard (*fo*). In an attempt to obtain more consistent conclusions, the statistical analyzes were performed considering the total of publications and only those studies that used FFD without replicates were considered, resulting in 40 papers for the investigation of experimental points.

Based on the test for one proportion, there is sufficient evidence to conclude that, in manufacturing processes, the factorial and axial points are used according to the standard values, independently of the number of control parameters, which confirms the second hypothesis raised in Section 3.2 (H2). This fact can be verified by comparing the observed frequency with the number of papers analyzed in each category, resulting in *p* values less than 5% for three and four control parameters (Table 6). Moreover, since in all categories there was full correspondence with values proposed in the literature, it is expected to obtain the same statistical demonstration for a larger amount of papers in the categories with two and five control parameters.

Table 7 reinforces these conclusions in terms of median and interquartile range (IQR), revealing that every component of variation in the total number of experiments comes from the use of center points (IQR not equal to 0.00). For instance, when evaluating papers with three control parameters, it was observed a median and an IQR of six and two center points, respectively. Similarly, for four parameters, it was observed a median of six and an IQR of 3.25 center points.

In the case of center points, however, there is insufficient evidence (*p* value = 0.437) to guarantee that most of the papers use the standard number of center points, although this occurs for factorial and axial points. Thus, the third hypothesis raised in Section 3 (H3) is rejected, that is, at the level of 95% confidence, it is shown that the percentage of publications that preserve the standard number of center points does not exceed 50%.

4.2.3 Response variables and correlated models

From the 49 papers, 123 response variables were obtained, which rise from a huge set of measurable characteristics of manufacturing processes. In machining processes, for example, surface roughness [106], cutting forces [96], MRR [108], chip thickness [104], hole taper [98], cantilever deflection [101], maximum deformation [103] were found.

In welding processes, for instance, depth of penetration [122], fracture stress [126], microhardness [124],

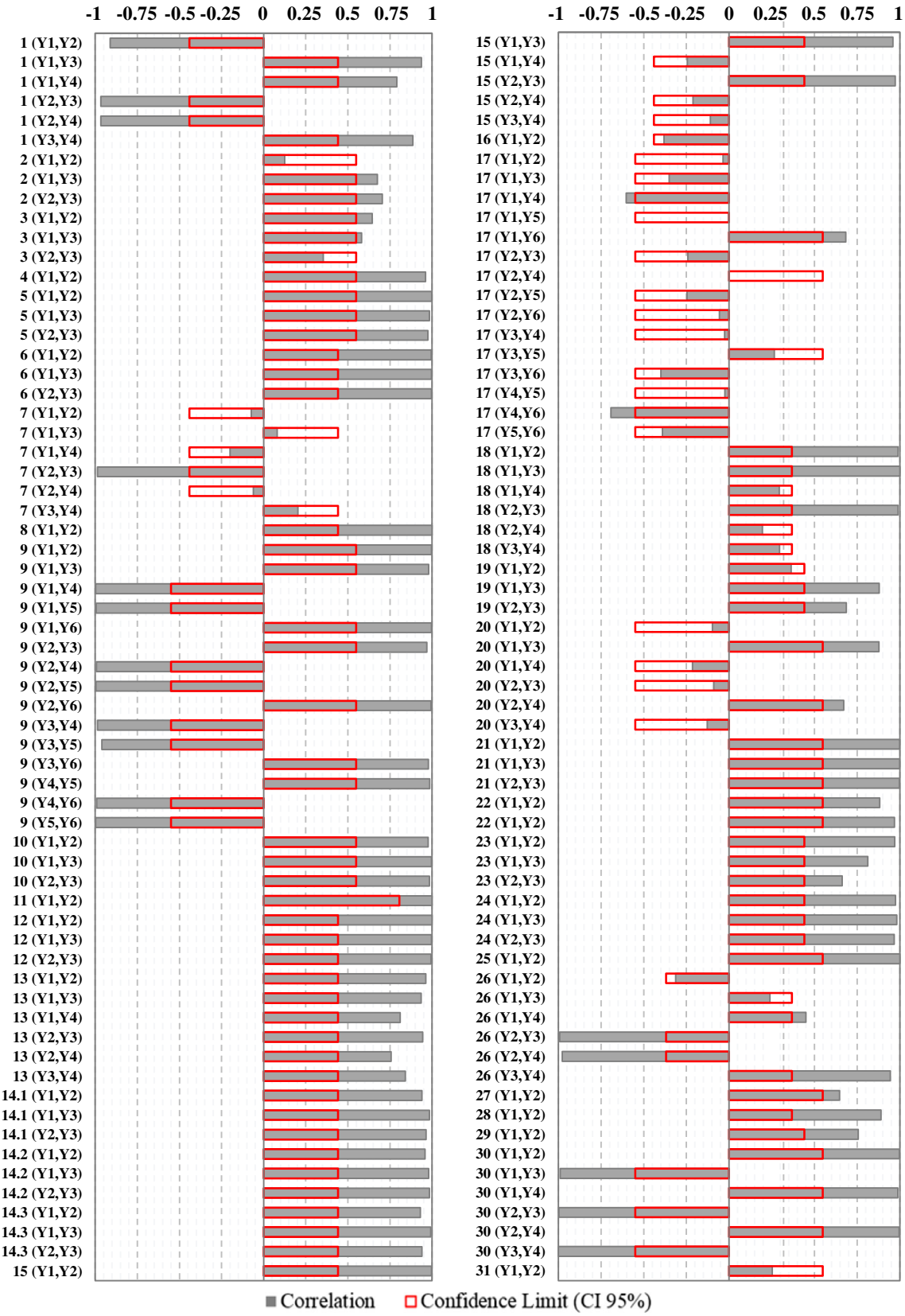

Fig. 16 Correlations observed between response surface models

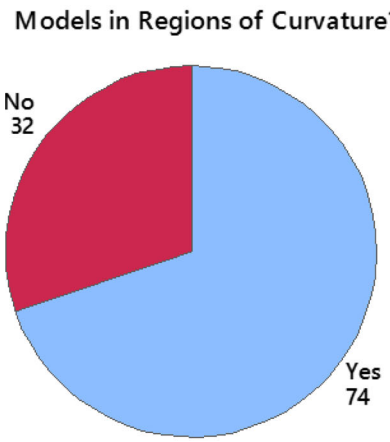

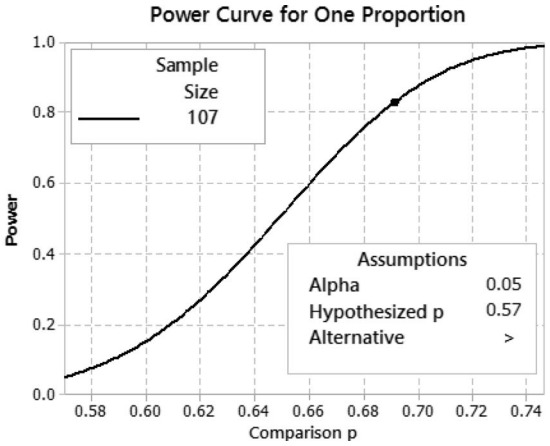

Test and CI for one proportion:
Test for p = 0.57 *vs* p > 0.57

Sample	X	N	Sample p	Lower Limit 95%
1	74	107	0.691589	0.610059

P-value: 0.006

Power and Sample Size:
tested p = 0.57 (*vs* > 0.57)

Sample	Comparison p	Size	Power
1	0.691589	107	0.831492

Fig. 17 One proportion test result for the models fitted in regions of curvature

thermomechanically affected zone [128], tensile strength [116], and impact toughness [119] were found.

In the other processes, the measured characteristics were even more diverse, ranging from pressure in a hydro-bulging process [136] to oxidant percent in a plasma spray coating process [132].

Response variables To test the fourth hypothesis raised in Section 3.2 (H4), the investigated papers were classified according to the number of response variables. Considering the minimum and maximum numbers of response variables, six categories were established, as shown in Table 8. The papers were also organized according to the main manufacturing processes identified: manufacturing (23 papers) and welding processes (14 papers). The other processes, which account for 12 of the 49 papers, were grouped into a separate category.

Table 8 also shows the chi-square goodness of fit tests and the tests for proportions of response variables in each category. To determine the most used number of variables, four tests, identified as test 1 (chi-squared tests), were performed. To verify if most of the papers measure multiple response variables, four other tests, indicated by test 2 (tests for proportions), were carried out. In all, eight tests were performed, considering the types of manufacturing processes and the total number of papers. With the application of test 1, it is observed, at a 95% level of confidence, that there is a significant difference between the numbers of variables measured in the papers investigated. This is demonstrated by a chi-squared statistic of 26.061 and a p value of 0.000. In specific terms, this is due to machining processes (p value = 0.009) and the other manufacturing processes (χ^2 = 12.000 and p value = 0.035), in which the same conclusions are observed.

In an overall analysis, therefore, it can be said that the category of papers that only measure one response variable represents, on an individual basis, most of the investigated papers. However, in aggregate terms, there is a significant preponderance of multiple response variables, as demonstrated with test 2 (Table 8). In other words, at a 95% level, there is enough evidence to infer that the proportion of papers that measure multiple response variables is more than 50% of the total of papers (63.27% in punctual terms). This result confirms the fourth hypothesis raised in Section 3.2 (H4) and preliminarily indicates the relevance of multivariate methods for manufacturing studies.

Correlated models In "Response Variables" section, the usage of multiple response variables has been shown to be recurrent in the investigations, confirming one of the hypotheses raised in Section 3.2. As mentioned previously, this result advocates the importance of multivariate techniques. However, in isolation, it does little to counter traditional multiobjective optimization, in which a single global function is minimized in the presence of convenient constraints, as discussed in Section 2.5.

In this sense, considering that this global function presupposes linear independence between the original functions, a

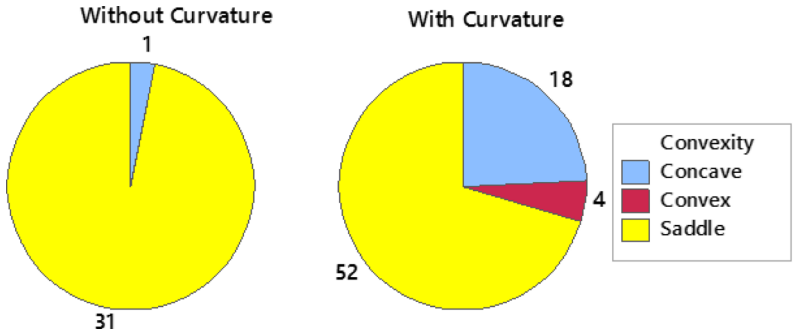

Tabulated Statistics: Curvature; Convexity

Rows: Curvature Columns: Convexity

	Concave	Convex	Saddle	All
Without curvature	1[a]	0	31	32
	5.736	1.208	25.057	
	3.910	1.208	1.410	
With curvature	18	4	52	74
	13.264	2.792	57.943	
	1.691	0.522	0.610	
All	19	4	83	106[b]

Cell Contents: Count
Expected count
Contribution to Chi-square

Chi-Square Pearson = 9.350; DF = 2; P-Value = 0.009

Likelihood Ratio Chi-Square = 12.314; DF = 2; P-Value = 0.002

Fig. 18 Chi-squared test result for the association between rotatability and convexity

fifth hypothesis was raised (H5), inferring on the fraction of models that present significant correlation. Then, to test H5, the Pearson correlation analyses were performed for each pair of models by paper.

As a result, 128 pairs of models were evaluated, of which 92 revealed significant correlation; from this, a test for one proportion was performed. With 95% confidence and power of 88.41%, it was verified that more than 60% of the pairs of models are correlated (p value = 0.000), reaching, in specific terms, 71.88% of the sample. Figure 15 details these results, confirming the fifth hypothesis raised in Section 3 (H5).

The overall result of the correlation analysis is shown in Fig. 16, where the magnitude of the correlation between the pairs and their significance levels are presented by investigated paper. To illustrate this result, some examples can be cited, since most of the investigated models exhibited a significant correlation. For instance, the tensile strength was highly correlated to hardness in the works of Ahmadnia et al. [116] and Safeen et al. [119], which investigated friction stir welding of aluminum alloys. This relationship was also obtained in the work of Pakseresht et al. [132], who investigated a plasma spray coating process.

Similarly, the surface roughness in any region of small beams presented a significant correlation with the cantilever deflection when subjected to the drilling process carried by Sonawane and Joshi [101]. In the work of Amdouni et al. [95], however, the average surface roughness was correlated to nano-hardness, measured in the ball-burnishing process of aluminum alloy 2017A-T451.

In the turning process analyzed by Daoud et al. [104], the cutting force showed high correlation with the chip thickness for the three investigated aluminum alloys (Al2024-T3, ρ =

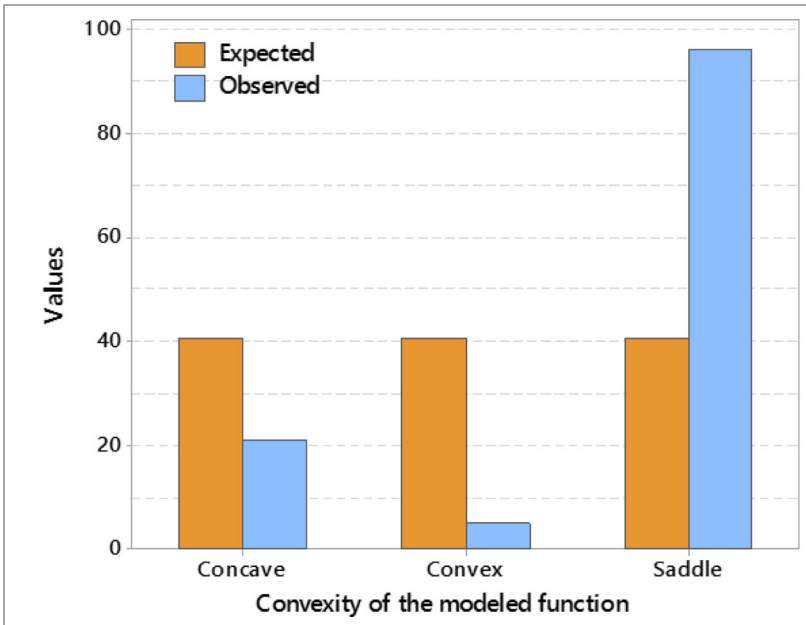

Chi-Square Goodness of Fit Test:
Variable – Number of Models

Category	Observed	Test proportion	Expected	Contribution to Chi-Sq
Concave	21	0.333333	40.6667	9.5109
Convex	5	0.333333	40.6667	31.2814
Saddle	96	0.333333	40.6667	75.2896

N	DF	Chi-Sq	P-value
122	2	116.082	0.000

Fig. 19 Chi-square test result for the number of models in each category of convexity

0.985; Al6061-T6, $\rho = 0.980$; Al7075-T6, $\rho = 0.992$). In the study of Hosseinzadeh and Mouziraji [130], however, the cutting force showed no significant correlation with any of the models of the tube drawing process.

A similar case occurred between the works of Yilmaz et al. [109] and Hourmand et al. [108]. On the one hand, the work of Yilmaz et al. [109] revealed a high correlation between material removal rate (MRR) and electrode wear rate (EWR), when investigating the electrical discharge drilling of aerosol alloys IN 718 (D2NiBr). On the other hand, however, the work of Hourmand et al. [108] showed a non-significant correlation between the same responses when studying an electrical discharge machining (EDM) of Al-Mg2Si metal matrix composite (MMC).

4.2.4 Curvature, convexity, and optimization direction

In the last sections, conclusions were drawn about the typical number of control parameters and response variables and the magnitude of correlations between models. The present section explores some of the statistical assumptions of the RSM raised in Sections 2.2 and 2.5. For this, 123 models were investigated regarding curvature, convexity, and optimization direction.

Regions of curvature In some particular cases, it was not possible to determine the existence of curvature in the experimental regions. This was due to the use of only one center point [135, 137, 139], to the obtaining of identical responses at the design center [102, 131], and to the hiding of data in some of the investigate studies [111, 114]. Then, disregarding 16 response variables, curvature tests were performed for 107 models.

Based on the test for one proportion provided by Fig. 17, it can be demonstrated, with 95% confidence and power of approximately 83.15%, that over 57% of the manufacturing models are fitted in regions of curvature (p value = 0.007), representing 69.16% of the sample.

Although these results prove, statistically, the sixth hypothesis raised in Section 3 (H6), the obtained results indicate that

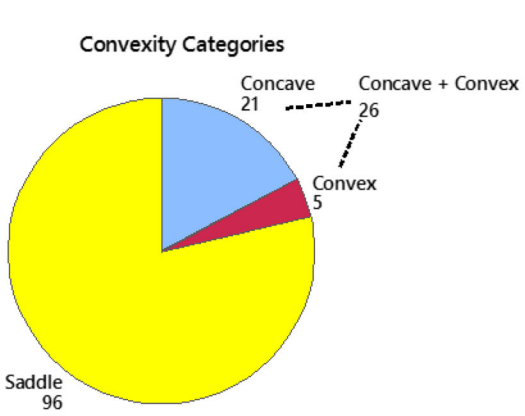

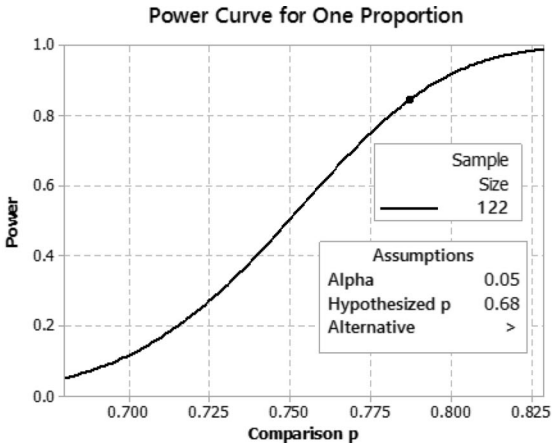

Test and CI for one proportion:
Test for p = 0.68 *vs* p > 0.68

Sample	X	N	Sample p	Lower Limit 95%
1	74	122	0.786885	0.716819
P-value: 0.006				

Sample	Comparison p	Size	Power
1	0.786885	122	0.833574

Fig. 20 One proportion test result for saddle-shaped models

there is still a large number of models fitted in regions without curvature. In other words, a little more than 30% of the functions are fitted in flat regions, where, according to the literature, the second-order models are not appropriate [2, 9, 38].

By investigating these functions in detail, it can be observed that almost all the models fitted in regions without curvature are saddle-shaped. That is, with the exception of the paper of Zhao et al. [127], which fitted a concave function, 31 of the 32 models of this category (96.86%) are saddle-shaped.

Furthermore, the model of Zhao et al. [127] belongs to a special class of convexity called rising ridge, in which the stationary point is not close to the design center [9]. That is, although the function has a maximum point, it does not reveal itself at all as a concave function, as formally defined in Section 2.3. It is suspected, therefore, that the fitting of models in regions without curvature presupposes the obtaining of some distortion, characterized, in general, by saddles.

To test this hypothesis, an association analysis between curvature and convexity was performed, as shown in Fig. 18. With the application of the chi-squared Pearson and likelihood ratio chi-squared tests, a significant association between curvature and convexity can be proven (the chi-squared Pearson p value = 0.009, likelihood ratio chi-squared p value = 0.002).

Likewise, when performing a test for one proportion, it was verified, with power of 83.15% and significance level of 5%, that the proportion of saddled-shaped functions corresponds to more than 83% of the models estimated in flat regions (p value = 0.019), confirming the seventh hypothesis raised in Section 3.2 (H7).

This conclusion is compatible with the core principles set forth in the literature since the non-existence of curvature presupposes only two options. On one hand, the curve region should be explored by applying methods of identification of the stationary point, such as SAM [2]. On the other, a first-order model should be fitted [9], as was the case in [78].

Convexity analysis In the convexity analyzes, 122 models were investigated, since one of the 123 models had to be excluded because the authors fitted a first-order model [78], as mentioned in "Regions of curvature" section. Three studies presented inconsistent models, by removing the main factors and preserving their interactions or quadratic terms [101, 119, 129]. In these cases, the hierarchy principle was not respected, since, in the absence of the main factors, all associated terms should be equally removed [9].

As a solution, for these papers, full quadratic models were adopted, in order to support accurate convexity analyzes. For the works of Ayyappan and Sivakumar [99], Huang et al. [137], Pakseresht et al. [132] and Yilmaz et al. [109], in which the models for the response variables were not provided, this procedure was also adopted. Then based on the original data

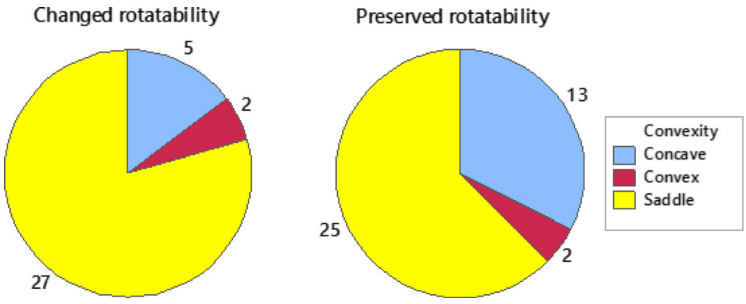

Tabulated Statistics: Rotatability; Convexity

Rows: Preserved Rotatability? Columns: Convexity

	Concave	Convex	Saddle	All
No	5	2	27	34
	8.270	1.838	23.892	
	1.293	0.014	0.404	
Yes	13	2	25	40
	9.730	2.162	28.108	
	1.099	0.012	0.343	
All	18	4	52	74

Cell Contents: Count
Expected count
Contribution to Chi-square

Chi-Square Pearson = 3.167; GL = 2; P-Value = 0.205
Likelihood Ratio Chi-Square = 3.273; GL = 2; P-Value = 0.195

Fig. 21 Chi-squared test result for the association between rotatability and convexity

set presented by the authors, for each response variable, a model was fitted.

For the study of Lotfi and Nourouzi [124], who added interactions between main factors and quadratic terms in the model, only the conventional terms were adopted for convexity analysis, so that there was no harm to the present study.

As can be seen in Fig. 19, an expressive portion of the analyzed models revealed saddle shape; in absolute terms, this represents 96 models out of 122. With the application of a chi-square goodness of fit test (also shown in Fig. 19), it can be demonstrated, with 95% confidence, that the proportion of saddle-shaped models exceeds the proportion of concave and convex functions individually; however, the convex functions were very uncommon, contributing with only five models.

When considering both the number of concave and convex models, this thesis is again confirmed. As shown in Fig. 20, by applying a test for one proportion, it is proven, at a 5% level and power of 0.8336, that the occurrence of saddle-shaped functions exceeds 68% of the models, reaching, in relative terms, 78.69% of the sample, thus confirming the eighth hypothesis raised in Section 3 (H8).

A credible explanation for this expressive occurrence of saddles in manufacturing processes was presented in "Regions of curvature" section when it was found that 31 of the 92 saddle-shaped models were fitted in flat regions. However, even in regions with significant curvature, saddle-shaped models were dominant.

Considering these results, the present paper has raised some related hypothesis. Firstly, it was hypothesized that changes in axial points could lead to distortions in the estimated models, since they allow more adequate estimates of the coefficients of the quadratic terms, as described in Section 2.2.

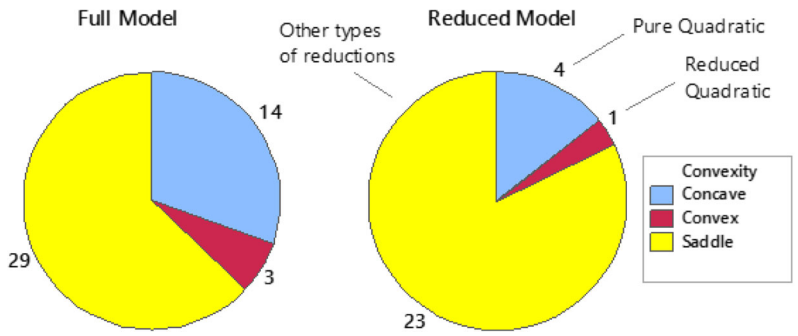

Tabulated Statistics: Model type; Convexity

Rows: Model Columns: Convexity

	Concave	Convex	Saddle	All
Full Model	14	3	29	46
	11.189	2.486	32.324	
	0.7061	0.1061	0.3419	
Reduced Model	4	1	23	28
	6.811	1,514	19.676	
	1.1600	0.1742	0.5617	
All	18	4	52	74

Cell Contents: Count
Expected count
Contribution to Chi-square

Chi-Square Pearson = 3.050; GL = 2; P-Value = 0.218

Likelihood Ratio Chi-Square = 3.202; GL = 2; P-Value = 0.202

Fig. 22 Chi-squared test result for the association between model type and convexity

Then, to test this hypothesis (H9), the models were investigated according to the presence or the absence of rotatability. For this, the convexity analysis was performed distinguishing studies that altered the standard distance to the axial points (absence of rotatability) of those who preserved it (presence of rotatability).

As presented in Fig. 21, by performing a new test of association, it is demonstrated, at a 5% level, that there is insufficient evidence to suppose a relationship between convexity and rotatability (in any of the tests, the *p*-values were higher than 5%; the chi-squared Pearson, *p* value = 0.205; likelihood ratio chi-squared, *p* value = 0.195). That is, the expressive occurrence of saddles in the investigated models does not depend on the design rotatability, which refutes the ninth hypothesis raised in Section 3.2 (H9).

In a way, this finding reduces the impacts of the usage of face-centered central composite design (FCCD) or selective modifications in the axial points, as it was found in the paper of Hassan et al. [133], for example. From another perspective, however, this conclusion widens the horizons of analysis, providing indications that this may be due to the exclusion of coefficients rather than less precise estimates, as initially proposed.

Despite this hypothesis (H10), no evidence was found that the terms used in the models have a real influence on the occurrence of saddles. As shown in Fig. 22, with 95% confidence, the null hypothesis cannot be refuted, indicating there

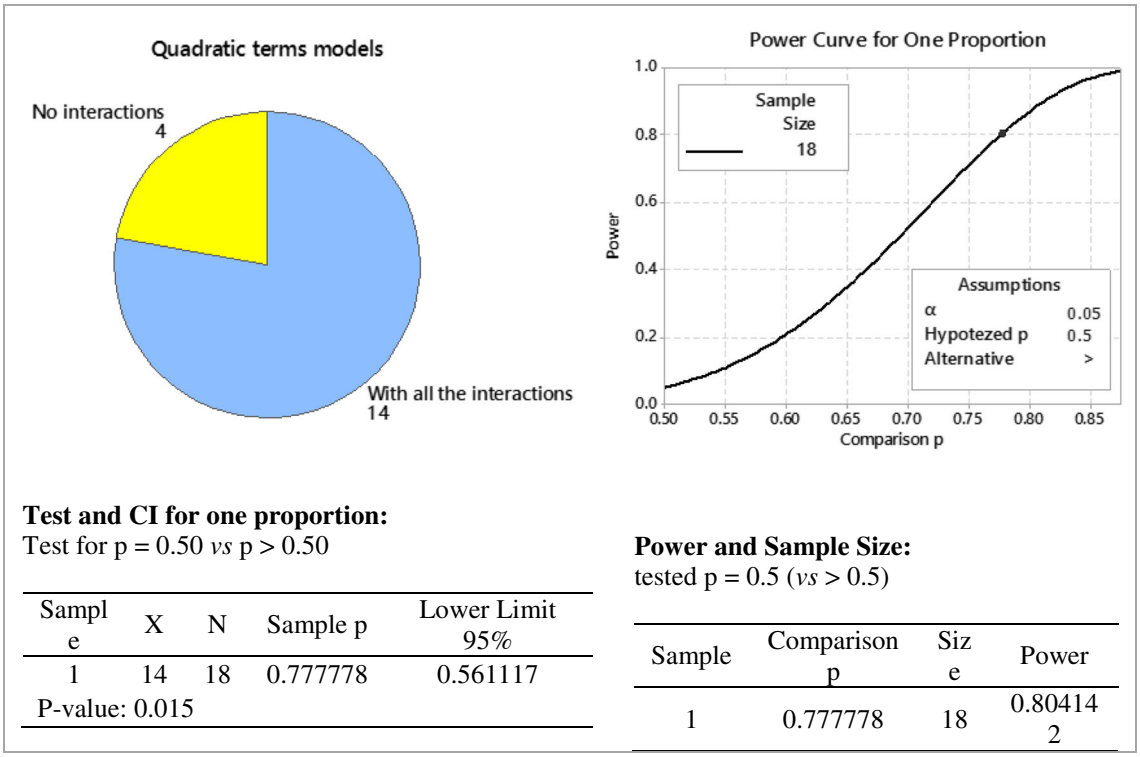

Test and CI for one proportion:
Test for p = 0.50 *vs* p > 0.50

Sample	X	N	Sample p	Lower Limit 95%
1	14	18	0.777778	0.561117
P-value: 0.015				

Power and Sample Size:
tested p = 0.5 (*vs* > 0.5)

Sample	Comparison p	Size	Power
1	0.777778	18	0.804142

Fig. 23 One proportion test result for the concave functions fitted to full quadratic models

is no significant association between model type and convexity.

On the other hand, all the 18 concave functions, fitted in regions with significant curvature, were modeled by full quadratic models (with or without interactions). Then, although it was found no explanation for the occurrence of saddles according to convexity, there seems to be some relationship between the fit of concave functions and the use of models containing all quadratic terms.

As can be seen in the analysis provided in Figs. 23 and 14 of the 18 concave, models were obtained by preserving all terms. With the application of a likelihood ratio chi-squared test for one proportion, it was observed that, at a 5% significance level and power of 80.41%, more than 50% of the concave functions come from full quadratic models, which confirms the tenth hypothesis raised in Section 3.2 (H10).

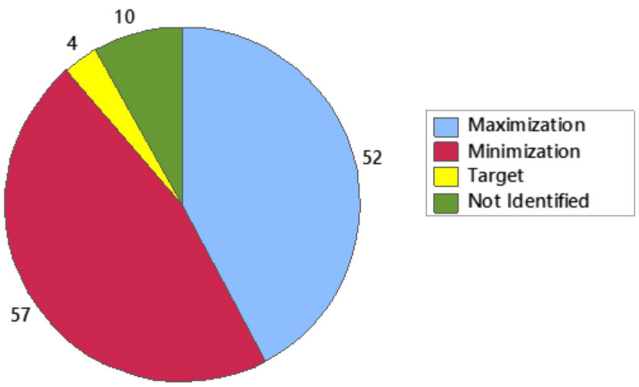

Fig. 24 Distribution of the models according to the optimization direction

Optimization direction In this section, all analyses involving the optimization directions of the investigated functions are discussed. For this, each of the 123 models was classified according to four categories, namely minimization, maximization, target, and not identified, which refers to the papers that did not present the optimization direction, resulting in some exclusions.

These exclusions account for the 10 models in the following 7 papers: [97] – 01, [98] – 02, [125] – 01, [129] – 01, [137] – 02, [136] – 02, and [140] – 01. The other 113 models were considered in the analysis, as shown in Fig. 24, which provides an overview of the models according to the optimization direction, revealing the small number of models to which target values were assigned.

In these cases, the authors did not propose classical optimization directions but optimized some functions toward specific values. Hashmi et al. [106], for instance, set a target value for surface roughness, rather than minimizing it, like most of the evaluated studies [78, 115]. Similarly, Hassan et al. [133] set a target value for the fiber volume fraction of aircraft composite structures.

As evidenced by Fig. 25, with the application of a chi-square goodness of fit test, at a 5% level, no significant difference was found between the numbers of maximized and minimized models, proving that, in the manufacturing processes,

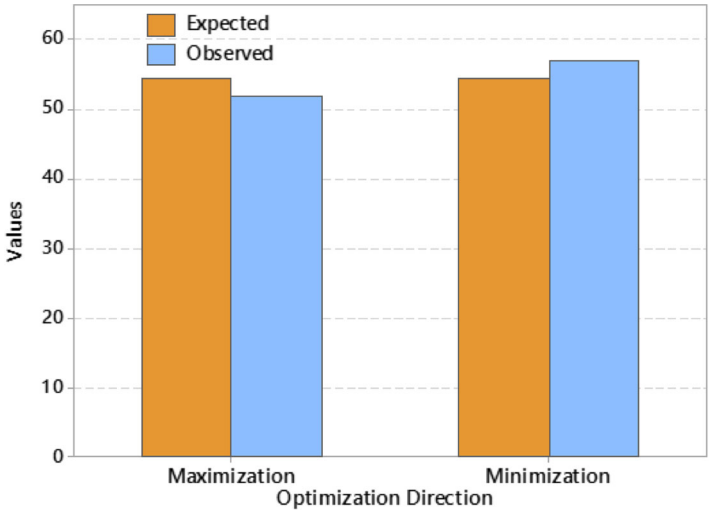

Chi-Square Goodness of Fit Test:
Variable – Number of Models

Category	Observed	Test proportion	Expected	Contribution to Chi-Sq
Maximization	52	0.5000	54.5000	0.114679
Minimization	57	0.5000	54.5000	0.114679

N	DF	Chi-Sq	P-value
109	1	0.229358	0.632

Fig. 25 Chi-squared test result for the number of models in each category of convexity

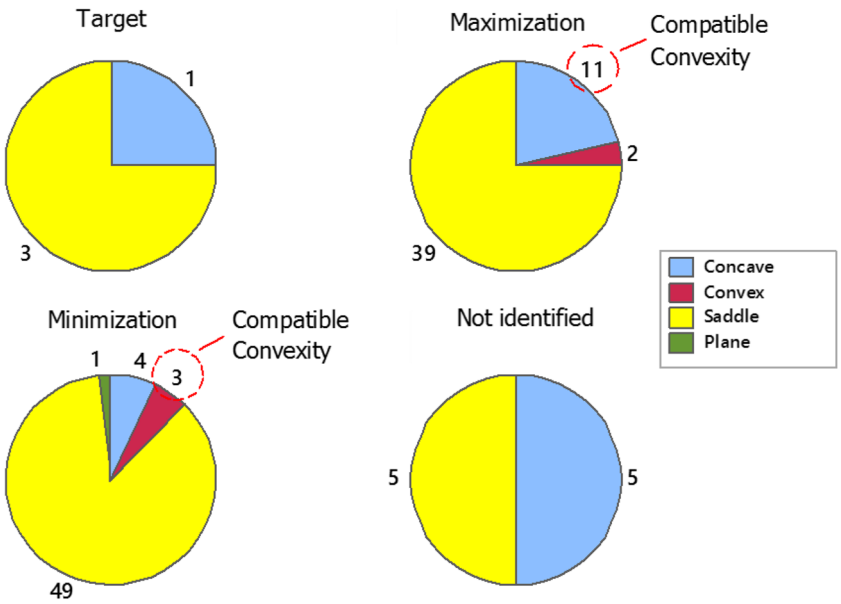

Fig. 26 Convexity of the studied models according to the optimization direction

Table 9 Levels of the selected parameters. Adapted from Campos [141] and Rocha et al. [100]

Coded level	Control parameters		
	Cutting speed *Vc* (m/min)	Feed rate *f* (mm/rev)	Depth of cut *d* (mm)
1.682	267.62	0.26	0.39
1.000	225.00	0.22	0.33
0.000	162.50	0.16	0.24
− 1.000	100.00	0.10	0.24
− 1.682	57.38	0.06	0.09

there is no dominance of one of the optimization directions, which confirms the eleventh hypothesis raised in Section 3.2 (H11).

In a compatibility analysis, the optimization direction and the convexity of the observed models were evaluated mutually. As can be seen in Fig. 26, only 14 models have convexity compatible with the optimization direction. By applying the test for one proportion, it is verified, with 95% confidence and 97.17% power, that more than 78% of the models in manufacturing processes have convexity incompatible with the desired optimization direction (p value = 0.007), reaching, in relative terms, 87.61% of the sample and, therefore, refuting the twelfth hypothesis raised in Section 3 (H12).

In spite of this, it was observed that only one paper makes clear the usage of the experimental region constraint for optimization [102]. This finding refutes the thirteenth hypothesis (H13) and provides insights for a relevant discussion, introduced in Section 2.4. That is, since most models do not have compatibility between convexity and optimization direction, most of the papers should use the experimental region constraint for process optimization.

Table 10 Factorial process investigated. Adapted from Campos [141] and Rocha et al. [100]

N	Levels of the parameters					
	Cutting speed		Feed rate		Depth of cut	
	Vc		*F*		*D*	
	(m/min)		(mm/rev)		(mm)	
	Cod.	Decod.	Cod.	Decod.	Cod.	Decod.
Factorial points						
1	− 1.00	100	− 1.00	0.10	− 1.00	0.15
2	1.00	225	− 1.00	0.10	− 1.00	0.15
3	− 1.00	100	1.00	0.22	− 1.00	0.15
4	1.00	225	1.00	0.22	− 1.00	0.15
5	− 1.00	100	− 1.00	0.10	1.00	0.33
6	1.00	225	− 1.00	0.10	1.00	0.33
7	− 1.00	100	1.00	0.22	1.00	0.33
8	1.00	225	1.00	0.22	1.00	0.33
Center points						
9	0.00	162.5	0.00	0.16	0.00	0.24
10	0.00	162.5	0.00	0.16	0.00	0.24
11	0.00	162.5	0.00	0.16	0.00	0.24
12	0.00	162.5	0.00	0.16	0.00	0.24
13	0.00	162.5	0.00	0.16	0.00	0.24

5 Hardened steel turning with PCBN wiper tool revisited

This section revisits a typical case of manufacturing process optimization by using RSM, considering the precepts discussed throughout this work. Using data available in one of the applications of Section 4.1, RSM was reproduced according to the roadmap of Fig. 2, presented in Section 2.1. In each of the steps, the critical aspects raised in Section 2, under a theoretical approach, and investigated in Section 4, under empirical analysis were discussed.

For this discussion, Rocha et al. [100] were chosen among the investigated papers for the following reasons: (a) the authors studied a manufacturing process controlled by three parameters, which, as demonstrated in Section 4.2.1, consists of the most common quantity of parameters in manufacturing processes; (b) the number of center points has been reduced, which, as demonstrated in Section 4.2.2, is a common practice; (c) the authors measured multiple response variables (three), which, as presented in "Response Variables" section, recurrently occurs; (d) significant correlation was observed between some of the estimated models, which, as shown in "Correlated Models" section, frequently occurs in these types of studies; (e) all the models were estimated in regions with curvature, which normally occurs, as shown in "Regions of curvature" section (69.16% of models are estimated in regions with curvature and 30.89% are estimated in regions with no curvature); (f) all the models presented a saddle format, which typically occurs with manufacturing processes response surface models, as presented in "Convexity Analysis" section; (g) the authors proposed both minimization and maximization optimization directions, which indeed occur with identical proportions in the investigated literature (50% max and 50% min), as demonstrated in "Optimization Direction" section; and (h) because of the findings of items 6 and 7, all models present a conflict between convexity and optimization direction, which, as proved in "Optimization Direction" section, occurs in more than 75% of cases.

Step 1: identify control parameters and other influencing factors on the process

Table 11 Response variables measured according to a factorial design with centers points. Adapted from Campos [141] and Rocha et al. [100]

N	Levels of the parameters						Response variables		
	Cutting speed		Feed rate		Depth of cut		Tool life	Surface roughness	Productivity
	Vc		*f*		*D*		*T*	*Ra*	*MRR/Fc*
	(m/min)		(mm/rev)		(mm)		(min)	(μm)	(cm^3/N min)
	Cod.	Decod.	Cod.	Decod.	Cod.	Decod.	–	–	–
Factorial points									
1	− 1.00	100	− 1.00	0.10	− 1.00	0.15	70.00	0.13	0.00438
2	1.00	225	− 1.00	0.10	− 1.00	0.15	35.00	0.09	0.01416
3	− 1.00	100	1.00	0.22	− 1.00	0.15	57.00	0.52	0.00778
4	1.00	225	1.00	0.22	− 1.00	0.15	32.50	0.26	0.03115
5	− 1.00	100	− 1.00	0.10	1.00	0.33	67.00	0.14	0.00739
6	1.00	225	− 1.00	0.10	1.00	0.33	33.00	0.12	0.03011
7	− 1.00	100	1.00	0.22	1.00	0.33	55.00	0.48	0.01634
8	1.00	225	1.00	0.22	1.00	0.33	31.50	0.45	0.06725
Center points									
9	0.00	162.5	0.00	0.16	0.00	0.24	46.50	0.15	0.01871
10	0.00	162.5	0.00	0.16	0.00	0.24	45.50	0.16	0.01881
11	0.00	162.5	0.00	0.16	0.00	0.24	47.50	0.14	0.01877
12	0.00	162.5	0.00	0.16	0.00	0.24	47.00	0.17	0.01888
13	0.00	162.5	0.00	0.16	0.00	0.24	46.50	0.16	0.01869

As shown in Section 2.1, the determination of the control parameters of a process can be accomplished through exploratory experiments or from previous experience, which can be reached by appropriate literature reviews. In this case of study, Rocha et al. [100] did not detail how the main control parameters and their respective levels were defined. Table 9 shows the levels of each parameter used by the authors.

As can be seen in Table 9, at the factorial points, the cutting speed varies from 100 to 200 m/min, the feed rate varies from 0.10 to 0.22 mm/rev, and the depth of cut ranges from 0.24 to 0.33 mm. At the center points, the cutting speed is 162.50 m/min, the feed rate is 0.16 mm/rev, and the depth of cut is 0.24 mm, which correspond to the midpoints of levels + 1 and − 1 of each control parameter.

At the axial points, placed at a distance of 1.682 according to Eq. 3 with $k = 3$, one can obtain cutting speeds of 57.38 and 267.62 m/min, feed rates of 0.06 and 0.26 mm/rev, and depths

Table 12 Curvature test for tool life (T)

Source	DF	Adj SS	Adj MS	*F* value	*p* value
Model	5	1882.61	376.52	823.64	0.000
Linear	3	1824.25	608.08	1330.18	0.000
Vc	1	1711.12	1711.12	3743.09	0.000
F	1	105.12	105.12	229.96	0.000
D	1	8.00	8.00	17.50	0.004
2-way interactions	1	55.12	55.12	120.59	0.000
Vc*f	1	55.12	55.12	120.59	0.000
Curvature	1	3.23	3.23	7.07	0.033
Error	7	3.20	0.46		
Lack-of-fit	3	1.00	0.33	0.61	0.645
Pure error	4	2.20	0.55		
Total	12	1885.81			

Table 13 Curvature test for surface roughness (Ra)

Source	DF	Adj SS	Adj MS	*F* value	*p* value
Model	8	0.273049	0.034131	262.55	0.000
Linear	3	0.208937	0.069646	535.74	0.000
Vc	1	0.015313	0.015313	117.79	0.000
F	1	0.189112	0.189112	1454.71	0.000
D	1	0.004512	0.004512	34.71	0.004
2-way interactions	3	0.015938	0.005313	40.87	0.002
Vc*f	1	0.006613	0.006613	50.87	0.002
Vc*d	1	0.007813	0.007813	60.10	0.001
f*d	1	0.001512	0.001512	11.63	0.027
3-way interactions	1	0.005512	0.005512	42.40	0.003
Vc*f*d	1	0.005512	0.005512	42.40	0.003
Curvature	1	0.042662	0.042662	328.17	0.000
Error	4	0.00052	0.00013		
Total	12	0.273569			

Table 14 Curvature test for productivity (MRR/Fc)

Source	DF	Adj SS	Adj MS	*F* value	*p* value
Model	7	0.003028	0.000433	81.1	0.000
Linear	3	0.002484	0.000828	155.22	0.000
Vc	1	0.001425	0.001425	267.21	0.000
F	1	0.000552	0.000552	103.58	0.000
D	1	0.000506	0.000506	94.86	0.000
2-way interactions	3	0.000506	0.000169	31.6	0.001
Vc*f	1	0.000218	0.000218	40.91	0.001
Vc*d	1	0.000205	0.000205	38.4	0.002
f*d	1	0.000083	0.000083	15.48	0.011
Curvature	1	0.000039	0.000039	7.26	0.043
Error	5	0.000027	0.000005		
Lack-of-fit	1	0.000027	0.000027	4500.84	0.000
Pure error	4	0.000000	0.000000		
Total	12	0.003055			

of cut of 0.09 and 0.39 mm, in the lower and higher levels respectively.

Step 2: analyze the influence of the factors on the responses variables

In some cases, when there is no certainty about the real influence of the factors suggested in step 1, it is necessary to choose those that govern surely the process investigated. In Section 2.1, some typical forms of analysis were discussed, such as the application of fractional factorial designs or the Taguchi designs (L8, L12, etc.). Rocha et al. [100] used the main effect plots for CCD data to illustrate the effect of each parameter on the response variables but should have explained why these parameters are the most influential.

Step 3: plan the experiment according to a factorial design with center points

As discussed throughout Sections 2.2 and 2.3, the factorial points allow the experimenter to identify the contributions of the control parameters on the investigated responses. The center points, in turn, have the purpose of enabling the correct location of the regions of curvature.

In the sequential approach of RSM, the factorial and center points are the first runs to be appreciated in the analysis. Table 10 presents the design formed by these points in coded (standardized values) and decoded (real values) units.

As can be seen in Table 10, Rocha et al. [100] reduced one center point in the design from six to five. The usage of several center points allows the experimenter to perform the curvature test, making possible a decisive step of RSM, as will be showed in step 5.

Step 4: carry out the experiments and measure the response variables (data collection)

After the structuring of the experimental design, the tests should be performed to data collection of response variables, as discussed in Section 2.1. In Section 4.2.3, several response variables were cited as typical outputs of manufacturing processes. In the case of study, Rocha et al. [100] selected tool

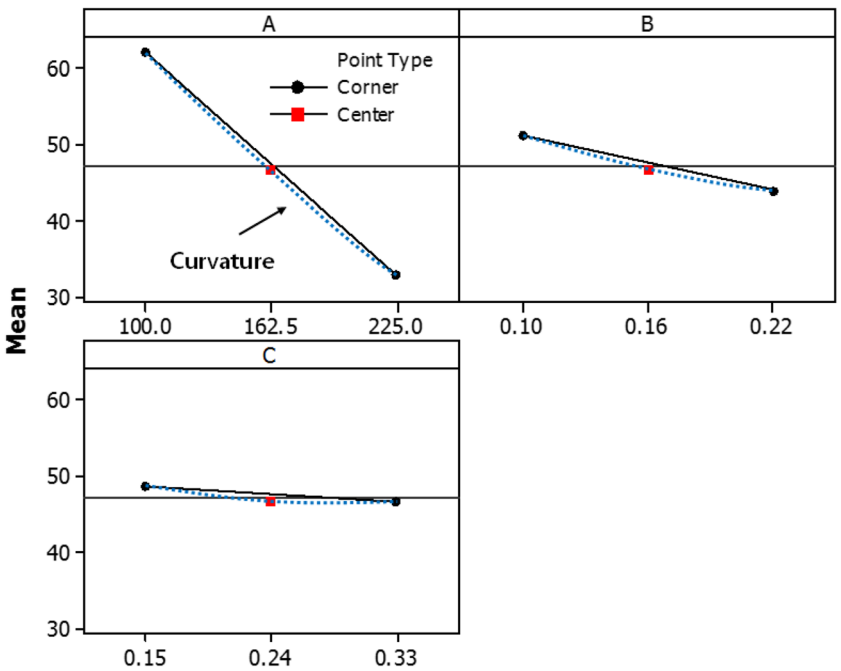

Fig. 27 Main factorial plot for tool life (T)

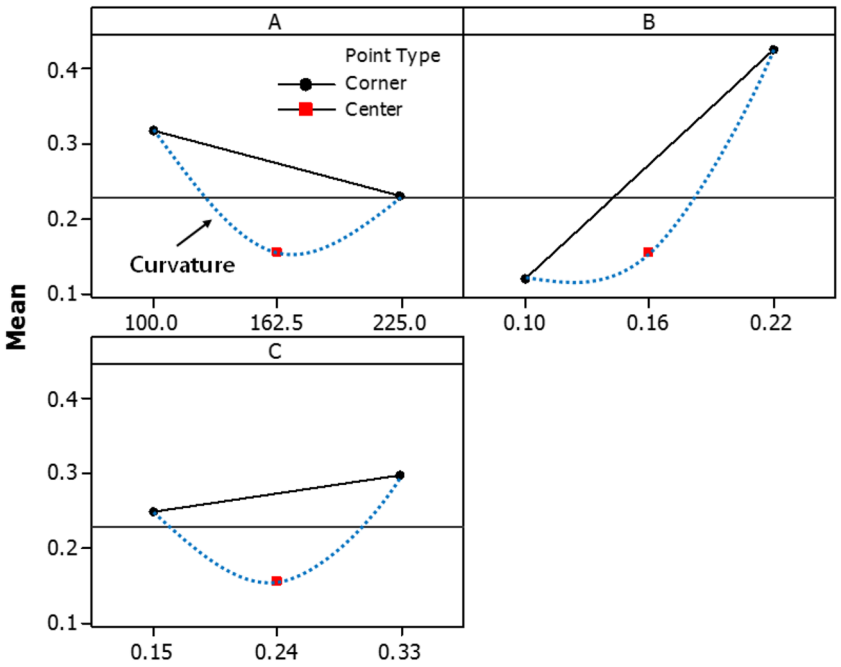

Fig. 28 Main factorial plot for surface roughness (Ra)

life, surface roughness, and productivity as responses variables of the hardened process investigated.

Table 11 presents the factorial design with center points of Table 10, including the responses measured in each test. In practical terms, this means that when performing the first experiment with a cutting speed of 100 m/min, a feed rate of 0.10 mm/rev, and a depth of cut of 0.15 mm, the experimenter obtained a tool life of 70 min, a surface roughness of 0.13 μm, and a productivity of 0.00438 cm^3/N min.

Step 5: perform curvature analysis of the experimental region

As discussed in Section 2.2, the existence of curvature in the experimental region is one of the main assumptions of RSM. Despite this, only one of the studies investigated in the present study commented on the usage of curvature tests as part of its scope of analysis [102].

Tables 12, 13, and 14 present ANOVA-based curvature tests for each of the responses of interest. With 95%

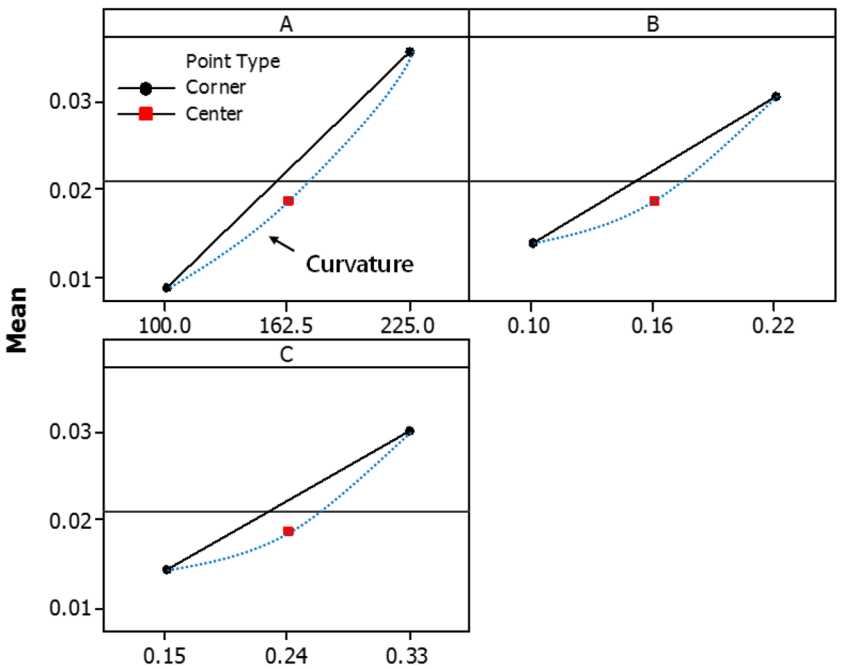

Fig. 29 Main factorial plot for productivity (MRR/Fc)

Table 15 Central composite design for data collection at axial points. Adapted from Campos [141] and Rocha et al. [100]

N	Levels of the parameters						Response Variables		
	Cutting speed		Feed rate		Depth of cut		Tool life	Surface Roughness	Productivity
	Vc		*f*		*d*		*T*	*Ra*	*MRR/Fc*
	(m/min)		(mm/rev)		(mm)		(min)	(μm)	(cm³/N min)
	Cod.	Decod.	Cod.	Decod.	Cod.	Decod.	-	-	-
Factorial points									
1	-1.00	100.00	-1.00	0.10	-1.00	0.15	70.00	0.13	0.00438
2	1.00	225.00	-1.00	0.10	-1.00	0.15	35.00	0.09	0.01416
3	-1.00	100.00	1.00	0.22	-1.00	0.15	57.00	0.52	0.00778
4	1.00	225.00	1.00	0.22	-1.00	0.15	32.50	0.26	0.03115
5	-1.00	100.00	-1.00	0.10	1.00	0.33	67.00	0.14	0.00739
6	1.00	225.00	-1.00	0.10	1.00	0.33	33.00	0.12	0.03011
7	-1.00	100.00	1.00	0.22	1.00	0.33	55.00	0.48	0.01634
8	1.00	225.00	1.00	0.22	1.00	0.33	31.50	0.45	0.06725
Center points									
9	0.00	162.50	0.00	0.16	0.00	0.24	46.50	0.15	0.01871
10	0.00	162.50	0.00	0.16	0.00	0.24	45.50	0.16	0.01881
11	0.00	162.50	0.00	0.16	0.00	0.24	47.50	0.14	0.01877
12	0.00	162.50	0.00	0.16	0.00	0.24	47.00	0.17	0.01888
13	0.00	162.50	0.00	0.16	0.00	0.24	46.50	0.16	0.01869
Axial points									
14	-1.68	57.39	0.00	0.16	0.00	0.24	*Experiments to be carried out*		
15	1.68	267.61	0.00	0.16	0.00	0.24			
16	0.00	162.50	-1.68	0.06	0.00	0.24			
17	0.00	162.50	1.68	0.26	0.00	0.24			
18	0.00	162.50	0.00	0.16	-1.68	0.09			
19	0.00	162.50	0.00	0.16	1.68	0.39			

confidence, one can guarantee that the experimental regions investigated for tool life (Table 12, p value = 0.033), surface roughness (Table 13, p value = 0.000) and productivity (Table 14, p value = 0.043) have significant curvatures.

Figures 27, 28, and 29 illustrate the "size" of the region of curvature for each response variable. As can be seen, the tool life has a small curvature (Fig. 27), the surface roughness is in a region of large curvature (Fig. 28) and the productivity in a region of intermediate curvature (Fig. 29). For the experimental conditions investigated, this means that improving tool life is not too natural as surface roughness.

Step 6A: add axial points to the experimental design

Once the condition imposed by step 5 is satisfied, the axial points can be included in the experimental design, completing the structuring of the CCD. As presented in Section 2.2, these points extrapolate the levels of each factor, each one, in turn, composing $2 \times k$ possible combinations according to Eq. 2 which allows a better estimation of the quadratic terms in the second-order model.

In the work of Rocha et al. [100], as $k = 3$, six axial points were correctly included (as discussed in Section 2.3), with a radius of 1.682, according to the calculation of Eq. 3. Table 15 provides the CCD, containing its three types of points.

Step 7: carry out new experiments and measure the response variables

With the application of experimental design of Table 15, new tests were performed to measure the response variables at the axial points, as shown in Table 16.

In Table 16, one can see that, since at the axial points the process is investigated under more "severe" conditions, extreme values are obtained in comparison to the original data set with factorial and center points. In the factorial design, for instance, the highest tool lives were observed when *Vc* was at 100 m/min (experiments 1 and 5). However, at experiment 15, when the *Vc* increased to 267.61 m/min, a smaller tool life was obtained (28.25 min).

Step 8: obtain an estimated model for each response and analyze the models

By applying OLS, one can estimate the models for each of the response variables measured. Tables 17, 18, and 19 provide the details of the estimated models, validated according to R^2adj values greater than 0.80.

When carrying the convexity analyses (Table 20), for all models eigenvalues with positive and negative signals were obtained, which indicates the occurrence of saddle-shaped functions, as shown in Fig. 30. This finding typifies one of

Table 16 Measurement of responses of interest in the machining process according to a factorial design with center points. Adapted from Campos [141] and Rocha et al. [100]

N	Levels of the parameters						Response variables		
	Cutting speed		Feed rate		Depth of cut		Tool life	Surface roughness	Productivity
	Vc		*F*		*d*		*T*	*Ra*	*MRR/Fc*
	(m/min)		(mm/rev)		(mm)		(min)	(μm)	(cm^3/N min)
	Cod.	Decod.	Cod.	Decod.	Cod.	Decod.	–	–	–
Factorial points									
1	− 1.00	100.00	− 1.00	0.10	− 1.00	0.15	70.00	0.13	0.00438
2	1.00	225.00	− 1.00	0.10	− 1.00	0.15	35.00	0.09	0.01416
3	− 1.00	100.00	1.00	0.22	− 1.00	0.15	57.00	0.52	0.00778
4	1.00	225.00	1.00	0.22	− 1.00	0.15	32.50	0.26	0.03115
5	− 1.00	100.00	− 1.00	0.10	1.00	0.33	67.00	0.14	0.00739
6	1.00	225.00	− 1.00	0.10	1.00	0.33	33.00	0.12	0.03011
7	− 1.00	100.00	1.00	0.22	1.00	0.33	55.00	0.48	0.01634
8	1.00	225.00	1.00	0.22	1.00	0.33	31.50	0.45	0.06725
Center points									
9	0.00	162.50	0.00	0.16	0.00	0.24	46.50	0.15	0.01871
10	0.00	162.50	0.00	0.16	0.00	0.24	45.50	0.16	0.01881
11	0.00	162.50	0.00	0.16	0.00	0.24	47.50	0.14	0.01877
12	0.00	162.50	0.00	0.16	0.00	0.24	47.00	0.17	0.01888
13	0.00	162.50	0.00	0.16	0.00	0.24	46.50	0.16	0.01869
Axial points									
14	− 1.68	57.39	0.00	0.16	0.00	0.24	63.00	0.29	0.00450
15	1.68	267.61	0.00	0.16	0.00	0.24	28.25	0.15	0.04608
16	0.00	162.50	− 1.68	0.06	0.00	0.24	42.50	0.12	0.00687
17	0.00	162.50	1.68	0.26	0.00	0.24	44.50	0.54	0.02879
18	0.00	162.50	0.00	0.16	− 1.68	0.09	54.50	0.15	0.00703
19	0.00	162.50	0.00	0.16	1.68	0.39	51.50	0.15	0.02822

Table 17 Estimated regression coefficients for tool life (T)

Term	Coef	SE Coef	*T* value	*p* value	VIF
Constant	46.590	1.650	28.28	0.000	
Vc	− 12.846	0.998	− 12.87	0.000	1.00
F	− 1.877	0.998	− 1.88	0.093	1.00
D	− 0.955	0.998	− 0.96	0.364	1.00
*Vc*Vc*	− 0.301	0.998	− 0.30	0.770	1.04
*f*f*	− 1.053	0.998	− 1.05	0.319	1.04
*d*d*	2.306	0.998	2.31	0.046	1.04
*Vc*f*	2.630	1.300	2.01	0.075	1.00
*Vc*d*	0.250	1.300	0.19	0.852	1.00
*f*d*	0.250	1.300	0.19	0.852	1.00
R^2	95.20%				
R^2_{adj}	92.79%				

Table 18 Estimated regression coefficients for surface roughness (Ra)

Term	Coef	SE Coef	*T* value	*p* value	VIF
Constant	0.1546	0.0181	8.55	0.000	
Vc	− 0.0429	0.0110	− 3.91	0.004	1.00
F	0.1418	0.0110	12.94	0.000	1.00
D	0.0139	0.0110	1.27	0.236	1.00
*Vc*Vc*	0.0302	0.0110	2.76	0.022	1.04
*f*f*	0.0691	0.0110	6.31	0.000	1.04
*d*d*	0.0055	0.0110	0.50	0.628	1.04
*Vc*f*	− 0.0288	0.0143	− 2.01	0.076	1.00
*Vc*d*	0.0313	0.0143	2.18	0.057	1.00
*f*d*	0.0137	0.0143	0.96	0.362	1.00
R^2	96.35%				
R^2_{adj}	92.71%				

Table 19 Estimated regression coefficients for productivity (MRR/Fc)

Term	Coef	SE Coef	*T* value	*p* value	VIF
Constant	0.018700	0.001170	15.93	0.000	
Vc	0.012939	0.000711	18.20	0.000	1.00
F	0.007567	0.000711	10.64	0.000	1.00
D	0.007268	0.000711	10.22	0.000	1.00
*Vc***Vc*	0.002727	0.000711	3.83	0.004	1.04
*f***f*	0.000090	0.000711	0.13	0.903	1.04
*d***d*	0.000017	0.000711	0.02	0.981	1.04
*Vc***f*	0.005223	0.000929	5.62	0.000	1.00
*Vc***d*	0.005060	0.000929	5.45	0.000	1.00
*f***d*	0.003212	0.000929	3.46	0.007	1.00
R^2	98.61%				
R^2_{adj}	97.21%				

the numerous cases found by the survey of Section 4.2.4. Moreover, since it is required the maximization of tool life and productivity and the minimization of surface roughness, one can conclude that all optimization directions are incompatible with the convexities of the functions, as can be seen in Table 20.

By performing the Pearson correlation analysis, moderate correlations were observed between T and Ra and between T and MRR/Fc ($\rho_{T,\,Ra} = 0.644$; $\rho_{T,\,MRR/Fc} = 0.582$). As described in Section 2.5, this result demonstrates that conventional optimization of a unique global function is not appropriate, since the objective functions have linear dependence.

Step 9: formulate and solve the optimization problem

By considering the models estimated in Step 8, the multiobjective problem can be expressed as follows:

$$\begin{aligned} &\text{Maximize} && Y1(\boldsymbol{x}) = T\,(Vc, f, d) \\ &\text{Minimize} && Y2(\boldsymbol{x}) = Ra\,(Vc, f, d) \\ &\text{Maximize} && Y3(\boldsymbol{x}) = d\,(Vc, f, d) \\ &\text{Subject to}: && \boldsymbol{x}^T\boldsymbol{x} \le \rho^2 \end{aligned} \tag{79}$$

Figure 31 illustrates the feasible region considering the three responses of interest.

Given the existence of correlations between some of the models, the multivariate techniques appear as convenient alternatives for the solution of the problem expressed by Eq. 76, as discussed in Section 2.5. For the study of this section, principal component analysis (PCA) was performed according to the proposed steps of Costa et al. [102]

Then, three principal components (PCs) were evaluated according to the eigenanalysis of the correlation matrix shown in Table 21. Since both the eigenvalues of PC1 and PC2 are greater than 1.000 and the cumulative proportion of the variance of PC2 exceeds 0.800, only PC1 and PC2 were used to describe the original variables.

Because the eigenvectors provide the relationships between the PCs and the original variables, PC1 was chosen to represent the variables T and MRR/Fc (eigenvectors of − 0.674 and 0.713, respectively), and PC2 to represent the variable Ra (eigenvector of 0.945).

By applying OLS, for each of the obtained components, models were estimated, resulting in the coefficients presented in Tables 22 and 23. Despite non-significant coefficients (*p*-values < 0.05), full models were adopted since they have the largest R^2adj values.

Table 24 provides the eigenvalues, convexities, and optimization directions of PC1 and PC2. As one can see, whereas for PC1, the convexity and the optimization direction are incompatible, for PC2 they are compatible. Figure 32 illustrates the response surfaces and the contour plots for PC1 and PC2.

By applying the steps and formulations of Costa et al. [102], this section employs an optimization method known as normal boundary intersection (NBI) to conclude RSM analysis. The generalized reduced gradient (GRG) algorithm is used as a subroutine of the NBI to obtain different optimal combinations for PC1 and PC2, prioritizing the minimization of PC1 (and therefore T and MRR/Fc) with smaller weights and prioritizing the minimization of PC2 (and therefore of Ra) with larger weights. The Pareto frontier for intervals of 0.05 units is provided in Fig. 33, where one of the optimal points is indicated with $T = 23.575$ min, Ra = 0.134 μm, and MRR/Fc = 0.042 cm^3/N min. Figure 34 shows the Pareto frontier inside the feasible region.

By applying Eq. 42 (Section 2.4), a confidence interval for the selected point in Fig. 33 is obtained as shown in Table 25. Then, to prove the effectiveness of the RSM study, confirmatory experiments must find a point inside the confidence intervals for each of the response variables.

Table 20 Convexity analysis and optimization direction

Response variable	Eigenvalues	Convexity	Optimization direction
T	[2.3249, − 2.0424, 0.6694]	Saddle	Maximization
Ra	[0.0739, 0.0352, − 0.0042]	Saddle	Minimization
MRR/Fc	[0.0058, − 0.0016, − 0.0015]	Saddle	Maximization

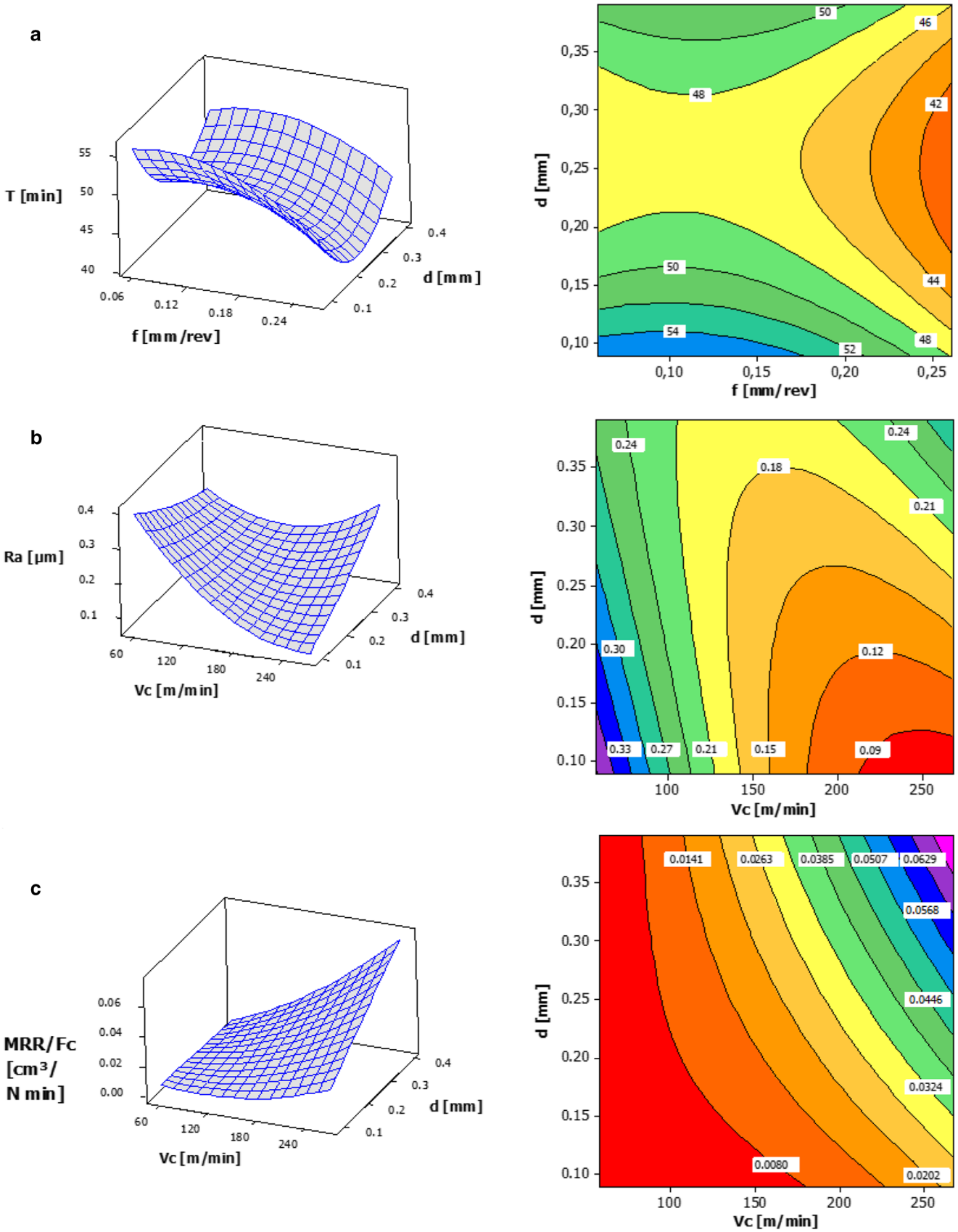

Fig. 30 Response surfaces and contour plots for: a) tool life (T), b) surface roughness (Ra), and c) productivity (MRR/Fc)

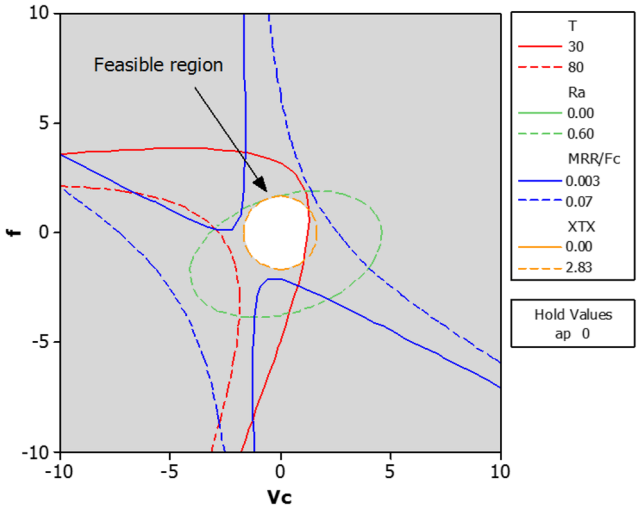

Fig. 31 Overlaid contour plot for tool life (T), surface roughness (Ra), productivity (MRR/Fc), and the experimental region constraint (XTX)

5.1 References on confirmatory experimental results

There are several ways of performing confirmatory experiments (also known as confirmation runs [14]). An appropriate method consists of first defining the sample size by using a statistical procedure, such as 1-sample *t* test. For this, the experimenter must define the power of the test, which is often greater than 0.80, the differences required to be detected, such as 0.5 (in standardized units), and the significance level (usually 0.05). After carrying the runs, a proper strategy consists of comparing the sample average with the confidence interval. If the average value lies within the confidence interval, then the RSM result is confirmed.

We can mention some IJAMT papers which employed similar strategies. Pereira et al. [26], for instance, used a *t* test considering a sample power greater than 0.90, a difference of 0.8297 (with a standard deviation of 0.51), and a 0.05 significance level. The authors found a sample of 8 runs and used the average values to demonstrate the effectiveness of the optimization via RSM of the surface roughness in the end milling of AISI 1045 steel since the average values lied within the confidence intervals.

Table 21 Eigenanalysis of the correlation matrix

	PC1	PC2	PC3
Eigenvalue	1.760	1.029	0.211
Proportion	0.587	0.342	0.070
Cumulative	0.587	0.930	1.000
Eigenvectors	PC1	PC2	PC3
T	− 0.674	0.322	− 0.665
Ra	0.193	0.945	0.262
MRR/Fc	0.713	0.048	− 0.700

Table 22 Estimated regression coefficients for PC1

Term	Coef	SE Coef	*T*	*p*
Constant	− 0.15107	0.14069	− 1.074	0.311
A	1.25168	0.08523	14.687	0.000
B	0.63093	0.08523	7.403	0.000
C	0.40062	0.08523	4.701	0.001
A*A	0.17941	0.08525	2.105	0.065
B*B	0.15236	0.08525	1.787	0.108
C*C	− 0.12159	0.08525	− 1.426	0.188
A*B	0.05197	0.11135	0.467	0.652
A*C	0.25537	0.11135	2.293	0.048
B*C	0.14915	0.11135	1.339	0.213
R^2	97.18%			
R^2_{adj}	94.36%			

Rodrigues et al. [29] employed the ANOVA one-way and the test to equal variance with a sample power of 0.998, a difference greater than 1.40, a standard deviation of 0.51, and a 0.05 significance level. Then, the researchers calculated the simple averages and the variances of 12 runs for the responses circularity and radial force measured in the helical milling of Al 7075 alloy. Regarding the confidence intervals, the authors concluded that the method based on RSM was able to find realistic solutions.

Pereira et al. [142] applied a statistical procedure with a sample power greater than 0.95, a difference of 5, standard deviations close to 1.00, and a 0.05 significance level for the machining forces measured in the helical milling of Al 7075 alloy. The authors showed that the method based on robust parameter design and RSM was able to find robust realistic solutions for the axial force because its average value lied within the confidence interval for all the noise conditions.

Table 23 Estimated regression coefficients for PC2

Term	Coef	SE Coef	*T*	*p*
Constant	− 0.49996	0.11323	− 4.415	0.002
A	− 0.57548	0.06860	− 8.389	0.000
B	0.86688	0.06860	12.638	0.000
C	0.08437	0.06860	1.230	0.250
A*A	0.19099	0.06861	2.784	0.021
B*B	0.40797	0.06861	5.946	0.000
C*C	0.09661	0.06861	1.408	0.193
A*B	− 0.09482	0.08962	− 1.058	0.318
A*C	0.21928	0.08962	2.447	0.037
B*C	0.10326	0.08962	1.152	0.279
R^2	96.88%			
R^2_{adj}	93.75%			

Table 24 Convexity analysis and optimization direction for principal components

Response variable	Eigenvalues	Convexity	Optimization direction
PC1	(0.2535, − 0.1799, 0.1366)	Saddle	Maximization
PC2	(0.4208, 0.2624, 0.0123)	Convex	Minimization

Other practical guides for performing confirmation runs after RSM analyses can be found in Gaudêncio et al. [143] who investigated the turning of AISI 12L14 steel; Naves et al. [144], who studied the methyl orange treatment with ozone; and Paiva et al. [145] who studied the hard turning of AISI 52100 with mixed ceramic tools.

6 Conclusions

RSM was introduced nearly 70 years ago by Box and Wilson (1951) and still has been studied by several authors. The development of a method capable of modeling and optimizing processes based on a small number of control parameters provided new directions for research in the twentieth century. In essence, RSM is the combination of design and analysis of experiments, modeling techniques, and optimization methods in a stronger approach that utilizes experimental data to obtain process improvements.

In this context, this paper presented the core theoretical principles and practical guidelines for carrying RSM analysis. Then, to investigate current RSM applications in manufacturing and raise some questions and research opportunities, this paper performed a survey literature review of 49 RSM-CCD

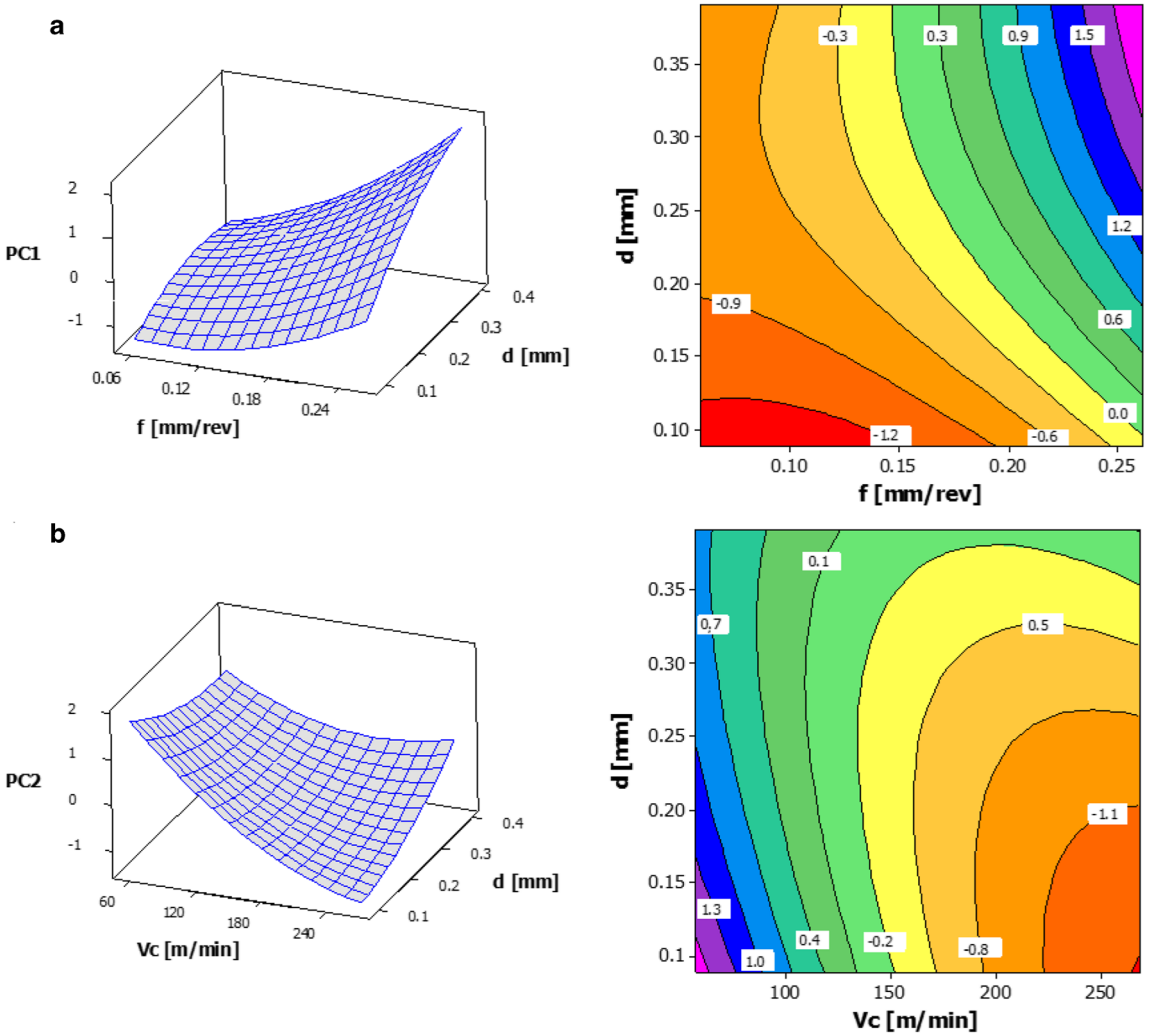

Fig. 32 Response surfaces and contour plots for: a) PC1 and b) PC2

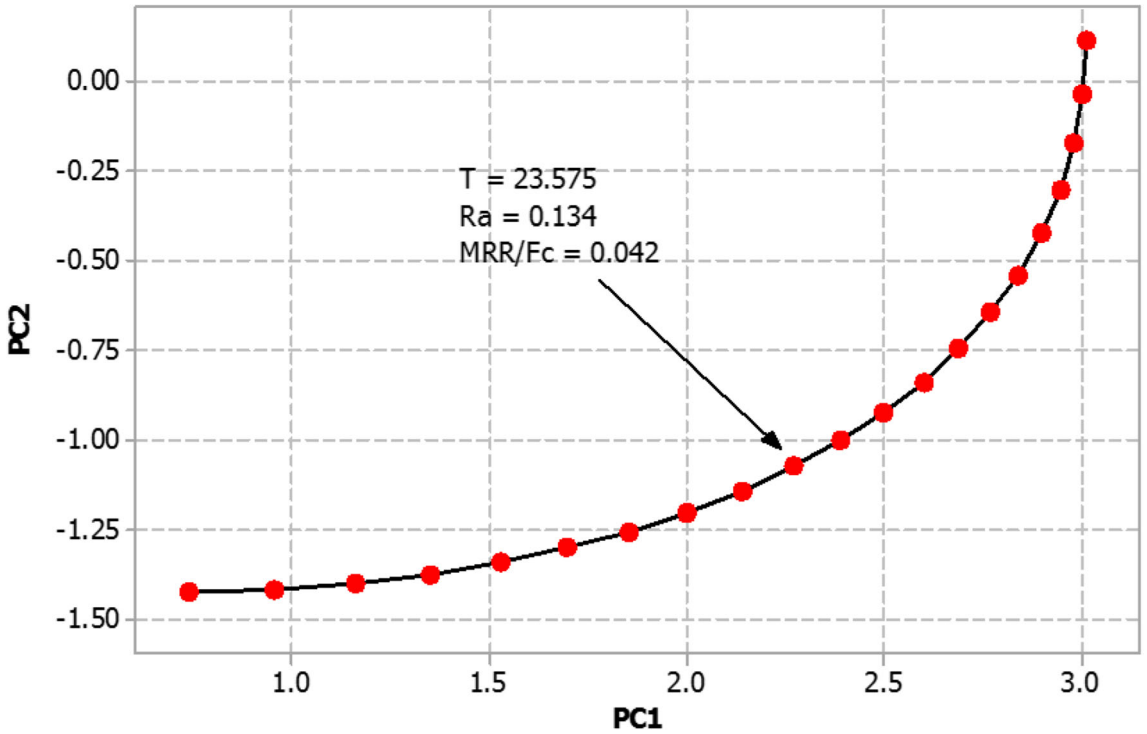

Fig. 33 Pareto frontier obtained from PCA-NBI method

papers published in the *International Journal of Advanced Manufacturing Technology* from 2014 and 2017.

For this, eight critical aspects and 13 research questions and related hypotheses were raised; to test these hypotheses, 123 response surfaces were investigated. The discussions were built based on several perspectives of RSM for advanced manufacturing technology optimization, such as the typical numbers of control parameters and response variables, the usage of CCD points, the regions where the models are fitted, the compatibility between convexity and optimization direction, the correlations between models, and the usage of experimental region constraint.

Then, considering the core theoretical principles and practical guidelines for RSM as well as the results obtained from the survey literature review, a typical case of advanced manufacturing technology optimization was revisited. One

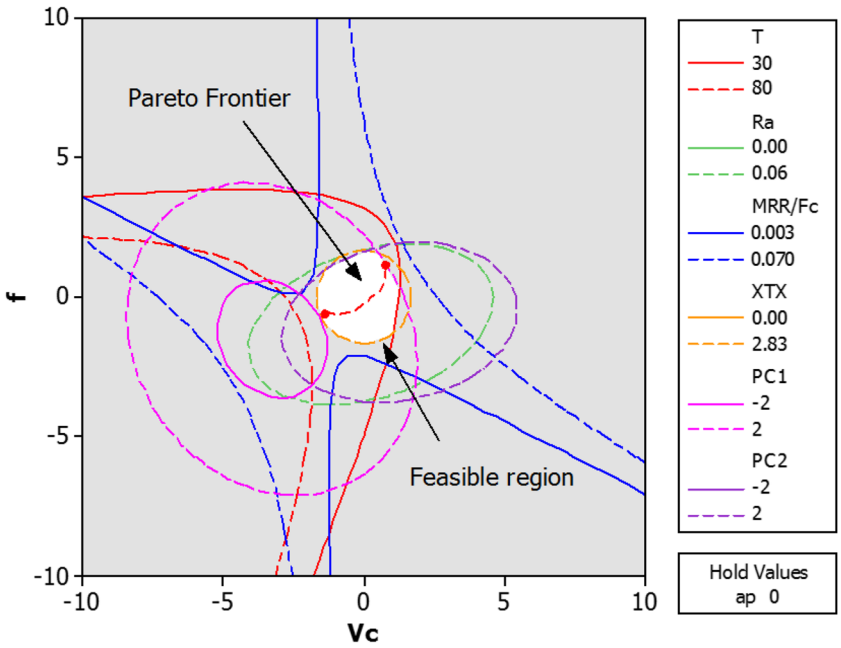

Fig. 34 Pareto frontier inside the feasible region

Table 25 Confidence intervals for the Pareto frontier point

Cutting parameters			Confidence intervals					
			T		Ra		MRR/Fc	
Vc	f	ap	Lower	Upper	Lower	Upper	Lower	Upper
266	0.14	0.29	17.18486	30.19373	0.077318	0.220114	0.03927	0.048537

of the main contributions of this paper is to provide theoretical discussions and empirical evidence to strength manufacturing optimization by using RSM.

Briefly, the main results of this work are as follows:

- The probability of an advanced manufacturing process being controlled by more than five parameters is almost null and, in general, these processes are controlled by three or four parameters;
- There is a consensus concerning the usage of the number of factorial and axial points prescribed in the literature, but not the number of center points. That is, it is as likely to find papers that use the number of center points prescribed in the literature as those that do not use it.
- Studies that measure multiple response variables occur with probability greater than 50%. In this investigation, they accounted for 63.27% of the sample.
- The probability of two models estimated for the same process be correlated is at least 60%. In the sample of the present study, 71.88% of the pairs of models presented a significant correlation.
- The probability of a quadratic model being estimated in the region of curvature is at least 57%. In this study, the proportion was 69.16% of the total of models.
- There is a significant association between curvature and convexity and the probability that an estimated quadratic model in the non-curvature region is a saddle function is greater than 83%. In the sample, the proportion of models in this condition was 96.86% of the total.
- The probability of a response surface model being saddle-shaped is at least 68%. In this study, these models represented 78.69% of the estimated total models.
- Changing the rotatability of the designs does not affect the convexity of the estimated models.
- Concave models are more likely to occur when using all model terms. In the sample, this happened with a frequency of 77.78%.
- There is no dominance of one of the optimization direction (maximization or minimization). Both occur equally.
- The probability of convexity and optimization direction being not compatible is at least 78%. In the investigated sample, this represented 87.61% of the cases.
- Only one of the investigated papers made clear the performing of curvature test and the usage of experimental region constraint for process optimization.

Future works will address the following issues:

- How have papers on manufacturing process optimization performed confirmatory experiments? How the sample size of confirmatory experiments should be determined?
- What are the typical approaches for calculating confidence intervals for the optimal points?
- What are the typical optimization methods employed in studies of advanced manufacturing technology optimization? What are the advantages and disadvantages of each of them?

Acknowledgements The authors also would like to acknowledge Prof. Ph.D. João Paulo Davim Tavares da Silva from the University of Aveiro, Portugal, who allowed and sponsored the consecution of experimental data set, the Foundation of Support Research of the State of Minas Gerais (FAPEMIG), and the anonymous reviewer for the careful reading of our paper and for the positive comments and suggestions.

Funding information This paper is supported by the Coordination for the Improvement of Higher Education Personnel (CAPES), through doctoral scholarships and project CAPES 9801-12.0 and the National Council for Scientific and Technological Development (CNPq) through projects CNPq 303586/2015-0 and CNPq 409318/2017-5.

References

1. Box GEP, Draper NR (1959) A basis for the selection of a response surface design. J Am Stat Assoc 54(287):622–654
2. Box GEP, Draper NR (2007) Response surfaces, mixtures, and ridge analyses, 2nd edn. Wiley, Hoboken
3. Carter WH, Chinchilli VM, Myers RH, Campbell ED (1986) Confidence intervals and an improved ridge analysis of response surfaces. Technometrics 28(4):339–346
4. Jackson MJ, Lathery E, Whitfield MD, Handy RG, Silva MB, Machado AR, Silva RB (2017) Computational analysis of turning G10530 steel to eliminate chip crowding using variable cutting speeds. Int J Adv Manuf Technol 92:2341–2363. https://doi.org/10.1007/s00170-017-0279-0
5. Suyama DI, Diniz AE, Pederiva R (2017) Tool vibration in internal turning of hardened steel using cBN tool. Int J Adv Manuf Technol 88:2485–2495. https://doi.org/10.1007/s00170-016-8964-y
6. Gamarra JR, Diniz AE (2018) Taper turning of super duplex stainless steel: tool life, tool wear and workpiece surface roughness. J Braz Soc Mech Sci Eng 40:39. https://doi.org/10.1007/s40430-018-0991-1
7. Loureiro D, Diniz AE, Farina AB, Delijaicov S (2017) The influence of turning parameters on surface integrity of nickel alloy 625. Proc Inst Mech Eng B J Eng Manuf 232(10):1837–1847

8. Myers RH, Carter WH (1973) Response surface techniques for dual response systems. Technometrics 15(2):301–317. https://doi.org/10.1080/00401706.1973.10489044
9. Myers RH, Montgomery DC (2009) Response surface methodology: process and product optimization using designed experiments, 3rd edn. Wiley, New York
10. Leithold L (1986) The calculus with analytic geometry, 5th edn. Harper & Row, New York
11. Box GEP (1954) Exploration and exploitation of response surfaces: some general considerations and examples. Biometrics 10(1):16–60. https://doi.org/10.2307/3001663
12. Biles WE (1975) A response surface method for experimental optimization of multi-response processes. Ind Eng Chem Process Des Dev 14(2):152–158. https://doi.org/10.1021/i260054a010
13. Stewart J (2012) Calculus, 7th edn. Cengage, Belmont
14. Montgomery DC (2017) Designs and analysis of experiments, 9th edn. Wiley, Hoboken
15. Teimouri R, Amini S, Mohagheghian N (2017) Experimental study and empirical analysis on effect of ultrasonicvibration during rotary turning of aluminum 7075 aerospace alloy. J Manuf Process 26:1–17. https://doi.org/10.1016/j.jmapro.2016.11.011
16. Ekici E, Motorcu AR (2014) Evaluation of drilling Al/SiC composites with cryogenically treated HSS drills. Int J Adv Manuf Technol 74(9):1495–1505. https://doi.org/10.1007/s00170-014-6085-z
17. Patel MGC, Krishna P, Parappagoudar MB (2016) An intelligent system for squeeze casting process – soft computing based approach. Int J Adv Manuf Technol 86(9):3051–3065. https://doi.org/10.1007/s00170-016-8416-8
18. Sivaraos, Milkeya KR, Samsudina AR, Dubeyb AK, Kiddc P (2014) Comparison between Taguchi method and response surface methodology (RSM) in modelling CO2 laser machining. Jordan J Mech Indust Eng 8(1):35–42
19. Bösiger P, Richard IMT, LeGat L, Michen B, Schubert M, Rossi RM, Fortunato G (2018) Application of response surface methodology to tailor the surface chemistry of electrospun chitosan-poly(-ethylene oxide) fibers. Carbohydr Polym 186:122–131. https://doi.org/10.1016/j.carbpol.2018.01.038
20. Vakili-Azghandi M, Fattah-alhosseini A, Keshavarz MK (2018) Optimizing the electrolyte chemistry parameters of PEO coating on 6061 Al alloy by corrosion rate measurement: response surface methodology. Measurement 124:252–259. https://doi.org/10.1016/j.measurement.2018.04.038
21. Ghaedi M, Hajjati S, Mahmudi Z, Tyagi I, Agarwal S, Maity A, Gupta VK (2015) Modeling of competitive ultrasonic assisted removal of the dyes - methylene blue and safranin-O using Fe3O4 nanoparticles. Chem Eng J 268:28–37. https://doi.org/10.1016/j.cej.2014.12.090
22. Dufreneix S, Legrand C, Di Bartolo C, Bremaud M, Mesgouez J, Tiplica T, Autret D (2017) Design of experiments in medical physics: application to the AAA beam model validation. Phys Med 41:26–32. https://doi.org/10.1016/j.ejmp.2017.05.068
23. Chitichotpanya P, Inprasit T, Chitichotpanya C (2017) In vitro assessment of antibacterial potential and mechanical properties of Ag-TiO2/WPU on medical cotton optimized with response surface methodology. J Nat Fibers 16:88–99. https://doi.org/10.1080/15440478.2017.1408520
24. Augustin G, Davila S, Udilljak T, Staroveski T, Brezak D, Babic S (2012) Temperature changes during cortical bone drilling with a newly designed step drill and an internally cooled drill. Int Orthop 36(7):1449–1456. https://doi.org/10.1007/s00264-012-1491-z
25. Seo J, Kim PJH, Myoungjae L, You K, Moon J, Lee DH, Paik U (2017) Multi-objective optimization of tungsten CMP slurry for advanced semiconductor manufacturing using a response surface methodology. Mater Des 117:131–138. https://doi.org/10.1016/j.matdes.2016.12.066
26. Pereira RBD, Hincapia CAA, Campos PHS, Paiva AP, Ferreira JR (2016) Multivariate global index and multivariate mean square error optimization of AISI 1045 end milling. Int J Adv Manuf Technol 87:3195–3209. https://doi.org/10.1007/s00170-016-8703-4
27. Roshan BS, Jooibari BM, Teimouri R, Asgharzadeh-Ahmadi G, Falahati-Naghibi M, Sohrabpoor H (2013) Optimization of friction stir welding process of AA7075 aluminum alloy to achieve desirable mechanical properties using ANFIS models and simulated annealing algorithm. Int J Adv Manuf Technol 69:1803–1818. https://doi.org/10.1007/s00170-013-5131-6
28. Yang A, Han Y, Pan Y, Xing H, Li J (2017) Optimum surface roughness prediction for titanium alloy by adopting response surface methodology. Results in Physics 7:1046–1050. https://doi.org/10.1016/j.rinp.2017.02.027
29. Rodrigues VFS, Ferreira JR, Paiva AP, Souza LGP, Pereira RBD, Brandão LC (2018) Robust modeling and optimization of borehole enlarging by helical milling of aluminum alloy Al7075. Int J Adv Manuf Technol 100:2583–2599. https://doi.org/10.1007/s00170-018-2832-x
30. Vairamani G, Kumar TS, Malarvizhi S, Balasubramanian V (2013) Application of response surface methodology to maximize tensile strength and minimize interface hardness of friction welded dissimilar joints of austenitic stainless steel and copper alloy. Trans Nonferrous Metals Soc China 23(8):2250–2259. https://doi.org/10.1016/S1003-6326(13)62725-9
31. Subramanian AVM, Nachimuthu MDG, Cinnasamy V (2017) Assessment of cutting force and surface roughness in LM6/SiCp using response surface methodology. J Appl Res Technol 15(3):283–296. https://doi.org/10.1016/j.jart.2017.01.013
32. Mostafaei M, Javadikia H, Naderloo L (2016) Modeling the effects of ultrasound power and reactor dimension on the biodiesel production yield: comparison of prediction abilities between response surface methodology (RSM) and adaptive neuro-fuzzy inference system (ANFIS). Energy 115:626–636. https://doi.org/10.1016/j.energy.2016.09.028
33. Costa DMD, Brito TG, Paiva AP, Leme RC, Balestrassi PP (2016a) A normal boundary intersection with multivariate mean square error approach for dry end milling process optimization of the AISI 1045 steel. J Clean Prod 135:1658–1672. https://doi.org/10.1016/j.jclepro.2016.01.062
34. Hadad M (2015) An experimental investigation of the effects of machining parameters on environmentally friendly grinding process. J Clean Prod 108:217–231. https://doi.org/10.1016/j.jclepro.2015.05.092
35. Prabhu R, Alwarsamy T (2017) Effect of process parameters on ferrite number in cladding of 317L stainless steel by pulsed MIG welding. J Mech Sci Technol 31(3):1341–1347. https://doi.org/10.1007/s12206-017-0234-x
36. Box GEP, Hunter JS (1957) Multi-factor experimental designs for exploring response surfaces. Ann Math Stat 28:195–241. https://doi.org/10.1214/aoms/1177707047
37. Paiva AP, Ferreira JR, Balestrassi PP (2007) A multivariate hybrid approach applied to AISI 52100 hardened steel turning optimization. J Mater Process Technol 189:26–35. https://doi.org/10.1016/j.jmatprotec.2006.12.047
38. Khuri AI, Cornell JA (1996) Response surface: design and analyses, 2nd edn. Marcel Dekker Inc., New York
39. Box GEP, Wilson KB (1951) On the experimental attainment of optimum conditions. J R Stat Soc 13(1):1–45
40. Mongomery DC (1999) Experimental design for product and process design and development. J R Stat Soc Ser D (Statistician) 48(2):159–177
41. Box GEP, Hunter JS (1961) The 2k-p fractional factorial designs part I. Technometrics 3(3):311–351

42. Box GEP, Hunter JS, Hunter WG (2005) Statistics for experimenters: design, innovation and discovery, 2nd edn. Wiley, New York
43. Del Castilho E (2007) Process optimization: a statistical approach. Springer, New York
44. Del Castilho E, Cahya S (2001) A tool for computing confidence regions on the stationary point of response surface. Am Stat 55(4): 358–365. https://doi.org/10.1198/000313001753272349
45. Myers RH, Kuri AI, Carter WH (1989) Response surface methodology: 1966-1988. Technometrics 31(2):137–157
46. Bezerra MA, Santelli RE, Oliveira EP, Villar LS, Escaleira LA (2008) Response surface methodology (RSM) as a tool for optimization in analytical chemistry. Talanta 76:965–977. https://doi.org/10.1016/j.talanta.2008.05.019
47. Khuri AI, Mukhopadhyay S (2010) Response surface methodology. Wiley Interdisciplinary Reviews: Computational Statistics 2(2):28–149. https://doi.org/10.1002/wics.73
48. Vadde KK, Syrotiuk VR, Montgomery DC (2006) Optimizing protocol interaction using response surface methodology. IEEE Trans Mob Comput 5(6):627–638. https://doi.org/10.1109/TMC.2006.82
49. Lundstedt T, Seifert E, Abramo L, Thelin B, Nystrom A, Pertensen J, Bergman R (1998) Experimental design and optimization. Chemom Intell Lab Syst 42:3–40. https://doi.org/10.1016/S0169-7439(98)00065-3
50. Goos P, Jones B (2011) Optimal design of experiments: a case study approach. Wiley, Chichester
51. Cheng SW, Wu CFJ (2001) Factor screening and response surface exploration. Stat Sin 11:553–604. https://doi.org/10.5705/ss.2012.210
52. Brightman HJ (1978) Optimization through experimentation: applying response surface methodology. Decis Sci 9(3):481–495. https://doi.org/10.1111/j.1540-5915.1978.tb00737.x
53. Yücel Y, Göycincik S (2015) Optimization of ethanol production from spent tea waste by Saccharomyces cerevisiae using statistical experimental designs. Biomass Conversion and Biorefinery 5: 247–255. https://doi.org/10.1007/s13399-014-0138-2
54. Lin YC, Tsao CC, Hsu CY, Hung SK, Wen DC (2012) Evaluation of the characteristics of the microelectrical discharge machining process using response surface methodology based on the central composite design. Int J Adv Manuf Technol 62:1013–1023. https://doi.org/10.1007/s00170-011-3745-0
55. Borkowski JJ (1995) Spherical prediction-variance properties of central composite and Box-Behnken designs. Technometrics 37(4):399–410. https://doi.org/10.2307/1269732
56. Duineveld CAA, Bruins CHP, Smilde AK, Bolhuis GK, Zuurman K, Doornbos DF (1994) Multicriteria steepest ascent. Chemom Intell Lab Syst 25(2):183–201. https://doi.org/10.1016/0169-7439(94)85042-9
57. Forbes C, Evans M, Hastings N, Peacock B (2010) Statistical distributions, 4th edn. Wiley, Hoboken. https://doi.org/10.1002/9780470627242.ch20
58. Hoerl RW (1985) Ridge analysis 25 years later. Am Stat 39(3): 186–192. https://doi.org/10.2307/2683926
59. Zavadskas EK, Turskis Z (2010) A new additive ratio assessment (ARAS) method in multicriteria decision-making. Technol Econ Dev Econ 16(2):159–172. https://doi.org/10.3846/tede.2010.10
60. Peterson JJ, Kuhn AM (2005) Ridge analysis with noise variables. Technometrics 47(3):274–283
61. Edwards JR (2007) Polynomial regression and response surface methodology. In: Ostroff C, Judge TA (eds) Perspectives on organizational fit. Jossey-Bass, San Francisco, pp 361–372
62. Lin DKJ, Peterson JJ (2006) Statistical inference for response surface optima. In: Khuri A (ed) Response Surface Methodology and related topics. World Scientific Publishing, Hackensack, pp 65–88
63. Sambucini V (2012) Confidence regions for the stationary point of a quadratic response surface based on the asymptotic distribution of its MLE. Stat Comput 22(3):739–751. https://doi.org/10.1007/s11222-010-9202-3
64. Rao SS (2009) Engineering optimization: theory and practice, 4th edn. Wiley, Hoboken
65. Deb K, Sindhya K, Hakanen J (2017) Multi-object/ive optimization. In: Sengupta RN, Gupta A, Dutta J (eds) Decision sciences: theory and practice. Taylor and Francis, Boca Raton, pp 146–179
66. Šaparauskas J, Zavadskas EK, Turskis Z (2011) Selection of facade's alternatives of commercial and public buildings based on multiple criteria. Int J Strateg Prop Manag 15(2):189–203. https://doi.org/10.3846/1648715X.2011.586532
67. Kant G, Sangwan KS (2014) Prediction and optimization of machining parameters for minimizing power consumption and surface roughness in machining. J Clean Prod 83:151–164. https://doi.org/10.1016/j.jclepro.2014.07.073
68. Öktem H, Erzurumlu T, Kurtaran H (2005) Application of response surface methodology in the optimization of cutting conditions for surface roughness. J Mater Process Technol 170:11–16. https://doi.org/10.1016/j.jmatprotec.2005.04.096
69. Kumar N, Mukherjee M, Bandyopadhyay A (2017) Comparative study of pulsed Nd:YAG laser welding of AISI 304 and AISI 316 stainless steels. Opt Laser Technol 88:24–39. https://doi.org/10.1016/j.optlastec.2016.08.018
70. Sudhagar S, Sakthivel M, Mathew PJ, Daniel SAA (2017) A multi criteria decision making approach for process improvement in friction stir welding of aluminium alloy. Measurement 108:1–8. https://doi.org/10.1016/j.measurement.2017.05.023
71. Song X, Zhang M, Pei ZJ, Wang D (2014) Ultrasonic vibration-assisted pelleting of wheat straw: a predictive model for energy consumption using response surface methodology. Ultrasonics 54(1):305–311. https://doi.org/10.1016/j.ultras.2013.06.013
72. Abuhabaya A, Fieldhouse J, Brown D (2013) The optimization of biodiesel production by using response surface methodology and its effect on compression ignition engine. Fuel Process Technol 113:57–62. https://doi.org/10.1016/j.fuproc.2013.03.025
73. Gomes JHF, Paiva AP, Costa SC, Balestrassi PP, Paiva EJ (2013) Weighted multivariate mean square error for processes optimization: a case study on flux-cored arc welding for stainless steel claddings. Eur J Oper Res 226:522–535. https://doi.org/10.1016/j.ejor.2012.11.042
74. Paiva AP, Paiva EJ, Ferreira JR, Balestrassi PP, Costa SC (2009) A multivariate mean square error optimization of AISI 52100 hardened steel turning. Int J Adv Manuf Technol 43:631–643. https://doi.org/10.1007/s00170-008-1745-5
75. Johnson RA, Wichern DW (2007) Applied multivariate statistical analysis, 6th edn. Pearson Prentice Hall, New Jersey
76. Kumara C, Dasa M, Paul CP, Singh B (2017) Experimental investigation and metallographic characterization of fiber laser beam welding of Ti-6Al-4V alloy using response surface method. Opt Lasers Eng 95:52–68. https://doi.org/10.1016/j.optlaseng.2017.03.013
77. Đặng TH, Chen BH, Lee DJ (2017) Optimization of biodiesel production from transesterification of triolein using zeolite LTA catalysts synthesized from kaolin clay. J Taiwan Inst Chem Eng 79:1–9. https://doi.org/10.1016/j.jtice.2017.03.009
78. Azam M, Jahanzaib M, Wasim A, Hussain S (2015) Surface roughness modeling using RSM for HSLA steel by coated carbide tools. Int J Adv Manuf Technol 78:1031–1041. https://doi.org/10.1007/s00170-014-6707-5
79. Bajíc D, Lela B, Živković D (2008) Modeling of machined surface roughness and optimization of cutting parameters in face milling. Metalurgija 47(4):331–334
80. Mia M, Khan MA, Dhar NR (2017) High-pressure coolant on flank and rake surfaces of tool in turning of Ti-6Al-4V:

investigations on surface roughness and tool wear. Int J Adv Manuf Technol 90(5):1825–1834. https://doi.org/10.1007/s00170-016-9512-5
81. Rocha LCS, Paiva AP, Paiva EJ, Balestrassi PP (2015) Comparing DEA and principal component analysis in the multiobjective optimization of P-GMAW process. J Braz Soc Mech Sci Eng 38:2513–2526. https://doi.org/10.1007/s40430-015-0355-z
82. Miettinen K (1999) Nonlinear multiobjective optimization. Kluwer, Norwell
83. Bratchell N (1989) Multivariate response surface modelling by principal components analysis. J Chemom 3:579–588. https://doi.org/10.1002/cem.1180030406
84. Purkayastha MD, Barthakur A, Mahanta CL (2015) Production of vegetable protein from rapeseed press-cake using response surface methodology, weighted multivariate index, and desirability function: a way to handle correlated multiple responses. Int J Food Prop 18:1248–1271. https://doi.org/10.1080/10942912.2014.891612
85. Gomes JHF, Salgado Júnior AR, Paiva AP, Ferreira JR, Costa SC, Balestrassi PP (2012) Global criterion method based on principal components to the optimization of manufacturing processes with multiple responses. J Mech Eng 58(5):345–353. https://doi.org/10.5545/sv-jme.2011.136
86. Routara BC, Mohanty SD, Datta S, Bandyopadhyay A, Mahapatra SS (2010) Combined quality loss (CQL) concept in WPCA-based Taguchi philosophy for optimization of multiple surface quality characteristics of UNS C34000 brass in cylindrical grinding. Int J Adv Manuf Technol 51:135–143. https://doi.org/10.1007/s00170-010-2599-1
87. Salmasnia A, Kazemzadeh RB, Seyyed-Esfahani M, Hejazi TH (2013) Multiple response surface optimization with correlated data. Int J Adv Manuf Technol 64:841–855. https://doi.org/10.1007/s00170-012-4056-9
88. Chadegani AA, Salehi H, Yunus MM, Farhadi H, Fooladi M, Farhadi M, Ebrahim NA (2013) A comparison between two main academic literature collections: Web of Science and Scopus Databases. Asian Soc Sci 9(5):18–26. https://doi.org/10.5539/ass.v9n5p18
89. Guz AN, Rushchitsky JJ (2009) Scopus: a system for the evaluation of scientific journals. Int Appl Mech 45(4):351–362. https://doi.org/10.1007/s10778-009-0189-4
90. Omrani E, Moghadam AD, Menezes PL, Rohatgi PK (2016) Influences of graphite reinforcement on the tribological properties of self-lubricating aluminum matrix composites for green tribology, sustainability, and energy efficiency – a review. Int J Adv Manuf Technol 83:325–346. https://doi.org/10.1007/s00170-015-7528-x
91. Pakseresht AH, Javadi AH, Nejati M, Shirvanimoghaddam K, Ghasali E, Teimouri R (2014) Statistical analysis and multiobjective optimization of process parameters in plasma spraying of partially stabilized zirconia. Int J Adv Manuf Technol 75:739–753. https://doi.org/10.1007/s00170-014-6169-9
92. Khoran M, Ghabezi P, Frahani M, Besharati MK (2015) Investigation of drilling composite sandwich structures. Int J Adv Manuf Technol 76:1927–1936. https://doi.org/10.1007/s00170-014-6427-x
93. Aggarwal V, Khangura SS, Garg RK (2015) Parametric modeling and optimization for wire electrical discharge machining of Inconel 718 using response surface methodology. Int J Adv Manuf Technol 79:31–47. https://doi.org/10.1007/s00170-015-6797-8
94. Mahesh G, Muthu S, Devadasan SR (2016) Prediction of surface roughness of end milling operation using genetic algorithm. Int J Adv Manuf Technol 77:369–381. https://doi.org/10.1007/s00170-014-6425-z
95. Amdouni H, Bouzaiene H, Montagne A, Nasri M, Iost A (2017) Modeling and optimization of a ball-burnished aluminum alloy flat surface with a crossed strategy based on response surface methodology. Int J Adv Manuf Technol 88:801–814. https://doi.org/10.1007/s00170-016-8817-8
96. Meddour I, Yallese MA, Khattabi R, Elbah M, Boulanouar L (2015) Investigation and modeling of cutting forces and surface roughness when hard turning of AISI 52100 steel with mixed ceramic tool: cutting conditions optimization. Int J Adv Manuf Technol 77:1387–1399. https://doi.org/10.1007/s00170-014-6559-z
97. Araby S, Zaied R, Haridy S, Kaytbay S (2017) Grooves into cylindrical shapes by wire electrochemical machining. Int J Adv Manuf Technol 90:445–455. https://doi.org/10.1007/s00170-016-9389-3
98. Rajesh P, Nagaraju U, Gowd GH, Vardhan TV (2015) Experimental and parametric studies of Nd:YAG laser drilling on austenitic stainless steel. Int J Adv Manuf Technol 93:65–71. https://doi.org/10.1007/s00170-015-7639-4
99. Ayyappan S, Sivakumar K (2014) Experimental investigation on the performance improvement of electrochemical machining process using oxygen-enriched electrolyte. Int J Adv Manuf Technol 75:479–487. https://doi.org/10.1007/s00170-014-6096-9
100. Rocha LCS, Paiva AP, Rotela Junior P, Balestrassi PP, Campos PHS (2017) Robust multiple criteria decision making applied to optimization of AISI H13 hardened steel turning with PCBN wiper tool. Int J Adv Manuf Technol 89:2251–2268. https://doi.org/10.1007/s00170-016-9250-8
101. Sonawane HA, Joshi SS (2015) Modeling of machined surface quality in high-speed ball-end milling of Inconel-718 thin cantilevers. Int J Adv Manuf Technol 78:1751–1768. https://doi.org/10.1007/s00170-014-6759-6
102. Costa DMD, Paula TI, Silva PAP, Paiva AP (2016b) Normal boundary intersection method based on principal components and Taguchi's signal-to-noise ratio applied to the multiobjective optimization of 12L14 free machining steel turning process. Int J Adv Manuf Technol 87:825–834. https://doi.org/10.1007/s00170-016-8478-7
103. Sundararaman KA, Guharaja S, Padmanaban KP, Sabareeswaran M (2014) Design and optimization of machining fixture layout for end-milling operation. Int J Adv Manuf Technol 73:669–679. https://doi.org/10.1007/s00170-014-5848-x
104. Daoud M, Jomaa W, Chatelain JF, Bouzid A (2015) A machining-based methodology to identify material constitutive law for finite element simulation. Int J Adv Manuf Technol 77:2019–2033. https://doi.org/10.1007/s00170-014-6583-z
105. Varun A, Venkaiah N (2015) Simultaneous optimization of WEDM responses using grey relational analysis coupled with genetic algorithm while machining EN 353. Int J Adv Manuf Technol 76:675–690. https://doi.org/10.1007/s00170-014-6198-4
106. Hashmi KH, Zakria G, Raza MB, Khalil S (2016) Optimization of process parameters for high speed machining of Ti-6Al-4V using response surface methodology. Int J Adv Manuf Technol 85:1847–1856. https://doi.org/10.1007/s00170-015-8057-3
107. Verma GC, Kala P, Pandey PM (2017) Experimental investigations into internal magnetic abrasive finishing of pipes. Int J Adv Manuf Technol 88:1657–1668. https://doi.org/10.1007/s00170-016-8881-0
108. Hourmand M, Farahany S, Sarhan AAD, Noordin MY (2015) Investigating the electrical discharge machining (EDM) parameter effects on Al-Mg2Si metal matrix composite (MMC) for high material removal rate (MRR) and less EWR–RSM approach. Int J Adv Manuf Technol 77:831–838. https://doi.org/10.1007/s00170-014-6491-2
109. Yilmaz O, Bozdana AT, Okka MA (2014) An intelligent and automated system for electrical discharge drilling of aerospace

alloys: Inconel 718 and Ti-6Al-4V. Int J Adv Manuf Technol 74: 1323–1336. https://doi.org/10.1007/s00170-014-6059-1
110. Jain AK, Pandey PM (2016) Experimental studies on tool wear in μ-RUM process. Int J Adv Manuf Technol 85:2125–2138. https://doi.org/10.1007/s00170-015-8248-y
111. Yue Z, Huang C, Zhu H, Wang J, Yao P, Liu Z (2014) Optimization of machining parameters in the abrasive waterjet turning of alumina ceramic based on the response surface methodology. Int J Adv Manuf Technol 71:2107–2114. https://doi.org/10.1007/s00170-014-5624-y
112. Liu JW, Baek DK, Ko TJ (2014a) Chipping minimization in drilling ceramic materials with rotary ultrasonic machining. Int J Adv Manuf Technol 72:1527–1535. https://doi.org/10.1007/s00170-014-5766-y
113. Zhao T, Shi Y, Lin X, Duan J, Sun P, Zhang J (2014) Surface roughness prediction and parameters optimization in grinding and polishing process for IBR of aero-engine. Int J Adv Manuf Technol 74:653–663. https://doi.org/10.1007/s00170-014-6020-3
114. Liu Z, Wang C, Chen M, Ge C, Li M (2014b) A coupling response surfaces methodology of multiple constraints (CRSMMC) for parameters optimization of broach tool in broaching of heat-resistant steel X12CrMoWVNb N-10-1-1. Int J Adv Manuf Technol 74: 1719–1732. https://doi.org/10.1007/s00170-014-6109-8
115. Zhou Y, Gong Y, Zhu Z, Gao Q, Wen X (2016) Modelling and optimisation of surface roughness from microgrinding of nickel-based single crystal superalloy using the response surface methodology and genetic algorithm. Int J Adv Manuf Technol 85: 2607–2622. https://doi.org/10.1007/s00170-015-8121-z
116. Ahmadnia M, Shahraki S, Kamarposhti MA (2016) Experimental studies on optimized mechanical properties while dissimilar joining AA6061 and AA5010 in a friction stir welding process. Int J Adv Manuf Technol 87:2337–2352. https://doi.org/10.1007/s00170-016-8636-y
117. Ramachandran KK, Murugan N, Kumar SS (2016) Performance analysis of dissimilar friction stir welded aluminium alloy AA5052 and HSLA steel butt joints using response surface method. Int J Adv Manuf Technol 86:2373–2392. https://doi.org/10.1007/s00170-016-8337-6
118. Hasan MM, Ishak M, Rejab MRM (2017) Influence of machine variables and tool profile on the tensile strength of dissimilar AA7075-AA6061 friction stir welds. Int J Adv Manuf Technol 90:2605–2615. https://doi.org/10.1007/s00170-016-9583-3
119. Safeen W, Hussain S, Wasim A, Jahanzaib M, Aziz H, Abdalla H (2016) Predicting the tensile strength, impact toughness, and hardness of friction stir-welded AA6061-T6 using response surface methodology. Int J Adv Manuf Technol 87:1765–1781. https://doi.org/10.1007/s00170-016-8565-9
120. Jahanzaib M, Hussain S, Wasim A, Aziz H, Mirza A, Ullah S (2017) Modeling of weld bead geometry on HSLA steel using response surface methodology. Int J Adv Manuf Technol 89: 2087–2098. https://doi.org/10.1007/s00170-016-9213-0
121. Shi H, Zhang K, Xu Z, Huang T, Fan L, Bao W (2014) Applying statistical models optimize the process of multi-pass narrow-gap laser welding with filler wire. Int J Adv Manuf Technol 75:279–291. https://doi.org/10.1007/s00170-014-6159-y
122. Korra NN, Vasudevan M, Balasubramanian KR (2015) Multi-objective optimization of activated tungsten inert gas welding of duplex stainless steel using response surface methodology. Int J Adv Manuf Technol 77:67–81. https://doi.org/10.1007/s00170-014-6426-y
123. Winiczenko R (2016) Effect of friction welding parameters on the tensile strength and microstructural properties of dissimilar AISI 1020-ASTM A536 joints. Int J Adv Manuf Technol 84:1657–1668. https://doi.org/10.1007/s00170-015-7751-5
124. Lotfi AH, Nourouzi S (2014) Predictions of the optimized friction stir welding process parameters for joining AA7075-T6 aluminum alloy using preheating system. Int J Adv Manuf Technol 73:1717–1737. https://doi.org/10.1007/s00170-014-5963-8
125. Xu WH, Lin SB, Fan CL, Zhuo XQ, Yang CL (2014) Statistical modelling of weld bead geometry in oscillating arc narrow gap all-position GMA welding. Int J Adv Manuf Technol 72:1705–1716. https://doi.org/10.1007/s00170-014-5799-2
126. Mostaan H, Shamanian M, Safari M (2016) Process analysis and optimization for fracture stress of electron beam welded ultra-thin FeCo-V foils. Int J Adv Manuf Technol 87:1045–1056. https://doi.org/10.1007/s00170-016-8553-0
127. Zhao S, Bi Q, Wang Y, Shi J (2017) Empirical modeling for the effects of welding factors on tensile properties of bobbin tool friction stir-welded 2219-T87 aluminum alloy. Int J Adv Manuf Technol 90:1105–1118. https://doi.org/10.1007/s00170-016-9450-2
128. Mostafapour A, Ebrahimpour A, Saeid T (2017) Finite element investigation on the effect of FSSW parameters on the size of welding subdivided zones in TRIP steels. Int J Adv Manuf Technol 88:277–289. https://doi.org/10.1007/s00170-016-8749-3
129. Cai Y, Wang XS, Yuan SJ (2016) Pre-form design for hydroforming of aluminum alloy automotive cross members. Int J Adv Manuf Technol 86:463–473. https://doi.org/10.1007/s00170-015-8160-5
130. Maji K, Pratihar DK, Nath AK (2016) Experimental investigations, modeling, and optimization of multi-scan laser forming of AISI 304 stainless steel sheet. Int J Adv Manuf Technol 83:1441–1455. https://doi.org/10.1007/s00170-015-7675-0
131. Guo W, Hua L, Mao H (2014) Minimization of sink mark depth in injection-molded thermoplastic through design of experiments and genetic algorithm. Int J Adv Manuf Technol 72:365–375. https://doi.org/10.1007/s00170-013-5603-8
132. Pakseresht AH, Ghasali E, Nejati M, Shirvanimoghaddam K, Javadi AH, Teimouri R (2015) Development empirical-intelligent relationship between plasma spray parameters and coating performance of yttria-stabilized zirconia. Int J Adv Manuf Technol 76:1031–1045. https://doi.org/10.1007/s00170-014-6212-x
133. Hassan MH, Othman AR, Kamaruddin S (2017) The use of response surface methodology (RSM) to optimize the acid digestion parameters in fiber volume fraction test of aircraft composite structures. Int J Adv Manuf Technol 90:3739–3748. https://doi.org/10.1007/s00170-016-9683-0
134. Rajakumar S, Balasubramanian V (2016) Diffusion bonding of titanium and AA 7075 aluminum alloy dissimilar joints—process modeling and optimization using desirability approach. Int J Adv Manuf Technol 86:1095–1112. https://doi.org/10.1007/s00170-015-8223-7
135. Hosseinzadeh M, Mouziraji MG (2016) An analysis of tube drawing process used to produce squared sections from round tubes through FE simulation and response surface methodology. Int J Adv Manuf Technol 87:2179–2194. https://doi.org/10.1007/s00170-016-8532-5
136. Zhang WW, Cong S (2016) Failure analysis of SUS304 sheet during hydro-bulging based on GTN ductile damage model. Int J Adv Manuf Technol 86:427–435. https://doi.org/10.1007/s00170-015-8199-3
137. Huang C, Radi B, Hami A (2016) Uncertainty analysis of deep drawing using surrogate model based probabilistic method. Int J Adv Manuf Technol 86:3229–3240. https://doi.org/10.1007/s00170-016-8436-4
138. Zhang P, Kou S, Lin B, Wang Y (2015) Optimization for radial knurling connection process of assembled camshaft using response surface method. Int J Adv Manuf Technol 77:653–661. https://doi.org/10.1007/s00170-014-6486-z
139. Liu S, Kovacevic R (2014) Statistical analysis and optimization of processing parameters in high-power direct diode laser cladding.

Int J Adv Manuf Technol 74:867–878. https://doi.org/10.1007/s00170-014-6041-y

140. Zhang WW, Han C, Yuan SJ (2016) Optimization of pre-form shapes by response surface methodology for hydro-forming of 780 MPa torsion beam. Int J Adv Manuf Technol 85:1227–1237. https://doi.org/10.1007/s00170-015-8043-9
141. Campos PHS (2015) DEA-OTS methodology: a contribution to the optimum selection of tools in the turning of hardened ABNT H13. Doctoral Dissertation, Federal University of Itajuba, Brazil
142. Pereira RBD, Leite RR, Alvim AC, Paiva AP, Balestrassi PP, Ferreira JR, Davim JP (2018) Multivariate robust modeling and optimization of cutting forces of the helical milling process of the aluminum alloy al 7075. Int J Adv Manuf Technol 95:2691–2715. https://doi.org/10.1007/s00170-017-1398-3
143. Gaudêncio JHD, Almeida FA, Turrioni JB, Quinino RC, Balestrassi PP, Paiva AP (2019) A multiobjective optimization model for machining quality in the AISI 12L14 steel turning process using fuzzy multivariate mean square error. Precis Eng. https://doi.org/10.1016/j.precisioneng.2019.01.001
144. Naves FL, Paula TI, Balestrassi PP, Moreira Braga WL, Sawhney RS, Paiva AP (2017b) Multivariate normal boundary intersection based on rotated factor scores: a multiobjective optimization method for methyl orange treatment. J Clean Prod 143:413–439. https://doi.org/10.1016/j.jclepro.2016.12.092
145. Paiva AP, Gomes JHF, Peruchi RS, Leme RC, Balestrassi PP (2014) A multivariate robust parameter optimization approach based on principal component analysis with combined arrays. Comput Ind Eng 74:186–198